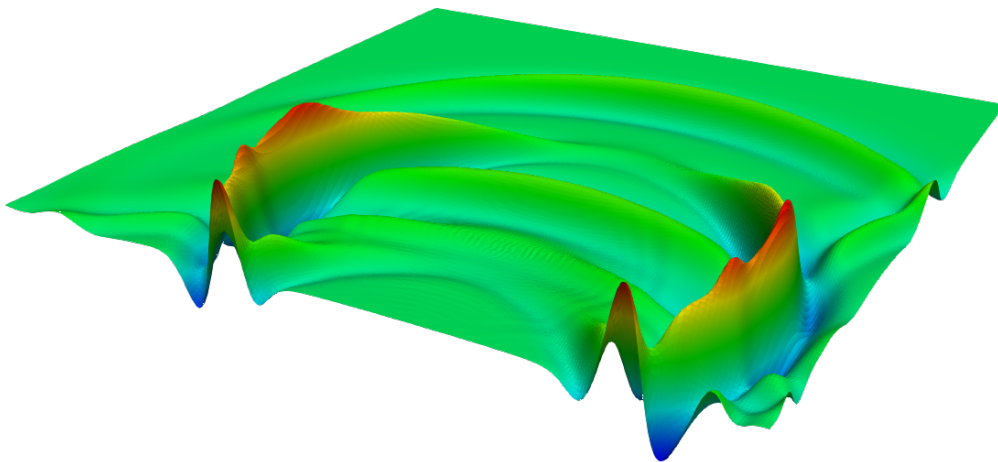




THE 2ND INTERNATIONAL CONFERENCE ON ADVANCED MODELLING OF WAVE PROPAGATION IN SOLIDS

THE ECCOMAS REGIONAL CONFERENCE

Edited by
Radek Kolman
Arkadi Berezovski
Alena Kruisová



Book of abstracts

THE 2ND INTERNATIONAL CONFERENCE
OF WAVE PROPAGATION IN SOLIDS

PRAGUE, CZECH REPUBLIC

SEPTEMBER 17–21, 2018

<http://wavemodelling2018.it.cas.cz>



EUROPEAN UNION
European Structural and Investment Funds
Operational Programme Research,
Development and Education

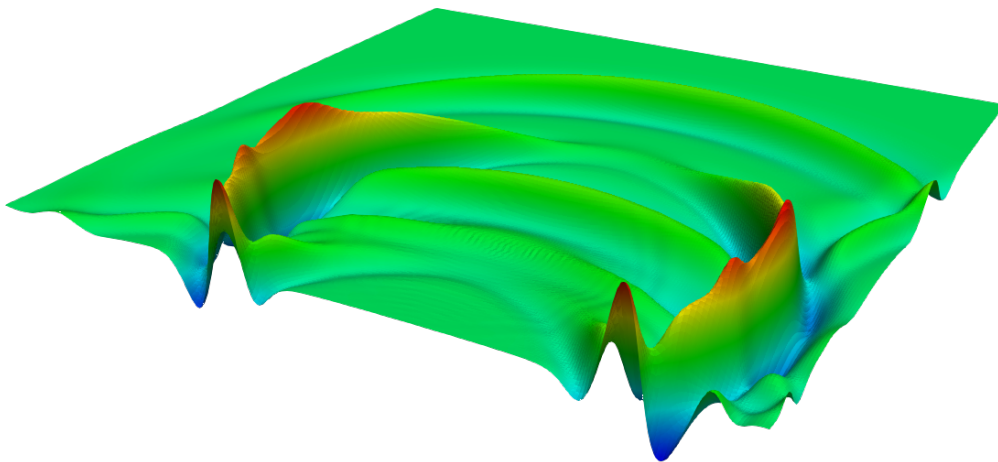




THE 2ND INTERNATIONAL CONFERENCE ON ADVANCED MODELLING OF WAVE PROPAGATION IN SOLIDS

THE ECCOMAS REGIONAL CONFERENCE

Edited by
Radek Kolman
Arkadi Berezovski
Alena Kruisová



Book of abstracts

THE 2ND INTERNATIONAL CONFERENCE
OF WAVE PROPAGATION IN SOLIDS

PRAGUE, CZECH REPUBLIC

SEPTEMBER 17–21, 2018

<http://wavemodelling2018.it.cas.cz>



EUROPEAN UNION
European Structural and Investment Funds
Operational Programme Research,
Development and Education



WAVE MODELLING 2018 - THE 2ND INTERNATIONAL CONFERENCE ON ADVANCED MODELLING OF WAVE PROPAGATION IN SOLIDS, THE ECCOMAS REGIONAL CONFERENCE, Prague, Czech Republic, September 17–21, 2018

organized by the Institute of Thermomechanics, The Czech Academy of Sciences, v.v.i.



under the auspices of the European Community on Computational Methods in Applied Science



the Central European Association for Computational Mechanics



the Czech Society for Mechanics



Centre of Excellence for Nonlinear Dynamic Behaviour of Advanced Materials in Engineering



EUROPEAN UNION
European Structural and Investment Funds
Operational Programme Research,
Development and Education



Edited by Radek Kolman, Arkadi Berezovski, Alena Kruisová

The abstracts are reproduced directly from author manuscripts. The authors are solely responsible for the contents and opinions expressed therein.

Note: The book of abstracts has been edited to the date August 10, 2018, including all electronically registered participants.

© 2018, Institute of Thermomechanics ASCR, v.v.i., Prague, <http://www.it.cas.cz>

Printed in Tiskárna a vydavatelství 999, s.r.o., Dolnokubínská 1451, 393 01 Pelhřimov, Czech Republic

ISBN: 978-80-87012-67-3

Number of pages: 128

Not for sale.

Chairmen

R. Kolman Institute of Thermomechanics, CAS, v.v.i., Prague
A. Berezovski Tallinn University of Technology, Tallinn

Scientific Committee

Prof. M. Ainsworth Brown University, Providence, USA
Dr. A. Berezovski Tallinn University of Technology, Tallinn, Estonia
Prof. A.-S. Bonnet-Ben Dhia CNRS-INRIA-ENSTA, Paris, France
Prof. C.-S. David Chen National Taiwan University, Taipei, Taiwan
Prof. W.-W. Chen Purdue University, West Lafayette, USA
Prof. J. Engelbrecht Tallinn University of Technology, Tallinn, Estonia
Prof. J. González University of Seville, Seville, Spain
Prof. H. Huh KAIST, Daejeon, Korea
Prof. A. Idesman Texas Tech University, Lubbock, USA
Prof. P. Joly CNRS-INRIA-ENSTA, Paris, France
Prof. D.M. Kochmann ETH, Zurich, Switzerland/Caltech, Pasadena, USA
Prof. D. Komatitsch CNRS and University of Aix-Marseille, Marseille, France
Prof. B.T. Maruszewski Poznan University of Technology, Poznan, Poland
Prof. M. Okrouhlík Czech Academy of Sciences, Prague, Czech Republic
Prof. W. J. Parnell University of Manchester, Manchester, UK
Prof. K.C. Park University of Colorado at Boulder, Boulder, USA
Dr. J. Plešek Czech Academy of Sciences, Prague, Czech Republic
Dr. Z. Převorovský Czech Academy of Sciences, Prague, Czech Republic
Prof. Z. Ren University in Maribor, Maribor, Slovenia
Prof. E. Rohan University of West Bohemia, Pilsen, Czech Republic
Prof. J. Sládek Slovak Academy of Sciences, Bratislava, Slovakia
Prof. S. Sorokin Aalborg University, Aalborg, Denmark
Dr. A. Tkachuk University of Stuttgart, Stuttgart, Germany
Prof. E. Zaretsky Ben-Gurion University of the Negev, Beer Sheva, Israel

Local Organizing Committee

Radek Kolman
Jiří Plešek
Miloslav Okrouhlík
Dušan Gabriel
Pavel Formánek
Alena Kruisová
Michal Mračko
Petr Pařík
Ján Kopačka
Jan Masák
Dagmar Tittlová

Conference webpage

<http://wavemodelling2018.it.cas.cz>

Preface

Wave propagation in solids remains to be an active topic of research in solid mechanics because of the development of new engineering materials required to meet advanced technological needs. The complex behavior of such materials demands a closer interaction between numerical analysts and experimentalists in order to provide a response to dynamical loadings.

Recent years have witnessed the development of innovative numerical schemes for the approximation of dynamic problems in solid mechanics. These methods have allowed the robust integration of very complex problems, often obtaining at the same time accurate pictures of the underlying dynamical behavior. Whereas the available integrators can handle very effectively standard models, there is still need to advance the capabilities in solving transient problems where multiple scales and physical phenomena interact, where the solution is non-smooth, and where computational cost remains a bottleneck.

The objective of this conference is to bring together researchers from the related fields to discuss recent advances and exchange new ideas on novel experimental and computational methods for the prediction of the response of heterogeneous materials at various strain rates and loading conditions. Topics for discussion at the conference include:

- Nonlinear, shock and plastic waves in solids
- Dynamics of complex materials
- Waves in heterogeneous and anisotropic materials
- Waves in metamaterials and periodic structures
- Waves in plates and shells
- Waves in composite materials
- Numerical methods for wave propagation
- Acoustic problems and fluid structure interactions
- Detection of defects in materials
- Nondestructive testing of materials
- Seismic waves
- Experimental methods in wave propagation problems

The selected papers will appear in special issues of the *Wave Motion* and in the *Computers & Mathematics with Applications*. The editors would like to thank all the contributors who made the conference and this book possible. Deep gratitude is also extended to all the members of the scientific committee, the members of the local organizing committee, and our colleagues, namely Jiří Plešek, Dušan Gabriel, Jan Masák, Michal Mračko, Pavel Formánek and Dagmar Tittlová.

VENUE, LOCATION and SOCIAL PROGRAMME

Conference Venue

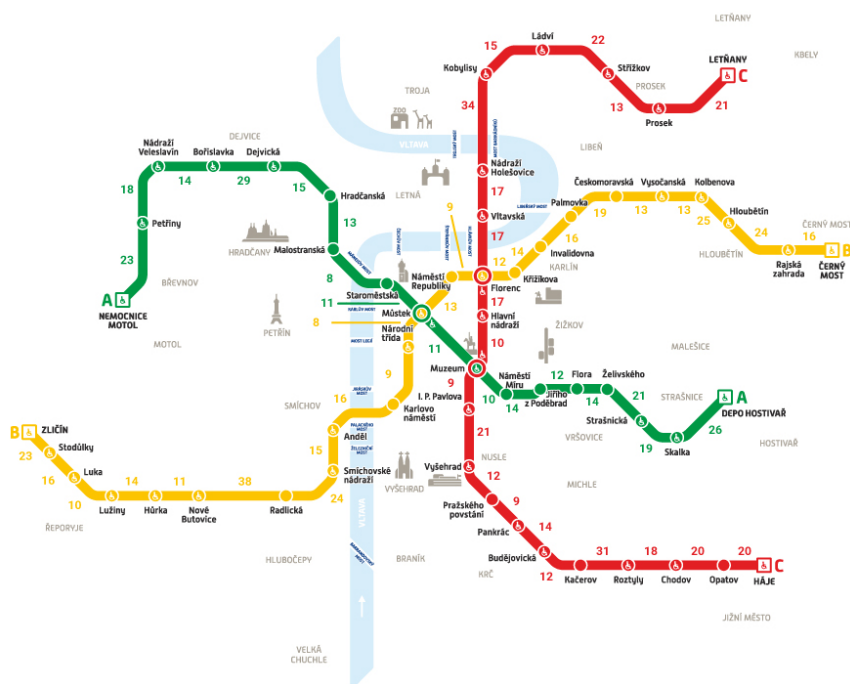
The conference room takes place at the J. Heyrovský Institute of Physical Chemistry of the CAS, v. v. i., Dolejškova 2155/3, 182 23 Prague 8.



Transportation

Air – There are direct connections from most major cities to Prague's Václav Havel Airport.

Ground – The best method of getting from Václav Havel Airport to the conference area is by taking bus line **119** to **Nádraží Veveslavín** and then metro **line A (green)** to **Muzeum** and metro **line C (red)** to **Ládví** station. This 50 minutes trip will cost 32CZK. Detailed info about public transportation can be found on Prague Public Transport website <http://www.dpp.cz/en/>. Here is the ground and tram transit scheme:



Vypočet: Český rozhlas s pomocí Mapy.cz, mapa linek metra: Dopravní podnik hl. m. Prahy

Social programme

The Welcome drink takes place at the **Pizzeria Giovanni** on Sunday, September 16, 2018, 5PM - 7PM. Address: Střelnická 1826/35, 182 00, Praha 8. The Metro station **Ládví, line C (red)**.

The conference banquet takes place at the terrace of the restaurant **Villa Richter** on Wednesday, September 19, 2018, 7PM - 9PM. Address: Staré zámecké schody 6/251, 118 00, Praha 1, Pražský hrad. The Metro station **Malostranská, line A (green)**.

CONTENTS

Abuziarov M.H.	21
3D METHOD AND CODES FOR FLUID STRUCTURE INTERACTION PROBLEMS IN EULER VARIABLES	
Acevedo R. , Kolman R., J. Trnka J., D. Mochar D. , Gabriel D.	23
BEHAVIOUR OF Ti6Al4V AUXETIC HONEYCOMB STRUCTURE UNDER DYNAMIC LOADING	
Adámek V. , Valeš F., Červ J.	25
TRANSIENT WAVES IN FUNCTIONALLY GRADED STRIP UNDER IMPACT LOADING	
Bar-On B.	27
STOMATAL MICRO-TO-MACRO MECHANICS: THE ROLE OF MECHANICAL ANISOTROPY ON BIO-MECHANICAL FUNCTION	
Baronian V., Bonnet-Ben Dhia A-S., Fliss S., Tjandrawidjaja Y.	29
THE HALF-SPACE MATCHING METHOD FOR LAMB WAVE SCATTERING IN ANISOTROPIC PLATES	
Berjamin H., Lombard B. , Chiavassa G., Favrie N.	31
NONLINEAR WAVES IN SOLIDS: VISCOELASTICITY, SOFTENING, AND FINITE-VOLUME METHODS	
Bonnet M. , Aquino W.	33
IDENTIFICATION OF HETEROGENEOUS ELASTIC MODULI USING A MODIFIED ERROR IN CONSTITUTIVE EQUATION FUNCTIONAL: THE CASE OF INTERIOR ELASTODYNAMIC DATA AND UNDERDETERMINED BOUNDARY CONDITIONS	
Chaillat S. , Amlani F., Loseille A.	35
ANISOTROPIC HIGH-ORDER ADAPTIVE BOUNDARY ELEMENT METHODS FOR 3D ACOUSTICS	

Colvez M. , Cottureau R., Lopez-Caballero F. INFLUENCE OF CRUST HETEROGENEOUS PROPERTIES CLOSE TO A FAULT ON SEISMIC WAVE PROPAGATION	37
Cottureau R. , Sevilla R. INFLUENCE OF MATERIAL HETEROGENEITY ON THE STABILITY OF EXPLICIT HIGH-ORDER SPECTRAL ELEMENT METHODS	39
Engelbrecht J. , Berezovski A., Peets T., Tamm K. WAVE ENSEMBLES IN COMPLEX MEDIA	41
Fíla T. , Zlámal P., Falta J., Adorna M. DIRECT IMPACT HOPKINSON BAR: APPLICATION ON 3D PRINTED AUXETIC LATTICES AND OTHER CELLULAR STRUCTURES	43
Joshi S., Franc J.-P., Ghigliotti G., Fivel M. SMOOTHED PARTICLE HYDRODYNAMICS SIMULATIONS OF CAVITATION BUBBLE COLLAPSE INDUCED PLASTICITY	45
Foglar M. , Hájek R., Stoller J., Pachman J. BLAST OVERPRESSURE PROPAGATION IN FUNCTIONALLY LAYERED CEMENTITIOUS COMPOSITES	47
Gabriel D. , Kopačka J., Kolman R., González J. A., Plešek J. 2D/3D EXPLICIT FINITE ELEMENT CONTACT-IMPACT ALGORITHM WITH BIPENALTY STABILIZATION	49
Gitman I. M. , Song Y. DISPERSIVE WAVE PROPAGATION IN MATERIAL WITH PERIODIC AND RANDOM MICROSTRUCTURE	51
González J. A. , Kopačka J., Kolman R., Cho S. S., Park K. C. RECIPROCAL MASS MATRICES FOR ISOGOMETRIC ANALYSIS VIA THE METHOD OF LOCALIZED LAGRANGE MULTIPLIERS	53

Grabec T. , Sedlák P., Seiner H., Landa M. RITZ-RAYLEIGH APPROACH: NUMERICAL CALCULATION OF WAVES IN PLATES OF HIGH ANISOTROPY	55
Hirse Korn S. ELASTIC WAVE PROPAGATION AND SCATTERING MODELLING ASSISTED NONDESTRUCTIVE TESTING AND MICROSTRUCTURED MATERIALS EVALUATION	57
Hora P. , Machová A., Červ J., Uhnáková A. ACOUSTIC EMISSION FROM FAST DISLOCATIONS IN 3D BCC IRON CRYSTALS	59
Hudspeth M., Chen W. WAVE DEVELOPMENT IN HIGH-PERFORMANCE YARNS UNDER TRANSVERSE IMPACT	61
Huh H. , Park C., Joo G. WAVE PROPAGATION IN MEASUREMENT OF FLOW STRESS WITH HOPKINSON BAR TESTS AT HIGH STRAIN RATES	63
Jeon W. ACOUSTIC BLACK HOLES: FROM GENERALIZATION TO REALIZATION	65
Khajehtourian R. , Rafsanjani A., Bertoldi K., Kochmann D. TRANSITION WAVES IN RECONFIGURABLE MULTISTABLE SOFT STRUCTURES	67
Klimeš L. REPRESENTATION THEOREM FOR VISCOELASTIC WAVES WITH A NON-SYMMETRIC STIFFNESS MATRIX	69
Kober J. , Chlada M., Zeman R. GEOMETRIC RAY TRACING APPLIED TO TIME REVERSED ACOUSTICS	71

Koller M. , Kruisová A., Seiner H., Sedlák P., Román-Manso B., Miranzo P., Belmonte M., Landa M. ACOUSTIC ENERGY FOCUSING IN ROBOCAST CERAMIC SCAFFOLDS	75
Kolman R. , Cho S.S., Park K.C., González J.A., Berezovki A., Hora P., Adámek V. A LOCAL TIME STEPPING FOR DISCONTINUOUS WAVE PROPAGATION IN A HETEROGENEOUS BAR SCAFFOLDS	73
Kruisová A. , Kolman R., Plešek J. TEMPORAL-SPATIAL DISPERSION ERRORS IN FEM MODELLING OF WAVE PROPAGATION AND IMPLICIT TIME INTEGRATION	77
Ledet L.S. , Sorokin S.V. EIGENFREQUENCY ANALYSIS OF ELASTIC STRUCTURES UNDER HEAVY FLUID LOADING BY MEANS OF THE BI-ORTHOGONALITY RELATIONS	79
Lints M. , Salupere A., Dos Santos S. NUMERICAL SIMULATION OF ULTRASONIC TIME REVERSAL ON DEFECTS IN CARBON FIBRE REINFORCED POLYMER	81
Lukáš D. , Malý L., Straková E., Schöberl J. PARALLEL TDNNS-FEM FOR ELASTODYNAMICS OF THIN-WALLED STRUCTURES	83
Mračko M. , Kolman R., Kober J., Převorovský Z., Plešek J. INFLUENCE OF TEMPERATURE IN COMPUTATIONAL TIME REVERSAL METHOD	85
Naimark O. DEFECT INDUCED METASTABILITY AND POWER UNIVERSALITY OF WAVE FRONTS IN SHOCKED CONDENSED MATTER	87

Ocaña J. L. , García-Beltrán A., Angulo I., Cordovilla F. NUMERICAL SIMULATION OF PLASMA DYNAMICS AND SHOCK-INDUCED RESIDUAL STRESSES IN THE LASER SHOCK PROCESSING OF METALLIC MATERIALS	89
Park K. C. TOWARD NUMERICAL REALIZATION OF SPLIT-HOPKINS PRESSURE BAR: A FONDEST HOPE BY A COMPUTATIONAL MECHANICIAN	91
Parma S. , Červ J., Plešek J. ON EQUIVALENCE OF THE STRESS AND DISPLACEMENT FORMULATION OF THE RAYLEIGH WAVES PROPAGATION PROBLEM IN TWO-DIMENSIONAL COMPOSITE MATERIAL	93
Porubov A. , Antonov I. CONTROL OF NONLINEAR STRAIN WAVES IN DI-ATOMIC CRYSTALLINE MEDIA	95
Převorovský Z. , Mračko M., Kober J., Krofta J., Kolman R. ACOUSTIC SOURCE LOCATION BY TIME REVERSAL SIGNAL TRANSFER FROM EXPERIMENT TO NUMERICAL MODEL (DIGITAL TWIN)	97
Rejani S. , Khamlichi A., El Hajjaji A. THE GENERALIZATION OF THE MPSM ALGORITHM IN CASE OF CSCAN FOR THE IMAGE RECONSTRUCTION OF TH DELAMINATION DEFECT IN COMPOSITES	99
Rohan E. , Nguyen V.-H., Naili S. HOMOGENIZATION AND BLOCH ANALYSIS OF WAVE DISPERSION IN HETEROGENEOUS FLUID SATURATED POROUS MEDIA	101
Růžek B. , Pšenčík I. INVERSION OF P-WAVE VSP TRAVELTIMES IN ANISOTROPIC MEDIA	103

Salupere A. , Ratas M. 2D DISCRETE SPECTRAL ANALYSIS AND EMERGENCE OF SOLITONIC STRUCTURES	105
Tkachuk A. , Schaeuble A.-K., Bischoff M. VARIATIONAL CONSTRUCTION OF RECIPROCAL MASS MATRICES FOR B-SPLINE-BASED FINITE ELEMENTS: MULTIPARAMETER TEMPLATES AND CUSTOMIZATION	107
Zakhmatov V. , Chernyshov M., Kwech O., Bojko V. EXPLOSION WAVE PROPAGATION IN MASS OF SOLID PARTICLES TO CREATION EXTINGUISHING WHIRLY FOR FAST, EFFECTIVE REMOTE CONTROL OF LARGE, POWER FIRES	109
Zaretsky E. , Frage N., Meshi L. SHOCK WAVES. WHAT MAY BE LEARNT FROM THEIR PROPAGA- TION THROUGH SOLIDS?	111
LIST of REGISTERED PARTICIPANTS	113

ABSTRACTS

3D METHOD AND CODES FOR FLUID STRUCTURE INTERACTION PROBLEMS IN EULER VARIABLES

M.H. Abuziarov

Research institute for mechanics of Nizhnii Novgorod state university, Russia; e-mail: abouziar@mech.unn.ru

Keywords: Godunov method, elastic plastic flows, fluid structure interaction

The 3D codes based on the explicit numerical method for modeling shock wave and fluid structure interaction problems in Euler variables are presented. The method is based on the modified Godunov scheme of increased accuracy, uniform for solving equations of fluid dynamics and elastic-plastic flows [1]. The increase of the scheme accuracy is achieved by using 3D spatial time dependent solution of the discontinuity problem (3D space time dependent Riemann's solver). The same solution is used to calculate the interaction at the fluid-solid surface (Fluid Structure Interaction problem).

These codes do not require complex 3D mesh generators, only the surfaces of the calculating objects as the STL files created by CAD systems, which greatly simplifies the preparing the task and makes it convenient to use directly by the designer at the design stage. To set the initial geometry and follow the deformation of the calculating domains in the process of interaction it is enough to take into account the interacting surfaces constituted by a set of triangles. Fixed Cartesian grid and local mobile grids associated with each triangle of the surface are used. The flow parameters are interpolated from the Cartesian grid to the local grids and vice versa.

The results of the test solutions and applications related to the generation and extension of the detonation and shock waves, loading the constructions are presented.

Acknowledgement

This work was supported by the RFBR grants (15-48-02333 R_povolzhe_a, 16-08- 00458 a, 14-08-00197 a).

References

- [1] Abouziarov M., Aiso H., Takahashi T. An application of conservative scheme to structure problems. Series from research institute of mathematics of Kyoto university. Mathematical analysis in fluid and gas dynamics. 2004, N2 1353 , pp. 192-201

BEHAVIOUR OF Ti6Al4V AUXETIC HONEYCOMB STRUCTURE UNDER DYNAMIC LOADING

R. Acevedo^{1,2*}, R. Kolman², J. Trnka², D. Mochar² and D. Gabriel²

¹Department of Mechanical Engineering, UFSC, Brazil

²Institute of Thermomechanics, CAS, *v.v.i.*, Prague, Czech Republic

Keywords: titanium alloy, selective laser melting, auxetic materials, impact loading.

Typically, most of the materials have a Poisson's ratio between 0.2 and 0.4. Poisson's ratio is a non-dimensional ratio defined as the fraction between longitudinal elongation and lateral compression after a uniaxial traction effort. It yields the definition as

$$\nu = -\frac{\varepsilon_{transverse}}{\varepsilon_{axial}} \quad (1)$$

This ratio allows the characterization of matter contraction perpendicular to the applied effort direction [1]. Considering only isotropic materials, the values for this elastic parameter are comprised in the interval [-1, 0.5]. The maximum value of ν is 0.5 and it corresponds to the case of an incompressible material (natural rubber) while that the case $\nu = 0$ corresponds to a very little or zero lateral expansion after a compression effort, as it is observed for cork.

Nevertheless, there is a class of materials which present a negative Poisson ratio, those are called auxetic (first introduced by Evans), derived from the Greek word *auxetikos*, defined as "that which tends to increase" [2]. Auxetic behaviour can be either intrinsic or obtained by several re-entrant geometries, as shown in Fig. 1 [2]. These geometries can also be extended in 3D.

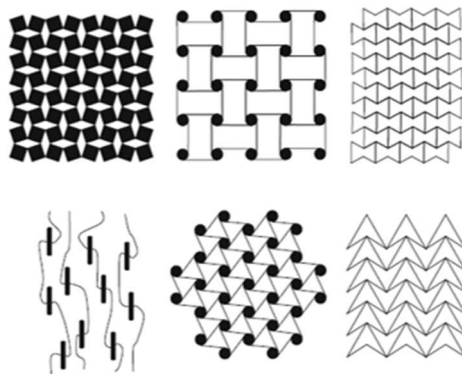


Figure 1: Geometries which show auxetic behaviour [2].

In this study, the following auxetic geometry was chosen (Fig.2), especially due to its easiness in parametrization and promising early simulation results. Elastic behaviour of this structure has been studied in [3,4].

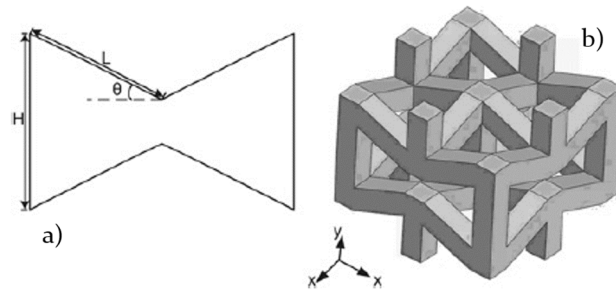


Figure 1: Auxetic geometry a) 2D detail and parameters; b) 3D rendering [3].

In this contribution, the behaviour of Ti6Al4V auxetic structures and bulk cylinders under impact loading is studied experimentally and numerically and results are compared among them. Using a destructive test approach (DT), these structures are impacted by a loader launched at a given height. The response of the structure on different impactors with different impact energy is monitored by a high-speed camera and radial displacement history is measured by a high speed vibrometer. The corresponding energy absorption in elasto-plastic regime is analysed. Besides, this experiment will allow to access the dynamic deformation behaviour of the structure under impact loading of both auxetic and bulk cylinder Ti6Al4V specimens.

Besides, a numerical model of the specimens will be performed using FEM method, especially with LS-DYNA. Finally, agreement of experimental data and simulation data will be discussed.

Acknowledgement

The work was supported by the Centre of Excellence for Nonlinear Dynamic Behaviour of Advanced Materials in Engineering CZ.02.1.01/0.0/0.0/15_003/0000493 (Excellence Research Teams) in the framework of Operational Program Research, Development and Education. The work of R. K. was supported by the grant projects with No. 17-22615S of the Czech Science Foundation (CSF) within institutional support RVO:61388998. Author R. A. acknowledges the support of CAPES – Brazil.

References

- [1] P.H. Mott, C.M. Roland. Limits to Poisson's ratio in isotropic materials. *Physical Review B*, **80**: 132104-1 – 132104-4, 2009.
- [2] T.C. Lim. *Auxetic Materials and Structures*. Engineering Materials series, Springer, 2015.
- [3] L. Yang, D. Cormier, H. West, O. Harryson, K. Knowlson. Non-stochastic Ti–6Al–4V foam structures with negative Poisson's ratio. *Materials Science & Engineering A*, **558**: 579–585, 2012.
- [4] X.-T. Wang, B. Wang, X.-W. Li, L. Ma. Mechanical properties of 3D re-entrant auxetic cellular structures. *International Journal of Mechanical Sciences*, **131**, 2017. DOI: 10.1016/j.ijmecsci.2017.05.048
- [5] S. Nedomová, L. Severa, J. Buchar, J. Trnka, P. Stoklasová. *Study of Hen's eggs behavior under impact loading*. Nova Science Publishers, 2011.

TRANSIENT WAVES IN FUNCTIONALLY GRADED STRIP UNDER IMPACT LOADING

Vítězslav Adámek^{1,*}, František Valeš² and Jan Červ³

¹NTIS - New Technologies for the Information Society, Faculty of Applied Sciences, University of West Bohemia, Pilsen, Czech Republic; e-mail: vadamek@kme.zcu.cz

²Institute of Thermomechanics AS CR, v.v.i., Pilsen, Czech Republic; e-mail: vales@it.cas.cz

³Institute of Thermomechanics AS CR, v.v.i., Prague, Czech Republic; e-mail: cerv@it.cas.cz

Keywords: transient waves, functionally graded material, plane stress problem, analytical solution

In this work we study the propagation of transient waves in a viscoelastic infinite strip made of a functionally graded material (FGM) under loads of impact character using semi-analytical approach. Wave phenomena in such a medium are described by a system of two partial integro-differential equations (PIDEs) of the second order in terms of the displacement components. Contrary to homogeneous elastic or viscoelastic case, this system of PIDEs is coupled so its solution for arbitrary variation of material properties is very difficult, if at all possible. For this reason, we decided to solve the problem as a problem of a multilayered medium with layers of constant material properties. This is one of possible approaches used to handle the wave propagation in FGMs (see [1], [2]). It is clear that this is only an approximation of real FGM and that the accuracy of this method mainly depends on the thickness of modelled layers. Further, there is a problem how to determine the material properties of each layer to properly represent the real behaviour of FGM. On the other hand, this approach enables us to derive analytical or semi-analytical solutions for FGMs with arbitrarily varying material properties, so we are not limited by exponential or power-law distributions as usual (see [3], [4], etc.). Moreover, wave propagation in media combining FGMs and thin layers can be investigated by using this approach, as well. This field of elastodynamics is of considerable interest and is related to the design of armours (see [5], [6]).

In the following, a strip infinite in the horizontal direction x and having a constant thickness and the height d will be assumed. Further, the strip material properties will change gradually in the vertical direction y according to an arbitrary function. The upper boundary of the strip is locally subjected to a dynamic load of impact character acting in the vertical direction y . The amplitude of this load will be constant through the strip thickness and it is described by an even function in the x direction. Thus a vertically symmetric plane stress problem is solved on a domain $\langle 0, +\infty \rangle \times \langle -d/2, d/2 \rangle$. Different boundary conditions at the bottom edge will be considered in this study, namely the problem for free, fixed and non-reflecting bottom boundary will be solved. As mentioned previously, the transient response of the strip will be investigated by using semi-analytical solution for a multilayered strip. In particular, the solution for the transient problem of a strip made of viscoelastic orthotropic layers presented in [7] was generalised and used for this purpose.

To demonstrate the results of our semi-analytical solution, the total velocity field in 100 mm long part of one half of the strip with $d = 40$ mm and with fixed bottom boundary is depicted at time $t \doteq 15.3 \mu\text{s}$ in Fig. 1. It is the transient response to the pressure pulse $\sigma(x, t) = \sigma_0 \cos\left(\frac{\pi x}{2h}\right) [H(t) - H(t - t_0)]$ lasting $t_0 = 2 \mu\text{s}$ and acting on the upper boundary on the small area of the length $2h = 4$ mm and having the amplitude $\sigma_0 = 1$ MPa. The material properties of the strip are fictitious in this study case. We assumed that the properties change according to parabolic distribution from elastic steel with $E = 2.1 \times 10^{11}$ Pa, $\rho = 7800$ kg/m³ and $\nu = 0.3$ at the top and at the bottom of the strip to viscoelastic properties of polyamide in the middle. It means that the relatively soft core of the strip is continuously stiffened by metal boundaries. The viscoelastic behaviour of the core is modelled using the standard linear viscoelastic solid as in [7] and the specific values of material parameters were taken from the work [8]. To approximate FGM, the strip was divided to 50 layers of same heights.

It is obvious from Fig. 1 that due to the continuous variation of material properties in the y direction, no wave reflections inside the strip occur. The velocities of P- and S-waves change continuously which

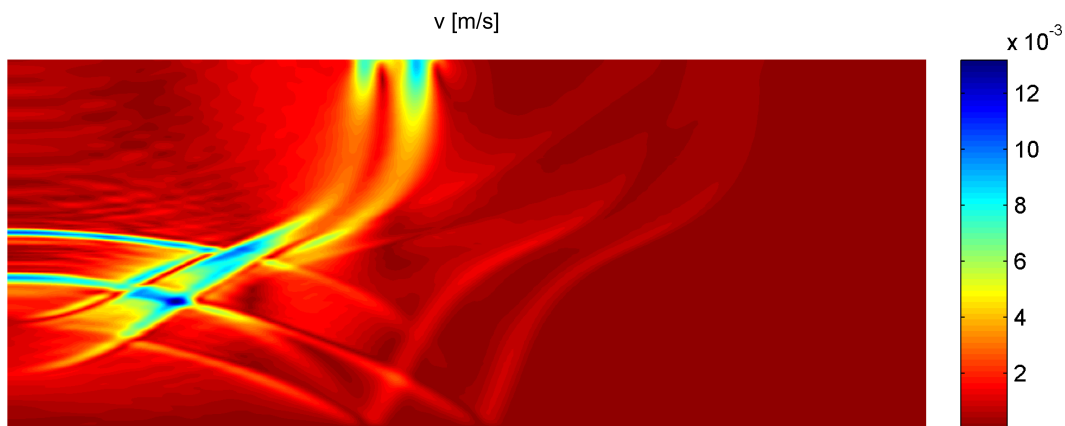


Figure 1: The distribution of the total velocity v at $t \doteq 15.3 \mu\text{s}$ in one half of the strip.

results in smooth distortion of all wave fronts. The dissipative effects of the viscous core are practically negligible due to the Fourier spectrum of applied load and relatively long relaxation time (see [8]). Further, the gradient of the material variation significantly influences the attenuation of R-waves with depth.

The presented solution can be used for detailed investigation and analysis of waves propagated in strip-like solids made of arbitrary FGM having elastic, viscoelastic and also orthotropic properties. Such results can then be used for optimal design of energy-absorbing FGM for many practical applications.

Acknowledgement

This publication was supported by the project LO1506 of the Czech Ministry of Education, Youth and Sports under the program NPU I and by the project GA CR 17-22615S.

References

- [1] H.A. Bruck. A one-dimensional model for designing functionally graded materials to manage stress waves. *International Journal of Solids and Structures*, **37**: 6383–6395, 2000.
- [2] A. Berezovski, J. Engelbrecht, G.A. Maugin. Numerical simulation of two-dimensional wave propagation in functionally graded materials. *European Journal of Mechanics A/Solids*, **22**: 257–265, 2003.
- [3] S. Qiao, X. Shang, E. Pan. Characteristics of elastic waves in FGM spherical shells, an analytical solution. *Wave Motion*, **62**: 114–128, 2016.
- [4] M. Dorduncu, M.K. Apalak, H.P. Cherukuri. Elastic wave propagation in functionally graded circular cylinders. *Composites: Part B*, **73**: 35–48, 2015.
- [5] Y. Wang, F. Wang, X. Yu, Z. Ma, J. Gao, X. Kang. Effect of interlayer on stress wave propagation in CMC/RHA multi-layered structure. *Composites Science and Technology*, **70**: 1669–1673, 2010.
- [6] A. Tasdemirci, G. Tunusoglu, M. Güden. The effect of the interlayer on the ballistic performance of ceramic/composite armors: Experimental and numerical study. *International Journal of Impact Engineering*, **44**: 1–9, 2012.
- [7] V. Adámek, F. Valeš, J. Červ. Propagation of non-stationary waves in viscoelastic strip composed of orthotropic layers. *Proceedings of the 6th International Conference on Computational Methods in Structural Dynamics and Earthquake Engineering*, National Technical University of Athens, Greece, 1322–1329, 2017.
- [8] V. Adámek, F. Valeš. Analytical solution of transient in-plane vibration of a thin viscoelastic disc and its multi-precision evaluation. *Mathematics and Computers in Simulation*, **85**: 34–44, 2012.

STOMATAL MICRO-TO-MACRO MECHANICS: THE ROLE OF MECHANICAL ANISOTROPY ON BIO-MECHANICAL FUNCTION

Benny Bar-On^{1,*}

¹Department of Mechanical Engineering, Ben-Gurion University of the Negev,
Beer-Sheva 8410501, Israel; e-mail: bbo@bgu.ac.il

Keywords: Stomata mechanics, Bio-composite, Finite-Elements modeling

Stomata are pores on the leaf surface, which are formed by a pair of mechanically anisotropic, curved, tubular guard cells. An increase in turgor pressure deforms the guard cells, resulting in the opening of the stomata. Recent studies employed numerical simulations, based on experimental data, to analyze the effects of various structural, chemical, and mechanical features of the guard cells on the stomatal opening characteristics; these studies all support the well-known qualitative observation that the mechanical anisotropy of the guard cells plays a critical role in stomatal opening. In this talk, I will introduce a computationally based analytical model that quantitatively establishes the relations between the degree of anisotropy of the guard cell, the bio-composite constituents of the cell wall, and the aperture and area of stomatal opening. The model introduces two non-dimensional key parameters that dominate the guard cell deformations - the inflation driving force and the anisotropy ratio - and it serves as a generic framework that is not limited to specific plant species.

Generally, the applied internal pressure (P) generates the stomatal deformations needed for pore opening while the cell wall stiffness - dominated by the two Young's moduli E_{Θ} and E_L - resists such deformations. The model could thus benefit from the introduction of another parameter, the normalized pressure, \hat{P} , a non-dimensional pressure parameter that reflects the effective *driving force* of stomatal deformations:

$$\hat{P} = \frac{P}{E_L} \approx P \cdot \frac{1 - \phi}{E_m} \quad (1)$$

where ϕ indicates the volume fraction of the micro-fibrils composing the cell wall and E_m represents the Young's modulus of the bio-polymeric matrix material that binds the micro-fibrils. Another key parameter with a marked effect on stomatal deformation is the degree of stiffness anisotropy of the cell wall. This characteristic is introduced by a non-dimensional *anisotropy* parameter - the modulus ratio, \hat{E} :

$$\hat{E} = \frac{E_{\Theta}}{E_L} \approx E_f \cdot \phi \cdot \frac{1 - \phi}{E_m} \quad (2)$$

where E_f represents the Young's modulus of the micro-fibrils. A series of FE simulations were conducted to identify the effect of the above parameters on the stomatal opening characteristics, namely, the stomatal aperture and opening area, which were found to be linearly correlated one another via approximated geometrical relations. Based on the FE simulations results, the following closed-form analytical model was introduced to the stomatal aperture (normalized by the pore length).

$$\hat{\delta}(\hat{P}, \hat{E}) = C \cdot f(\hat{E}) \cdot \hat{P}, \quad f(\hat{E}) = 1 - \exp\left(-\left(\frac{\hat{E} - b}{\lambda}\right)^k\right) \quad (3)$$

According to the FE-based analytical model, despite the substantial non-linear deformations of the guard cell upon inflation, the stomatal aperture is identified to be linearly related to driving force \hat{P} and thus to the internal turgor pressure. The stomatal compliance is dependent on the non-dimensional mechanical anisotropy \hat{E} ; when a threshold \hat{E}^{\bullet} is crossed - the compliance reaches maximal asymptotic value. From a material-level perspective, the cellulose microfibrils constitute the stiff, load-bearing portion of the stomatal cell wall, while soft matrix is essential to the ability of stomata to open. Thus,

a stiffer matrix will generate a small opening and will promote swelling deformation mode. These findings may indicate a biomechanical role for differences in stomatal cell wall composition across different plant species.

The predictions of the proposed theoretical modeling are in line with a wide range of previous experimental studies, and its analytical formulation sheds new light on the relations between the structure, mechanics, and function of stomata. Moreover, the model provides an analytical tool to back-calculate the elastic characteristics of the matrix that composes the guard cell walls, which, to the best of our knowledge, cannot be probed by direct nano-mechanical experiments. Indeed, the estimations of the proposed model are in good agreement with recently published results of independent numerical optimization schemes. The emerging insights from the stomatal structure-mechanics "design guidelines" may promote the development of miniature, yet complex, multiscale composite actuation mechanisms for future engineering platforms.

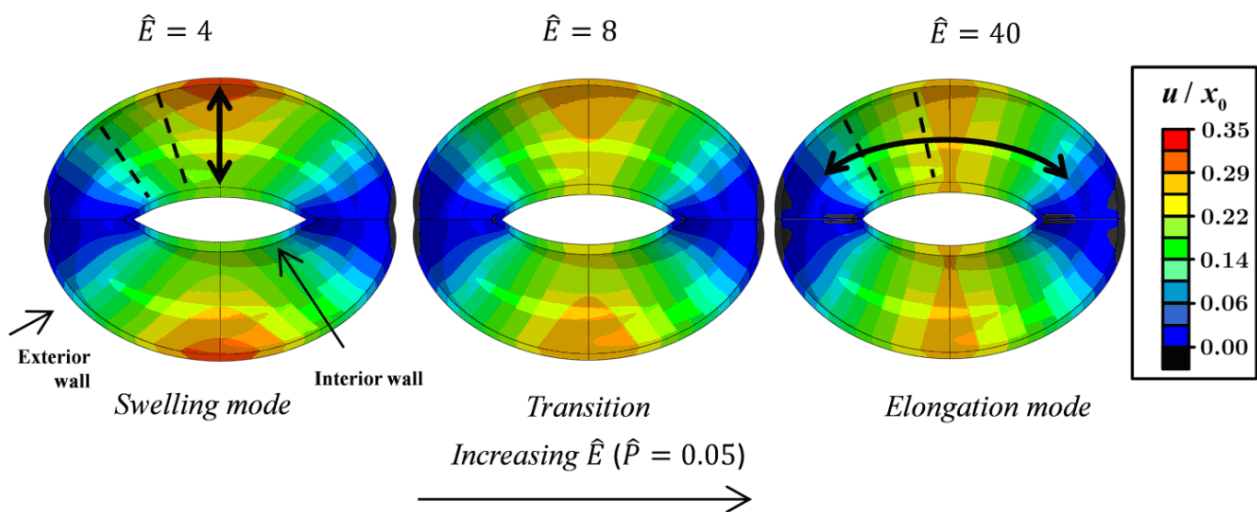


Figure 1: Displacement maps of stomatal opening for increasing \hat{E} values - showing the swelling, transition and elongation modes. Selected guard cell cross sections are illustrated by dashed lines.

Acknowledgement

This research was supported by the ISRAEL SCIENCE FOUNDATION (grant No. 1429/16).

References

- [1] Z. Marom, I. Shtein, B. Bar-On. Stomatal opening: the role of cell-wall mechanical anisotropy and its analytical relations to the bio-composite characteristics. *Frontiers in plant science*, **8**, 2017.
- [2] I. Shtein, Y. Shelef, Z. Marom, E. Zelinger, A. Schwartz, Z. Popper, B. Bar-On, S. Harpaz-Saad. Stomatal cell wall composition: distinctive structural patterns associated with different phylogenetic groups. *Annals of botany*, **119**(6): 1021–1033, 2017.

THE HALF-SPACE MATCHING METHOD FOR LAMB WAVE SCATTERING IN ANISOTROPIC PLATES

Vahan Baronian¹, Anne-Sophie Bonnet-Ben Dhia², Sonia Fliss³ and Yohanes Tjandrawidjaja^{4,*}

¹CEA-LIST, Saclay, France; e-mail: vahan.baronian@cea.fr

²POEMS (CNRS-INRIA-ENSTA), Palaiseau, France; e-mail: anne-sophie.bonnet-bendhia@ensta-paristech.fr

³POEMS (CNRS-INRIA-ENSTA), Palaiseau, France; e-mail: sonia.fliss@ensta-paristech.fr

⁴CEA-LIST and POEMS, France; e-mail: yohanes.tjandrawidjaja@ensta-paristech.fr

Keywords: scattering, Lamb modes, Fourier-integral operators, finite elements

We would like to simulate the interaction of Lamb waves with a defect in an anisotropic elastic plate, in the framework of non-destructive testing. The strategy is to generalize the Half-Space Matching method that we have previously developed in the 2D case. In the present case, it consists in coupling a finite element representation of the solution around the defect with semi-analytic representations of the solution in 4 semi-infinite plates. The semi-analytic representations are obtained by combining a Fourier Transform with a modal decomposition on Lamb modes. Ensuring that all the representations of the solution match yields a system of equations which couples, via Fourier-integral operators, the FE representation in the bounded perturbed domain with the displacement and the normal stress of the solution on the infinite bands limiting the half-plates. Compared to integral methods, this method avoids the expensive calculation of the Green function of the anisotropic plate.

1 The half-space matching formulation

We are interested in solving the following time-harmonic elastodynamic problem: find \mathbf{u} such that

$$\begin{cases} \operatorname{div}(\sigma(\mathbf{u})) + \rho\omega^2\mathbf{u} = \mathbf{f} & \text{in } \Omega, \\ \sigma(\mathbf{u})\nu = 0 & \text{on } z = \pm h \text{ and } \partial\mathcal{O}, \end{cases} \quad (1)$$

where $\Omega = \mathbb{R}^2 \times [-h, h] \setminus \mathcal{O}$ represents an elastic plate, \mathcal{O} represents a set of bounded defects in the plate, $\operatorname{supp}(f)$ is bounded.

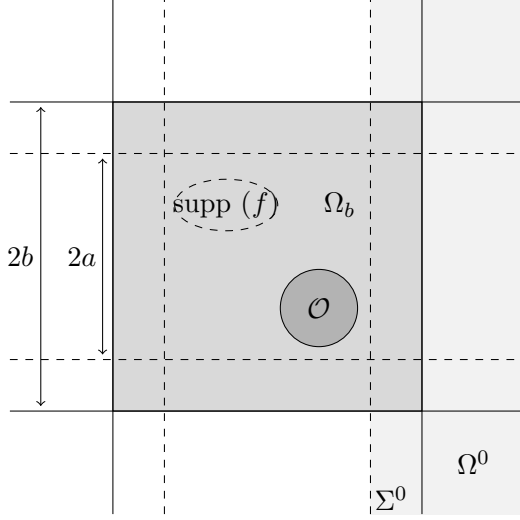
The idea of this method has been introduced in [1, 2] in the 2D case. To apply it to the 3D problem (1), we decompose the domain into 5 overlapping sub-domains: a bounded domain $\Omega_b = [-b, b]^2 \times [-h, h]$, where all perturbations (defects, source terms, inhomogeneities) are located, and 4 homogeneous semi-infinite half-plates $\Omega^j, j \in \{0, 1, 2, 3\}$:

$$\Omega^0 = \Omega \cap \{x \geq a\}, \quad \Omega^1 = \Omega \cap \{y \geq a\}, \quad \Omega^2 = \Omega \cap \{x \leq -a\}, \quad \Omega^3 = \Omega \cap \{y \leq -a\},$$

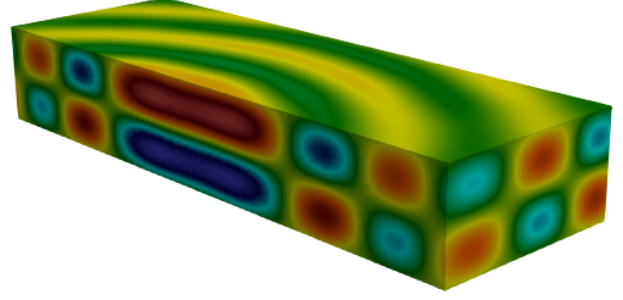
with $a < b$ (see Figure 1 for top view). Their artificial boundaries are denoted as

$$\Sigma^0 = \Omega \cap \{x = a\}, \quad \Sigma^1 = \Omega \cap \{y = a\}, \quad \Sigma^2 = \Omega \cap \{x = -a\}, \quad \Sigma^3 = \Omega \cap \{y = -a\}.$$

We can derive an explicit representation of $\mathbf{u}^j := \mathbf{u}$ in Ω^j with only the knowledge of the displacement and the normal stress tensor on Σ^j (see next section). To ensure the compatibility of the half-plate representations in the zones where they coexist, we write integral equations linking the unknowns on the bands Σ^j . Coupled with the finite element representation of \mathbf{u}_b , the restriction of \mathbf{u} in the bounded domain Ω_b , we obtain a system of equations with 1 volume unknown \mathbf{u}_b and 8 surface unknowns: 4 displacement tensors φ^j and 4 normal stress tensors ψ^j . After solving the system of equations, we can reconstruct the field \mathbf{u}^j in each half-plate Ω^j using φ^j and ψ^j , hence we have the solution in the whole domain Ω .



1. Domain decomposition: top view.

2. Real part of the first component of \mathbf{u}^0 in Ω_a^0 with only one excited Lamb mode.

2 The half-space representation

The main technical difficulty compared to the 2D case lies in the derivation of the half-plate representations \mathbf{u}^j . Consider for example the half-plate Ω^0 and suppose that we know the displacement and normal stress tensors on Σ^0 :

$$\mathbf{u}^0 = \boldsymbol{\varphi}^0 \text{ and } \sigma(\mathbf{u}^0)\nu = \boldsymbol{\psi}^0 \text{ on } \Sigma^0. \quad (2)$$

By applying the Fourier transform in the infinite direction, we get a family of equations for each Fourier variable ξ set in a semi-infinite strip $[-h, h] \times [a, +\infty)$.

We are looking for a solution expanded on outgoing modes:

$$\hat{\mathbf{u}}^0(x, \xi, z) = \sum_{n \in \mathbb{N}} a_n^0 \mathcal{U}_n^+(\xi, z) e^{i\beta_n^\xi(x-a)}, \quad (3)$$

where $(\mathcal{U}_n^+(\xi, z), \beta_n^\xi)$ are the modes. The amplitudes a_n^0 can be obtained by using the bi-orthogonality relation of the modes at $x = a$:

$$a_n^0 = \frac{1}{J_n^0} \int_{-h}^h \boldsymbol{\varphi}^0 \cdot \mathcal{T}_n^- - \mathcal{U}_n^- \cdot \boldsymbol{\psi}^0 \text{ where } J_n^0 = \int_{-h}^h \mathcal{U}_n^+ \cdot \mathcal{T}_n^- - \mathcal{U}_n^- \cdot \mathcal{T}_n^+, \quad (4)$$

where $\mathcal{T}(\xi, z)$ denotes the modal normal stress associated to the mode $(\mathcal{U}_n(\xi, z), \beta_n^\xi)$.

Using the inverse Fourier transform, we have an explicit formulation for each half-plate. This has been implemented in the isotropic case (see Figure 2), where we can use $\mathcal{U}_n^+(0, z)$ to obtain $\mathcal{U}_n^+(\xi, z)$, $\forall \xi \in \mathbb{R}$ by a simple rotation formula.

References

- [1] A-S. Bonnet-Ben Dhia, S. Fliss, A. Tonnoir. The Halfspace Matching method: a new method to solve scattering problem in infinite media. *JCAM*, vol. 338, 2018.
- [2] A. Tonnoir. Transparent conditions for the diffraction of elastic waves in anisotropic media. *Ecole Polytechnique, Ph.D. thesis*, 2015.

NONLINEAR WAVES IN SOLIDS: VISCOELASTICITY, SOFTENING, AND FINITE-VOLUME METHODS

Harold Berjamin¹, Bruno Lombard^{1,*}, Guillaume Chiavassa² and Nicolas Favrie³

¹Aix Marseille Univ, CNRS, Centrale Marseille, LMA, Marseille, France

²Centrale Marseille, CNRS, Aix Marseille Univ, M2P2 UMR 7340, 13451 Marseille Cedex 20, France

³Aix Marseille Univ, UMR CNRS 7343, IUSTI, Polytech Marseille, 13453 Marseille Cedex 13, France

Keywords: Continuum mechanics, Numerical methods, Nonlinear resonance

Rocks and concrete are known to soften under a dynamic loading, i.e. the speed of sound diminishes with forcing amplitudes. This softening occurs over a time scale larger than the period of the dynamic loading, which highlights the phenomenon of *slow dynamics*. Moreover, a hysteresis curve is obtained when the speed of sound is represented with respect to the strain. All these phenomena are accentuated when the forcing amplitude is increased [1].

In recent works, the authors have proposed a 3D model in the framework of continuum mechanics with internal variables [2]. A variable g is introduced in order to modify the elastic moduli of a nonlinear elastic solid. Also, an evolution equation for g is provided. By construction, the model is thermodynamically admissible and dissipative. Contrary to models of isotropic damage, the variable g may increase (softening) or decrease (recovery).

The resulting set of equations writes as a hyperbolic system of conservation laws with relaxation terms, which is solved numerically using finite-volume methods. In one space dimension, the numerical method is validated using analytical solutions [3]. Nonlinear viscoelasticity of Zener type is accounted for by using additional internal variables [4]. The numerical tool is used to reproduce qualitatively resonance experiments (NRUS) and dynamic acousto-elastic testing (DAET), by implementing realistic boundary conditions. Wave propagation simulations are performed in 2D. In particular, one observes that P-waves and S-waves are not decoupled, which is a classical feature of nonlinear elastodynamics.

References

- [1] M. Lott, M. C. Remillieux, P.-Y. Le Bas, T. J. Ulrich, V. Garnier, C. Payan. From local to global measurements of nonclassical nonlinear elastic effects in geomaterials, *J. Acoust. Soc. Am.* **140**: EL231, 2016.
- [2] H. Berjamin, N. Favrie, B. Lombard, G. Chiavassa. Nonlinear waves in solids with slow dynamics: an internal-variable model, *Proc. R. Soc. A* **473**: 20170024, 2017.
- [3] H. Berjamin, B. Lombard, G. Chiavassa, N. Favrie. Analytical solution to 1D nonlinear elastodynamics with general constitutive laws, *Wave Motion* **74**: 35–55, 2017.
- [4] H. Berjamin, B. Lombard, G. Chiavassa, N. Favrie. Modeling longitudinal wave propagation in nonlinear viscoelastic solids with softening, *Int. J. Solids Struct.*, in press, 2018.

IDENTIFICATION OF HETEROGENEOUS ELASTIC MODULI USING A MODIFIED ERROR IN CONSTITUTIVE EQUATION FUNCTIONAL: THE CASE OF INTERIOR ELASTODYNAMIC DATA AND UNDERDETERMINED BOUNDARY CONDITIONS

Marc Bonnet^{1,*}, Wilkins Aquino²

¹POems (UMR 7231 CNRS-INRIA-ENSTA), ENSTA, Palaiseau, France; e-mail: mbonnet@ensta.fr

²Dept. of Civil and Env. Eng., Duke University, Durham, USA; e-mail: wilkins.aquino@duke.edu

Keywords: modified error in constitutive equation, elastodynamics, full waveform inversion, interior data

Background. This work is concerned with the reconstruction of heterogeneous elastic moduli (i.e. elasticity imaging) from experimental data on the elastodynamic response of the sample subjected to time-harmonic excitations. This classical kind of inverse problem has applications in e.g. geophysics (in which context it is often called “full waveform inversion”, see e.g. [8]) or medicine (with application to elastography, see e.g. [9]). Our investigation, while set in the common general framework of PDE-constrained optimization, departs from the conventional use of output least-squares (OLS) objective functionals. Instead, our inversion approach is based on the minimization of a modified error in constitutive equation (MECE) functional. MECE functionals additively combine an energy-based error on the constitutive equation and an output least-squares functional that incorporates the measured data, the relative weights of the two components being tunable by means of an adjustable parameter ξ (that can be interpreted as the reciprocal of a regularization parameter typically associated with Tikhonov regularization). They are widely used for constitutive parameter identification and FE model updating since over two decades, see e.g. [2, 5, 7]. Solving constitutive identification problems using this framework entails minimizing MECE functionals with respect to three variables, namely a kinematically admissible displacement field, a dynamically admissible stress field, and the sought spatially-dependent elasticity tensor. This minimization process is often treated in alternate-direction fashion, where each step consists in solving a linear coupled two-field stationarity problem yielding optimal admissible fields for given moduli (partial minimization with frozen moduli) and then performing a constitutive update (partial minimization with frozen admissible fields). The weighting parameter ξ can be adjusted using Morozov’s discrepancy principle (MDP), whereby $\xi \rightarrow \infty$ in the ideal case of perfect (i.e. noiseless) data with our conventions.

MECE functionals applied to interior data and underspecified boundary conditions. We have been investigating the formulation and application of MECE-based methods to the reconstruction of spatially-varying elastic or viscoelastic moduli, under time-harmonic [1, 4] or transient conditions [3] over the last few years, with preliminary applications to elastography presented in [6]. This communication addresses the application of MECE-based formulations to elasticity imaging by means of interior kinematical data obtained under time-harmonic conditions and over a region of interest (RoI) that can be a subset of the sample being tested, while boundary conditions (BCs) may be underspecified due to insufficient relevant experimental data (e.g. if the computational domain is to be limited to the RoI). The latter provision implies in particular that, contrary to most formulations of inverse problems, a forward problem cannot be clearly defined.

The main contribution we wish to present consists, for this class of imaging problems, in establishing useful mathematical properties of the MECE-based identification methodology:

- First, we prove that the coupled two-field problem that arises from the first-order optimality conditions associated with the partial minimization with frozen moduli is well-posed (in the functional-analytic sense) at any operating frequency, and even when available data is such

that BCs are underdetermined (subject, in this case, to a condition on the interior kinematic measurements ensuring that it is sufficiently abundant to compensate for insufficient BC data). The latter implies, importantly, that the lack of a well-defined forward problem is no impediment for undertaking the (alternate-direction) minimization of the MECE functional.

- Then, we also prove that the Hessian of the reduced MECE functional (considered as a function of the moduli only, through the moduli-dependent stationarity solution) is positive in the $\xi \rightarrow \infty$ limit, thereby providing mathematical insight to abundant available computational evidence showing reduced MECE functionals to be “more convex” than OLS functionals. The reduced MECE functional is therefore better behaved than OLS functionals (for which no such convexity result is available), allowing for faster convergence and avoidance of unwanted local minima.

These properties will be given precise statements, and their proof sketched. They make MECE-based imaging a quite attractive tool for applications in e.g. elastography (as done in [6]), as it can be applied on a computational domain reduced to the RoI and is insensitive to eigenfrequencies.

In addition, the above main theoretical results will be demonstrated on numerical experiments, whose results will be shown and discussed. Those experiments will in particular highlight the well-posedness of the stationarity problem at all frequencies and the asymptotic convexity of the reduced MECE Hessian. Results on a full elasticity imaging example will also be presented, including automatic adjustment of the weighting parameter ξ by means of MDP.

References

- [1] Banerjee, B., Walsh, T. F., Aquino, W., Bonnet, M. Large scale parameter estimation problems in frequency-domain elastodynamics using an error in constitutive equation functional. *Comp. Meth. Appl. Mech. Eng.*, **253**:60–72 (2013).
- [2] Barthe, D., Deraemaeker, A., Ladevèze, P., Le Loch, S. Validation and updating of industrial models based on the constitutive relation error. *AIAA Journal*, **42**:1427–1434 (2004).
- [3] Bonnet, M., Aquino, W. Three-dimensional transient elastodynamic inversion using an error in constitutive relation functional. *Inverse Probl.*, **31**:035010 (2015).
- [4] Diaz, M., Aquino, W., Bonnet, M. A modified error in constitutive equation approach for frequency-domain viscoelasticity imaging using interior data. *Comp. Meth. Appl. Mech. Eng.*, **296**:129–149 (2015).
- [5] Feissel, P., Allix, O. Modified constitutive relation error identification strategy for transient dynamics with corrupted data: the elastic case. *Comp. Meth. Appl. Mech. Eng.*, **196**:1968–1983 (2007).
- [6] Ghosh, S., Zou, Z., Babaniyi, O., Aquino, W., Diaz, M. I., Bayat, M., Fatemi, M. Modified error in constitutive equations (MECE) approach for ultrasound elastography. *J. Acoust. Soc. Am.*, **142** (2017).
- [7] Ladevèze, P., Nedjar, D., Reynier, M. Updating of finite element models using vibration tests. *AIAA Journal*, **32**:1485–1491 (1994).
- [8] Métivier, L., Brossier, R., Virieux, J., Operto, S. Full waveform inversion and the truncated Newton method. *SIAM J. Sci. Comput.*, **35**:B401–B437 (2013).
- [9] Park, E., Maniatty, A. M. Shear modulus reconstruction in dynamic elastography: time harmonic case. *Phys. Med. Biol.*, **51**:3697–3721 (2006).

ANISOTROPIC HIGH-ORDER ADAPTIVE BOUNDARY ELEMENT METHODS FOR 3D ACOUSTICS

Stéphanie Chaillat^{1,*}, Faisal Amlani¹ and Adrien Loseille²

¹POEMS, CNRS-ENSTA-INRIA, Palaiseau, France; e-mail: chaillat@ensta.fr, amlani@ensta.fr

²Project Team Gamma3, INRIA Paris-Saclay, Palaiseau, France; e-mail: adrien.loseille@inria.fr

Keywords: accelerated boundary element methods, anisotropic mesh adaptation, high-order methods

1 Context

The main advantage of the Boundary Element Methods (BEMs) is that only the domain boundaries (and possibly interfaces) are discretized leading to a drastic reduction of the total number of degrees of freedom. In addition, they are well suited to problems in large-scale or infinite domains since they exactly account for radiation conditions at infinity. In traditional BE implementation the dimensional advantage with respect to domain discretization methods is offset by the fully-populated nature of the BEM coefficient matrix, with set-up and solution times rapidly increasing with the problem size.

Mesh adaptation is a technique to reduce the computational cost of a numerical method. The principle is to optimize the positioning of a given number of degrees of freedom on the geometry of the obstacle, in order to yield simulations with superior accuracy compared to those obtained via the use of uniform meshes. For wave scattering problems, adaptation is particularly important for obstacles that contain geometric singularities, i.e., edges and vertices, which lead to a rapid variation of the surface solution near these singularities. In addition, we may exploit the directionality of the waves in order to further reduce the number of degrees of freedom. The best strategy to achieve these goals is via so-called "anisotropic" mesh adaptation for which an extensive literature exists for volume-based methods [1]. However, there is relatively little research attention being paid to mesh adaptation in a boundary element context. One possible explanation is the large computational cost of standard BEMs. With the development of fast BEMs such as the Fast Multipole accelerated BEM (FM-BEM) [3] or H-matrix accelerated BEM (H-BEM) [5], the capabilities of the BEMs are greatly improved such that efficient adaptive mesh strategies are needed not only to optimize further the computational cost, but also to certify the numerical results by assessing that the theoretical convergence order is observed during the computations. Most current BEM adaptivity methods, like those relying on Dörfler marking, have been confined to isotropic techniques. In addition, most works are restricted to Galerkin discretizations and are formulated specifically for a system of equations [2].

2 Methodology

The first novelty of the present work is the extension of metric-based anisotropic mesh adaptation (AMA) to the collocation BEM where it has never been used. The metric-based AMA proposed in [6] does not employ a Dörfler marking strategy but rather generates a sequence of non-nested meshes with a specified complexity. The different meshes are defined according to a metric field derived from the evaluation of the linear interpolation error of the (unknown) exact solution on the current mesh. From a theoretical point of view, a continuous metric is derived from the Hessian of the exact solution. From a practical point of view, an approximate metric is derived from the numerical solution only. In AMA, the size, shape, and orientation of elements are adjusted simultaneously. The advantages of this approach are that it is ideally suited to solutions with anisotropic features, it is independent of the underlying PDE and discretization technique (collocation, Galerkin, etc.), and it is inexpensive. The second novelty of this work is the combination of two acceleration techniques, namely metric-based anisotropic mesh adaptivity and Fast Multipole acceleration. If no fast BEM is used, the capabilities of

anisotropic mesh techniques cannot be fully demonstrated for realistic large scale scattering scenarios. Since geometric representation, numerical implementation and discretisation strategy are a handful of factors that determine the effectiveness of BEMs for wave scattering problems, we also extend the methodology presented in [4] to high order BEMs. The main difficulties are: (i) to relate the interpolation error to the metric driving the adaptation and (ii) to define the optimal metric in the context of non-planar curved elements.

3 Numerical results illustrating the efficiency of the strategy

This original combination permits us to show the performance of AMA strategy for complex real-world scattering problems such as acoustic scattering. More precisely, we show via a variety of numerical examples that it allows to recover optimal convergence rates for \mathbb{P}_0 , \mathbb{P}_1 or \mathbb{P}_2 interpolation and for domains with geometric singularities: a planar screen, a sphere with aperture, a cube with cavity (Fig. 1a), and a F15 jet (Fig. 1b-c). These optimal convergence rates cannot be achieved when using uniform refinement since the rapid variation of the boundary solution near geometric singularities requires special meshing treatment.

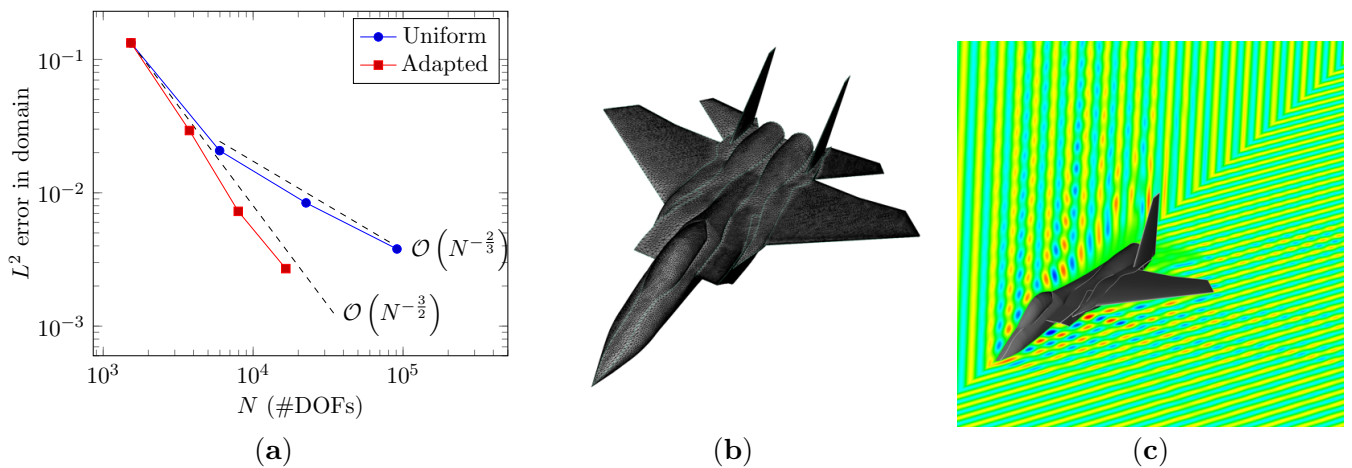


Figure 1: (a) Sound-soft cube with cavity: Relative L^2 errors for uniform and adapted meshes, $k = 10$; F15: (b) Mesh after AMA and (c) Real part of the total field in $x = 0$ and $z = 0$ planes.

References

- [1] M. Ainsworth and J. T. Oden. *A posteriori error estimation in finite element analysis*, John Wiley & Sons, 2011.
- [2] M. Bakry, S. Pernet, and F. Collino. A new accurate residual-based a posteriori error indicator for the BEM in 2D-acoustics. *Computers & Mathematics with Applications*, **73**: 2501–2514, 2017.
- [3] S. Chaillat, M. Bonnet and J.F. Semblat. A multi-level fast multipole BEM for 3-D elastodynamics in the frequency domain. *Comput. Methods Appl. Mech. Engrg.*, **197**: 4233–4249, 2008.
- [4] S. Chaillat, S. Groth and A. Loseille. Metric-based anisotropic mesh adaptation for 3D acoustic boundary element methods. *Under review*.
- [5] S. Chaillat, L. Desiderio and P. Ciarlet. Theory and implementation of \mathcal{H} -matrix based iterative and direct solvers for Helmholtz and elastodynamic oscillatory kernels. *J. Comput. Phys.*, **351**: 165–186, 2017.
- [6] A. Loseille and F. Alauzet. Continuous mesh framework part I: well-posed continuous interpolation error. *SIAM Journal on Numerical Analysis*, **49**: 38–60, 2011.

INFLUENCE OF CRUST HETEROGENEOUS PROPERTIES CLOSE TO A FAULT ON SEISMIC WAVE PROPAGATION

Martin Colvez^{1,*}, Régis Cottureau¹ and Fernando Lopez-Caballero¹

¹Laboratoire MSSMat, UMR CNRS 8579, CentraleSupélec, Université Paris-Saclay, France

* Corresponding author: martin.colvez@centralesupelec.fr

Keywords: wave propagation, heterogeneities, strong localization

In the close vicinity of seismic faults, the rock is densely fractured by both the tectonic movements and the seismic activity [1]. The objective of this presentation is to discuss the effect of this particular fractured structure on the elastic wave propagation at several distance from the source to some recording points .

For such problems, numerical approximation requires the use of large scale computational models. The Spectral Element Method is well-suited to compute huge dimensional problems with the possibility to obtain a good scaling of performance on thousands of computing cores.

As mentioned above, the model developed in this study includes heterogeneities close to seismic faults (some meters). In a first approximation, the network of fractures is modeled by stochastic fields of properties of the medium near the fault. In order to quantify the effect of inclusion of heterogeneities, the obtained response at some recording points is compared to the homogeneous one.

Some numerical issues appear with dealing wave propagation in strong heterogeneous medium. For instance, the stability of explicit scheme and the implementation of PMLs. Those particular points will be discussed in this work.

The results highlight the effects of strong localization of the wave propagation and the resulting multiple scattering next to the seismic source. A part of the energy spectrum stays trapped near to the seismic source. Consequently, the frequency content of the seismic signal is modified by the presence of heterogeneous fields near the fault and thus, the high frequencies have wider trend to be blocked than low frequencies.

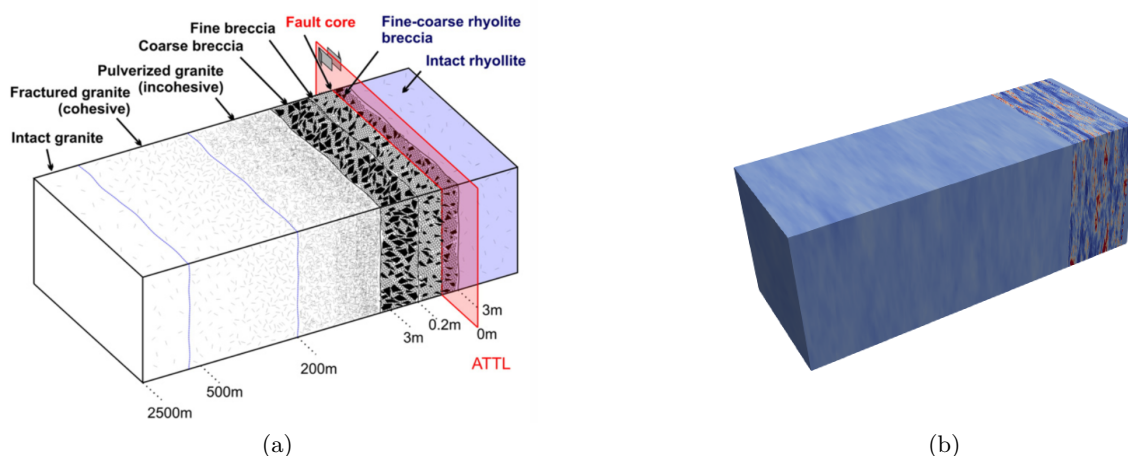


Figure 1: a) Schematic diagram of the strongly asymmetric damage structure on the ATTL [1] and b) An example of visualisation of stochastic field representing the fractured structure

References

- [1] Mitchell, TM and Ben-Zion, Y and Shimamoto, T *Pulverized fault rocks and damage asymmetry along the Arima-Takatsuki Tectonic Line, Japan*. Earth and Planetary Science Letters, Elsevier, 2011.

INFLUENCE OF MATERIAL HETEROGENEITY ON THE STABILITY OF EXPLICIT HIGH-ORDER SPECTRAL ELEMENT METHODS

Rgis Cottereau^{1,*} and Ruben Sevilla²

¹Laboratoire MSSMat, CNRS, CentraleSuplec, Université Paris-Saclay, France

²Zienkiewicz Centre for Computational Engineering, College of Engineering, Swansea University, UK

Keywords: spectral element method, explicit time integration, stability, heterogeneous media, high-order.

This talk [2] describes precisely the influence of material heterogeneity on the stability of explicit time marching schemes for the high-order spectral element discretization of wave propagation problems. Two different types of heterogeneity are considered. In a first part, it consists in a periodic fluctuation of the density and stiffness parameters, whose period is related to the characteristic element size of the mesh. A new stability criterion is derived analytically for quadratic and cubic one-dimensional spectral elements in heterogeneous materials, which may in some situations replace the current rule of thumb. The analysis presented reveals the origin of instabilities that are often observed when the stability limit derived for homogeneous materials [1] is adapted by simply changing the velocity of the wave to account for the material heterogeneity (see Fig. 1). In a second part, a more complete heterogeneity is considered and precise stability estimates are obtained based on Irons and Treharne theorem [3] and general eigenvalue bounds. Finally, in a third part, very simple estimates are obtained for rapidly fluctuating media. Several extensions of the results are discussed, including higher order approximations, higher dimensions and random media. Extensive numerical results demonstrate the validity of the new stability estimates.

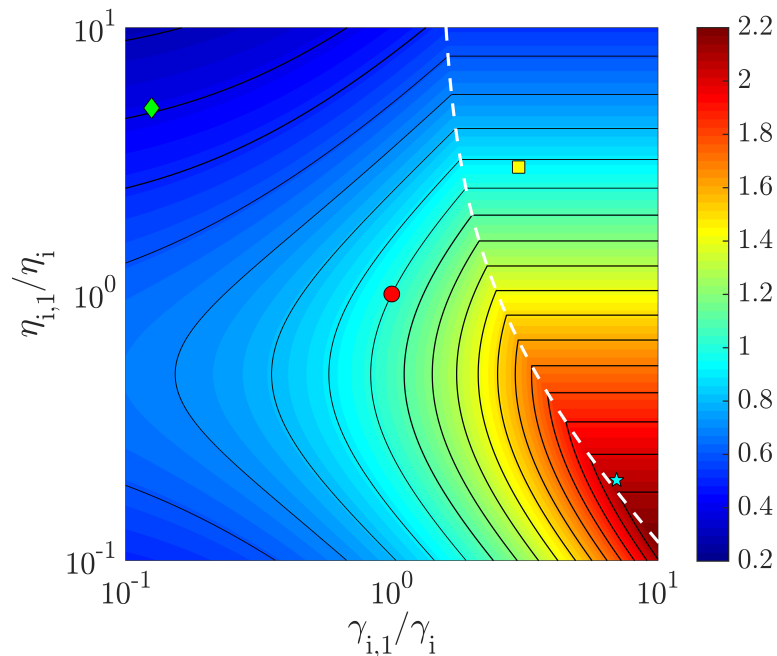


Figure 1: Ratio between the value of the critical time step for the heterogeneous and homogeneous cases for different values of the ratios of parameter values inside the element and on its vertices. The red dot indicates the homogeneous case and the white discontinuous line represents the change of definition of the critical time step given by the maximum in the two eigenvalues of the dispersion matrix.

References

- [1] G. Cohen. *Higher-order numerical methods for transient wave equations*. Scientific Computation. Springer, 2001.
- [2] R. Sevilla and R. Cottureau. Influence of material heterogeneity on the stability of explicit high order spectral element methods. *J. Comput. Phys.*, 2017. Submitted for publication.
- [3] A. J. Wathen. An analysis of some element-by-element techniques. *Comp. Meths. Appl. Mech. Engr.*, 74:271–287, 1989.

WAVE ENSEMBLES IN COMPLEX MEDIA

Jüri Engelbrecht*, Arkadi Berezovski, Tanel Peets and Kert Tamm

Department of Cybernetics, School of Science, Tallinn University of Technology
e-mails: je@ioc.ee, berez@ioc.ee, tanelp@ioc.ee and kert@ioc.ee

Keywords: ensemble of waves, microstructured materials, biomembranes

Interdisciplinary studies into the complexity of wave processes in continua take into account the various types of interactions: wave-wave, wave-field, wave-internal structure, and others [1]. Often the interactions can be nonlinear. For example, in classical theory the longitudinal and transverse waves are uncoupled but in a nonlinear medium a separate transverse wave cannot exist [2]. The resulting observable behaviour of waves depends on interactions and is governed by thermodynamic constraints. As a result, a wave process may involve an ensemble of waves: a set of coupled waves propagating together as a whole.

In what follows, two typical cases of the emergence of wave ensembles are presented: (i) the propagation of waves in a microstructured thermoelastic material; (ii) the propagation of signals in nerve fibres. In both cases the emergent ensemble involves several waves that can be generated by one input. The emergence is dependent on the coupling forces.

(i) Waves in microstructured thermoelastic materials. The dynamical processes in microstructured materials are characterized by variables at macro- and microlevels. In case of a thermoelastic solid, one has to distinguish (in 1D setting) between longitudinal macro-displacement u together with the macro-temperature Θ and micro-deformation α together with the micro-temperature φ . The latter variables can be treated as internal variables and they describe the changes in the embedded microstructure. The microtemperature means actually the fluctuations of temperature due to the different properties of macro- and microstructure. By using the concept of internal variables [3], the governing equations are described in the following form [4]:

$$\rho_0 u_{tt} = (\lambda + 2\mu)u_{xx} + m\Theta_x + A\alpha_x + M\varphi_{xx}, \quad (1)$$

$$\rho_0 c_p \Theta_t = (k\Theta_x)_x + m\Theta_0 u_{xt} + Q\varphi_t^2, \quad (2)$$

$$I\alpha_{tt} = C\alpha_{xx} - Au_x - B\alpha, \quad (3)$$

$$I_0\varphi_{tt} + Q\varphi_t = N\varphi_{xx} + Mu_{xx}. \quad (4)$$

Here the constants are specified following the physical considerations [4] and indices here and further indicate differentiation. System (1)-(4) contains three hyperbolic equations (Eqs (1), (3), (4)) and one parabolic equation (Eq. (2)) for macro-temperature. The processes at the micro-level are coupled with the longitudinal wave u at the macro-level. When the longitudinal wave u is generated, then an ensemble of waves emerges. The notable effect is that the heat conduction at the macro-level (Eq. (2)) is affected by the micro-temperature φ and this coupling can induce the wave-like propagation of the macro-temperature contrary to the uncoupled case of the diffusion-type process.

(ii) The signals in nerve fibres. Apart from the analysis of the action potential (AP) as the main carrier of information along nerve fibres, the recent studies have shown also the existence of accompanying waves in the axoplasm and in the surrounding biomembrane [5]. These waves are of the mechanical character. A robust mathematical model for describing all coupled waves is recently proposed [6]. In the first approximation the AP is described by the FitzHugh-Nagumo model

$$z_t = z(z - (a_1 + b_1))(1 - z) - j + Dz_{xx}, \quad (5)$$

$$j_t = \varepsilon(-j + (a_2 + b_2)z). \quad (6)$$

The pressure wave in the axoplasm is governed by the 1D Navier-Stokes model

$$\rho(v_t + vv_x) + \bar{p}_x - \mu_\nu v_{xx} = F_1(z). \quad (7)$$

The longitudinal wave in the surrounding biomembrane is described by a Boussinesq-type model [6] involving the displacement-type nonlinearity due to the lipid structure of the biomembrane

$$u_{tt} = [(c_0^2 + pu + qu^2)u_x] - h_1 u_{xxxx} + h_2 u_{xxtt} + F_2(z, v). \quad (8)$$

Equation (8), contrary to the model proposed in [5], takes also the inertia of the lipid structure into account. The possible transverse (observable) displacement can be easily calculated like in the rods

$$w = -kru_x. \quad (9)$$

Above the AP is denoted by z , the velocity of a wave in the axoplasm by v , and the longitudinal displacement in the biomembrane by u while j denotes the ion current; \bar{p} is the pressure and ρ is density of the axoplasm. The constants are defined from physical considerations [6]. If the AP is generated by an input above the threshold then an ensemble of waves emerges. The nonlinearities and coupling forces play a crucial role in all the process. Here further experimental studies could specify the details. The remarkable property of such an emerging ensemble is the adjustment of velocities dictated by the velocity of the AP.

In conclusion, the ensembles of waves demonstrate the properties which are not summed up from properties of single waves – a clear evidence of complexity. This is a characteristic to many dynamical processes in solids, fluids and tissues.

Acknowledgement

This research was supported by the European Union through the European Regional Development Fund (Estonian Programme TK 124) and by the Estonian Research Council (projects IUT 33-24, PUT 434).

References

- [1] J. Engelbrecht. Complexity in engineering and natural sciences. *Proceedings of the Estonian Academy of Sciences*, **64(3)**: 249–255, 2015.
- [2] D.R. Bland. *Nonlinear Dynamic Elasticity*. Blaisdell, 1969.
- [3] P. Ván, A. Berezovski, J. Engelbrecht. Internal variables and dynamic degrees of freedom. *Journal of Non-Equilibrium Thermodynamics*, **33**: 235–254, 2008.
- [4] A. Berezovski, J. Engelbrecht, P. Ván. Weakly nonlocal thermoelasticity for microstructured solids: microdeformation and microtemperature. *Archive of Applied Mechanics*, **84(9-11)**: 1249–1261, 2014.
- [5] S.S.L. Andersen, A.D. Jackson, T. Heimburg. Towards a thermodynamic theory of nerve pulse propagation. *Progress in neurobiology*, **88(2)**: 104–13, 2009.
- [6] J. Engelbrecht, T. Peets, K. Tamm, M. Laasmaa, M. Vendelin. On complexity of signal propagation in nerve fibres. *Proceedings of the Estonian Academy of Sciences*, 2018, in press.

DIRECT IMPACT HOPKINSON BAR: APPLICATION ON 3D PRINTED AUXETIC LATTICES AND OTHER CELLULAR STRUCTURES

Tomáš Fíla^{1,*}, Petr Zlámal¹, Jan Falta¹ and Marcel Adorna¹

¹Czech Technical University in Prague, Faculty of Transportation Sciences,
Konviktská 20, Prague, Czech Republic; e-mail: fila@fd.cvut.cz

Keywords: Direct Impact Hopkinson Bar, impact testing, auxetic lattices, cellular materials

Modern manufacturing technologies like additive manufacturing, 3D printing and foaming of metals allow for production of an advanced cellular materials with structure optimized for energy absorption applications. Moreover, the production methods allow for manufacture of a functional graded structures with properties optimized for the desired application. Numerical simulations are used as a tool for the optimization of the structures. Relevant material models reliably representing the behavior of the materials at a given rate of impact have to be used in the simulations. Experimental analysis is commonly used for the estimation of the material model parameters.

Recently, a number of papers concerning high rate impact testing of auxetic materials and metal foams using Split-Hopkinson Pressure Bar (SHPB) were published, e. g. [1, 2, 3]. SHPB is a well established experimental technique for characterization of materials at high strain-rates. However, testing of materials designed for energy absorption requires compression to high strains at constant strain-rates. In this field, standard SHPB has several significant limitations: i) maximum strain in the specimen is proportional to length of the striker bar and its impact velocity, ii) strain-rate is proportional to the striker bar impact velocity, iii) dynamic equilibrium has to be achieved in the specimen and iv) dimensions of the specimen are strictly limited. Thus, testing of cellular structures in conventional SHPB requires setup with high performance, long striker bars and relatively small specimens. Impact compression at different strain-rates is also limited as achievable maximum strain decreases with decreasing striker impact velocity. These limitations can be reduced using an upgrades of the setup or by introduction of an advanced measurement methods.

In this contribution, an Open Hopkinson Pressure Bar (OHPB) apparatus [4] was used for high strain-rate compression of the additively manufactured auxetic lattices and selected cellular metals. The principle of OHPB is based on Direct Impact Hopkinson Bar (DIHB). Instead of striker bar, the incident bar is accelerated in the gas-gun and it hits directly the specimen mounted on the face of the transmission bar. The incident bar is instrumented using strain-gauges and so, in contrast with Taylor anvil test, strain histories corresponding to the both contact faces of the specimen are measured and thus are known. Unlike conventional SHPB test, OHPB allows for high maximum strain in the specimen at constant strain-rate with good conditions of dynamic equilibrium as the strain waves propagate from the specimen boundaries [4].

For the experimental tests, OHPB consisting of a gas-gun, two high-strength aluminum alloy bars (EN-AW-7075) with nominal diameter 20 mm and length 1600 mm, and a damper was used. The incident bar was partially loaded in the barrel of the gas-gun with available stroke for acceleration 1400 mm. The impact face of the incident bar was guided using low friction linear guidance system TW-04-12 (Igus, Germany). Both bars were equipped with foil strain-gages (3/120 LY61, HBM, Germany) in half-bridge arrangement located 200 mm from the specimen faces. The half-bridge circuits were realized using custom built switchboard that allows powering and balancing of circuits. Due to small sensitivity of the foil strain gauges high emphasis was put on elimination of noise in the measurement chain. On the input of the chain, the battery power supply with excitation voltage 4 V was used to power of strain gauge circuit to minimize the noise of strain gauge signal. The measured noise of the signal of the strain gauge circuit in unloaded state with this battery source was approximately 3.5 mV_{pp}. To maximize the signal-to-noise ratio of the output signal it was necessary to use the active differential low noise amplifier (EL-LNA-2, Elsys AG, Switzerland). Gain of amplifier was set to 100

with 15 MHz bandwidth. High speed 16-bit digitizer (PCI-9826H, ADLINK Technology, Inc., Taiwan) with maximal 20 MHz sample rate and 1 MOhm input impedance was used to sample the amplified strain gauge signal. Limited time interval of the record given by on-board memory of the digitizer and time synchronization of the data flow required triggering of the OHPB test. Thus, a two pairs of laser through-beam photoelectric sensors (FS/FE 10-RL-PS-E4, Sensopart, Germany) were installed on the barrel of the gas-gun. The OHPB was designed with focus on advanced optical techniques (e.g. DIC - digital image correlation technique) for strain assessment. Both types of triggers can be used with many types of high-speed cameras. The tests with auxetic structures were observed using a high-speed digital camera (FASTCAM SA5, Photron, Japan) with $20\ \mu\text{m}$ square CMOS sensor with maximal 1,000,000 fps at a 64×16 px image pixel resolution (maximal frame rate depends on image resolution and vice versa). As a compromise between the image resolution and frame rate $124,000$ fps and 192×216 px image resolution were set. A pair of high intensity LED lights (Constellation 60, Veritas, USA) was attached on main frame of the setup for illumination of the sample surface. The area of impact was equipped with shield made from transparent polymer to protect the high-speed camera and lights against sample's fragments. Data acquisition, source synchronization as well as control of instruments during the OHPB test were implemented as custom virtual instrument in Labview (National Instruments, USA).

Three types of the auxetic lattices (2D re-entrant, 3D re-entrant, missing-rib) and selected types of cellular metals were tested using OHPB. The results were compared with previous tests carried out using SHPB apparatus [2]. DIC technique was used to evaluate displacement and strain fields in the specimen and to analyze Poisson's ratio of the structures. DIC results were also compared with the results obtained using SHPB.

Acknowledgement The research was supported by the internal grant of the Czech Technical University in Prague (project no. SGS17/148/OHK2/2T/16).

References

- [1] M. Peroni et al. *Development of a Hopkinson Bar Apparatus for Testing Soft Materials: Application to a Closed-Cell Aluminum Foam*. *Materials* **9**(1): 27, 2016.
- [2] T. Fíla et al. *Impact Testing of Polymerfilled Auxetics Using Split Hopkinson Pressure Bar*. *Advanced Engineering Materials* **19**: 1700076, 2017.
- [3] M. A. Islam et al. *Mechanical response and dynamic deformation mechanisms of closed-cell aluminium alloy foams under dynamic loading*. *Int. J. Impact Eng.* **114**, 111-122 (2018) *International Journal of Impact Engineering* **114**: 111-122, 2018.
- [4] R. A. Govender, R. J. Curry. *The "Open" Hopkinson Pressure Bar: Towards Addressing Force Equilibrium in Specimens with Non-uniform Deformation*. *Journal of dynamic behavior of materials* **2**: 43-49, 2016.

SMOOTHED PARTICLE HYDRODYNAMICS SIMULATIONS OF CAVITATION BUBBLE COLLAPSE INDUCED PLASTICITY

Shrey Joshi¹, Jean-Pierre Franc², Giovanni Ghigliotti² and Marc Fivel^{1*}

¹Univ. Grenoble Alpes, CNRS, Grenoble-INP, Science and Engineering of Materials and Process, Grenoble, France; e-mail: Marc.Fivel@simap.grenoble-inp.fr

²Univ. Grenoble Alpes, CNRS, Grenoble-INP, Laboratoire des Ecoulements Géophysiques et Industriels, Grenoble, France.

Keywords: SPH, cavitation erosion, bubble collapse, plasticity, damage.

Cavitation erosion is a major concern in many industrial applications such as water pump, marine propellers, hydroelectric turbines, fuel injectors, or even in health science like for heart valves. Cavitation erosion is the consequence of mass loss of a solid material subjected to multiple impacts of collapsing bubbles in the fluid. The bubbles are generally nucleated in the flow at locations where the local pressure decreases below vapour pressure, i.e. in the regions of high velocity. They will later collapse when the velocity will decrease. In the case the collapsing bubble is located close to a solid interface, the dynamics of the collapse is not symmetric and a liquid microjet is formed toward the solid interface as depicted in Figure 1b. When the microjet hits the opposite side of the bubble (Figure 1c), a shock wave is generated in the fluid. The liquid microjet will then reach the solid surface (Figure 1d) at a velocity of several meters per second leading to high strain rates in the material. With time, the solid/liquid interface will experience a large number of impacts that will cumulate plasticity in the material. This will finally lead to the nucleation of a crack at the origin of mass loss.

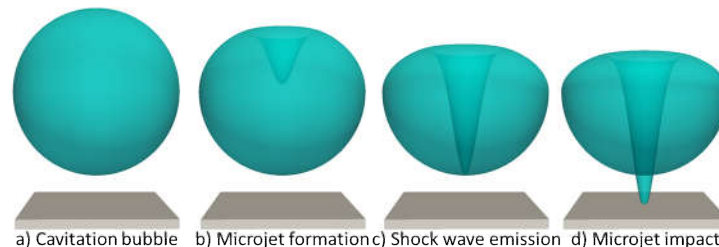


Figure 1: Snapshots of the dynamics a cavitation bubble collapse near a solid interface.

The objective of this paper is to simulate the plasticity induced in the solid material by bubble collapses. Very few attempts have been conducted so far. Typical simulations consist of using a Finite Element (FE) solver where the load corresponding to the bubble collapse is introduced via a pressure distribution at the solid boundary. However, it is extremely difficult to measure experimentally such a load distribution. Indeed, measurements based on PVDF only give an integration of multiple bubble collapses on the entire sensor area with a poor temporal resolution. An alternative solution consists of realizing Computational Fluid Dynamics (CFD) simulations but a key point is to accurately account for the deformation of the solid interface. This could be done within a classical fluid/structure interaction framework, for example using an Arbitrary Lagrangian Eulerian description of the fluid domain and a strong coupling between the CFD code and the FE solver [1]. In the present paper, we chose to use a meshless method in order to solve both the fluid and the solid domain in the same code. Smoothed Particle Hydrodynamics (SPH) method is a Lagrangian meshless method for which the dynamics of particles representative of an infinitesimal part of the continuum domain is computed based on a set of constitutive equations [2]. Although originally developed to numerical studies of planetary collisions [3], SPH is nowadays mostly dedicated to fluid mechanics for which the code can easily handle compressibility and subsequent wave propagations.

Starting from the 2D open-source software SPHysics dedicated to fluid mechanics and jointly developed at Johns Hopkins University and the University of Rome, La Sapienza [4], we have modified the code so that it could account for elasto-visco-plastic media within axisymmetric conditions. The solid solver has been validated by comparisons with FE simulations in simple situations such as the case of indentation. The fluid solver has been verified by computing the velocity field during a spherical bubble collapse in an infinite fluid domain and comparing the result of the analytical Rayleigh-Plesset solution.

The code has then been applied to the case of a spherical bubble collapsing near an Al-2205 aluminum alloy sample for which the constitutive parameters have been identified experimentally. Different standoff positions of the bubble have been tested. Namely, we have investigated the case of a detached cavity for which the standoff ratio, SR, defined as the distance to the wall divided by the bubble radius is greater than 1 and the case of an attached cavity for which $SR < 1$.

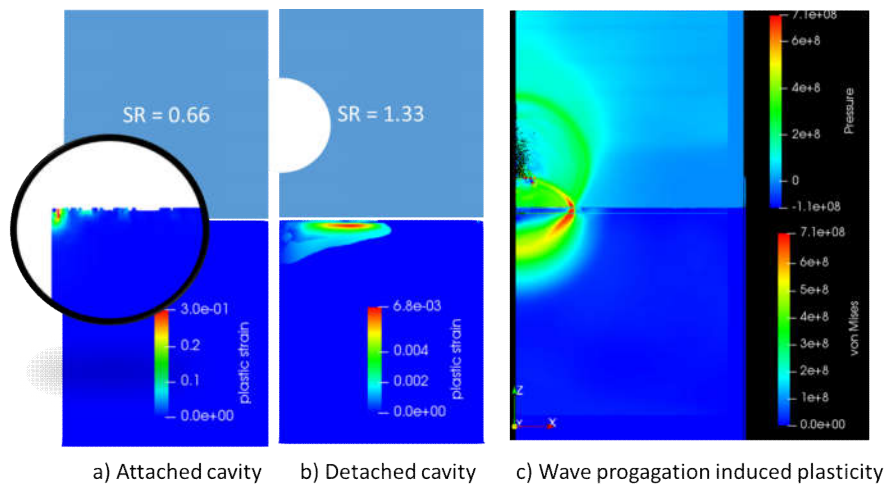


Figure 2: SPH results of plasticity induced by an attached cavity (a) compared to a detached cavity (b). Illustration of the Von Mises stress induced by the wave propagation in the case of a detached cavity (c).

It is observed that the attached cavities induce a much more localized plastic zone precisely located along the symmetry axis (Figure 2a). The detached cavity behaves differently because of the shock wave generated during the bubble collapse which cumulates plasticity outside the symmetry axis (Figure 2b) although it is not the location of the highest pressure induced by the fluid. The plasticity expansion process is attributed to inertial effects induced by the elastic wave traveling in the solid (Figure 2c). It is concluded that numerical investigations of cavitation erosion should not be limited to pressure distribution at the interface.

Acknowledgement

This project has received funding from the European Union's Horizon 2020 research and innovation program under the Marie Skłodowska-Curie grant agreement No 642536.

References

- [1] M. Fivel, J.-P. Franc and S.C. Roy, Towards numerical prediction of cavitation erosion, *Interface Focus*, **5**(5), 20150013, 2015.
- [2] J.J. Monaghan, Smoothed Particle Hydrodynamics, *Annu. Rev. Astron. Astrophys.*, **30**:543-574, 1992.
- [3] W. Benz, W.L. Slattery, A.G.W Cameron, The origin of the moon and the single-impact hypothesis I, *Icarus*, **66**:515-535, 1986.
- [4] SPHYSICS available at dual.sphysics.org

BLAST OVERPRESSURE PROPAGATION IN FUNCTIONALLY LAYERED CEMENTITIOUS COMPOSITES

Marek Foglar^{1*}, Radek Hájek¹, Jiri Stoller² and Jiri Pachman³

¹Czech Technical University in Prague, Prague, Czech Republic; e-mail: marek.foglar@fsv.cvut.cz

²University of Defence, Brno, Czech Republic; e-mail: jiri.stoller@unob.cz

³University of Pardubice, Pardubice, Czech Republic; e-mail: jiri.pachman@upce.cz

Keywords: cementitious composites, blast overpressure propagation

The presented research builds on multiple runs of full-scale experiments focused on blast performance of cementitious composites. The specimens are real-scale reinforced concrete bridge decks 6m in span, cross-section 0.3 x 1.5m.

In the year 2016, the three specimens were tested. Ultra-high performance fiber reinforced concrete (UHPFRC) was used for the specimens. The heterogeneity of the specimens was further increased by basalt meshes or recycled textile sheets. The blast overpressure propagation was recorded by PDV and the damage was tested using ultra-sound measurement. On the contrary to previous runs of the experiments, the specimens were cast in a way that the material creates construction joints that further increase the heterogeneity of the specimens, i. e. the specimens are functionally layered.

The paper presents the findings and compares them to previous runs of the experiments. Conclusions are drawn with respect to the modified fabrication method.

Acknowledgement

Financial support from Grant Agency of the Czech Republic project no. 17-23067S is gratefully acknowledged.

References

- [1] M. Foglar, M. Kovar. Conclusions from experimental testing of blast resistance of FRC and RC bridge decks. *International Journal of Impact Engineering*, **59**: 18-28, 2013.
- [2] M. Foglar, R. Hajek, M. Kovar, J. Štoller. Blast performance of RC panels with waste steel fibers. *Construction and Building Materials*, **94**: 536-546, 2015.
- [3] M. Foglar, R. Hajek, J. Fládr, J. Pachman, J. Stoller. Full-scale experimental testing of the blast resistance of HPFRC and UHPFRC bridge decks. *Construction and Building Materials*, **145**: 588-601, 2017.
- [4] R. Hajek, M. Foglar. Numerical and Experimental Analysis of the Effect of Rigid Barriers on Blast Wave Propagation. *ASCE Journal of Structural Engineering*, **141**. 2015
- [5] R. Hajek, M. Foglar, J. Fládr. Influence of Barrier Material and Barrier Shape on Blast Wave Mitigation. *Construction and Building Materials*, **120**: 54 - 64, 2016.

2D/3D EXPLICIT FINITE ELEMENT CONTACT-IMPACT ALGORITHM WITH BIPENALTY STABILIZATION

Dušan Gabriel^{1,*}, Ján Kopačka¹, Radek Kolman¹, José A. González² and Jiří Plešek¹

¹Institute of Thermomechanics AS CR, v.v.i., Prague, Czech Republic; e-mail: {gabriel,kopacka,kolman,plesek}@it.cas.cz

²Escuela Técnica Superior de Ingeniería, Universidad de Sevilla, Spain; e-mail: japerez@us.es

Keywords: bipenalty method, contact-impact, finite element method, explicit dynamics

It is well known that in contact-impact problems the stiffness penalty method tends to decrease the critical time step in conditionally stable time integration schemes [1]. This is due to the fact that the stiffness penalty can greatly enlarge the maximum eigenfrequency of a system. In the dynamic transient analysis, the penalty method can also be applied to the mass matrix. This technique is known as the mass penalty or the inertia penalty method. In contrast to the stiffness penalty approach, it significantly reduces one or more eigenfrequencies. Askes *et al.* [3] proposed a bipenalty method, in which both penalty formulations were used simultaneously. The goal of this method is to find the optimum of the so-called critical penalty ratio (CPR) defined as the ratio of stiffness and mass penalty parameters so that the maximum eigenfrequency and the critical time step are preserved. The calculation of CPR requires an analysis of the full bipenalised problem. Owing to mathematical difficulty, it limits the classes of elements that can be taken into account. In order to overcome this problem, a simple relationship between the CPR of an element and its maximum unpenalised eigenfrequency was derived in [4]. Thus, the multiple constraints and more complex element formulations can be directly accounted for [5].

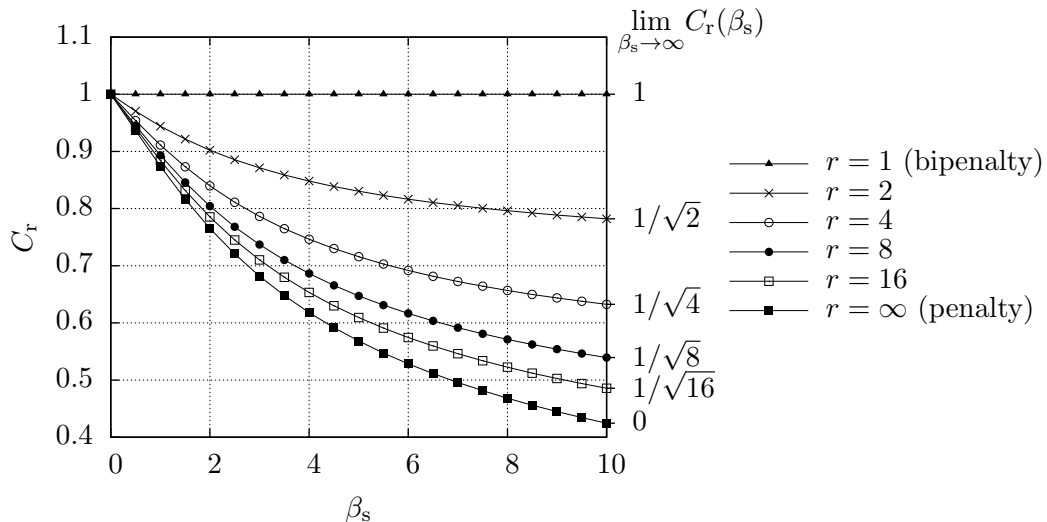


Figure 1: Dependence of the critical Courant number C_r on the dimensionless stiffness penalty β_s for selected dimensionless penalty ratios r .

Belytschko and Neal [1] derived an upper bound of the stiffness penalty for which the stability of time integration scheme is preserved. Kopačka *et al.* [7] generalized this estimation for the bipenalty method. It is based on the solution of 1D Signorini problem depicted in Figure 1, where the dependence of the Courant number C_r on the dimensionless stiffness penalty β_s is plotted. Note that the dimensionless penalty ratio r is employed as the parameter. The curve for $r \rightarrow \infty$ corresponds to the standard stiffness penalty method presented in [1]. It illustrates the main disadvantages of the stiffness penalty method: the Courant number C_r rapidly decrease with increasing dimensionless stiffness penalty β_s . On the other hand, the curve for $r = 1$ confirms the existence of the CPR, for which the stable time

step remains unchanged for an arbitrary value of the dimensionless stiffness penalty β_s . It is clear that the bipenalty method with the penalty ratio equal to the CPR is superior over the standard stiffness penalty method.

In this work, the bipenalty approach is extended for multidimensional contact-impact problems using symmetry preserving explicit finite element contact-impact algorithm developed by authors [2]. Several numerical examples are presented including the impact of two tubes and the longitudinal impact of two thick plates, for which an analytical solution is available. In all cases, the superiority of the bipenalty method over the standard penalty method is clearly demonstrated.

Acknowledgement

The work of D. Gabriel, R. Kolman, J. Plešek was supported by the European Regional Development Fund under Grant No. CZ.02.1.01/0.0/0.0/15.003/0000493 (Centre of Excellence for Nonlinear Dynamic Behaviour of Advanced Materials in Engineering). The work of J. Kopačka was supported by the Czech Science foundation under grant number 16-03823S within institutional support RVO:61388998.

References

- [1] T. Belytschko, M.O. Neal. Contact-impact by the pinball algorithm with penalty and lagrangian methods. *International Journal for Numerical Methods in Engineering*, **31**: 547–572, 1991.
- [2] D. Gabriel, J. Plešek, M. Ulbin. Symmetry preserving algorithm for large displacement frictionless contact by the pre-discetization penalty method. *International Journal for Numerical Methods in Engineering*, **61**: 2615–2638, 2004.
- [3] H. Askes, M. Caramés-Saddler, A. Rodríguez-Ferran. Bipenalty method for time domain computational dynamics. *Proceedings of the Royal Society A*, **466**: 1389–1408, 2010.
- [4] J. Hetherington, A. Rodríguez-Ferran, H. Askes. A new bipenalty formulation for ensuring time step stability in time domain computational dynamics. *International Journal for Numerical Methods in Engineering*, **90**: 269–286, 2012.
- [5] J. Hetherington, A. Rodríguez-Ferran, H. Askes. The bipenalty method for arbitrary multipoint constraints. *International Journal for Numerical Methods in Engineering*, **93**: 465–482, 2013.
- [6] J. Hetherington, H. Askes. A mass matrix formulation for cohesive surface elements. *Theoretical and Applied Fracture Mechanics*, **69**: 110–117, 2014.
- [7] J. Kopačka, A. Tkachuk, D. Gabriel, R. Kolman, M. Bischoff, J. Plešek. On stability and reflection-transmission analysis of the bipenalty method in contact-impact problems: a one-dimensional, homogeneous case study. *International Journal for Numerical Methods in Engineering*, **113**: 1607–1629, 2017.

DISPERSIVE WAVE PROPAGATION IN MATERIAL WITH PERIODIC AND RANDOM MICROSTRUCTURE

Inna M. Gitman^{1,*}, Yilang Song¹

¹The University of Sheffield, Sheffield, UK; e-mail: i.gitman@sheffield.ac.uk

Keywords: stop-band, wave filter, composite material, laminate, randomness, wave propagation.

In this presentation the influence of mechanical and geometrical properties of a heterogeneous periodic composite material, both deterministic and stochastic in nature, on wave propagation will be discussed from the position of stop band phenomenon.

We will discuss numerical analyses used to identify parameters that have the most significant effect on the wave filtering properties of the medium.

The discussion will start with a one dimensional solid periodic laminate material. Further, randomness will be added to the material properties (mechanical and geometrical) to investigate its effect on the stop band properties. The stop band phenomenon will also be studied for two dimensional samples with deterministic and random material microstructure.

In order to identify the characteristic influences of the relative Young's moduli, densities and unit cell length on the band-gap structures, numerical analysis (see for details [1]) of longitudinal wave propagation through a finite domain occupied by the composite material will be performed, predicting the associated transmission coefficient. The value of the obtained transmission coefficient will indicate a stop-band or pass-band. The results indicated that (see Figure 1): (a) increasing the contrast in Youngs moduli of phases, leads to a band-gap at lower frequency and the transmission coefficient in the pass-band drops slightly; (b) increasing the contrast in density leads to a significant increase in the width of the first stop-band and the transmission coefficient associated with the second pass-band also decreases; (c) increasing the unit cell length whilst keeping overall length fixed gives rise to a stop-band at lower frequency.

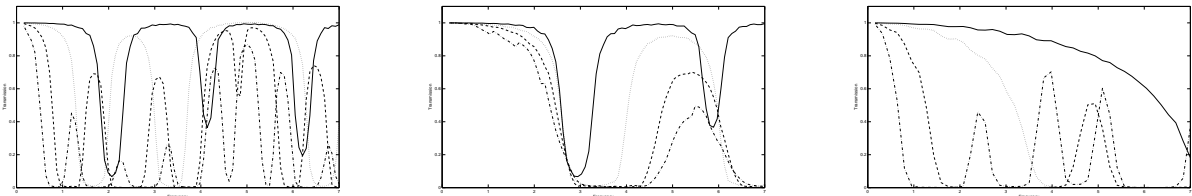


Figure 1: Contrast in Youngs moduli of phases (left), contrast in densities (middle), different unit cell lengths (right)

As the next step the randomness in the material properties (mechanical and geometrical) was introduced. The results reported little or no influence of randomness of material parameters (Young's moduli and densities), however introducing randomness to the geometrical properties has proven to be more beneficial.

To show the aforementioned result a random, 1D Fibonacci bar has been constructed [2] and longitudinal wave has been sent propagating through the material.

The transmission coefficient of random (Fibonacci based) bar are then compared with the transmission coefficient results of a wave propagating through a periodic material. This comparison is shown in Figure 2. As it can be seen, geometrical randomness can significantly reduce the value of the transmission coefficient in the second pass band compared to periodic laminate material.

Similar effect has been shown in two dimensional case, where randomness has been introduced through

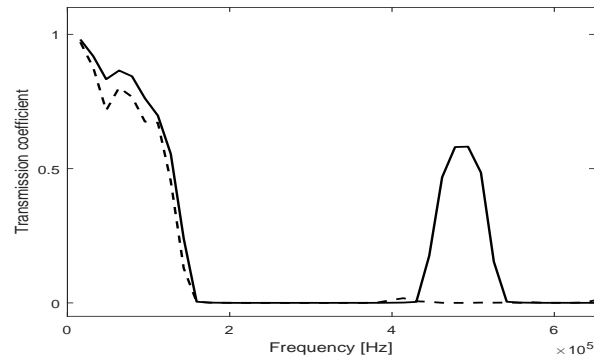


Figure 2: Quasi-random (dashed line) compared with periodic case (solid line).

the two dimensional Fibonacci square (see Figure 3).

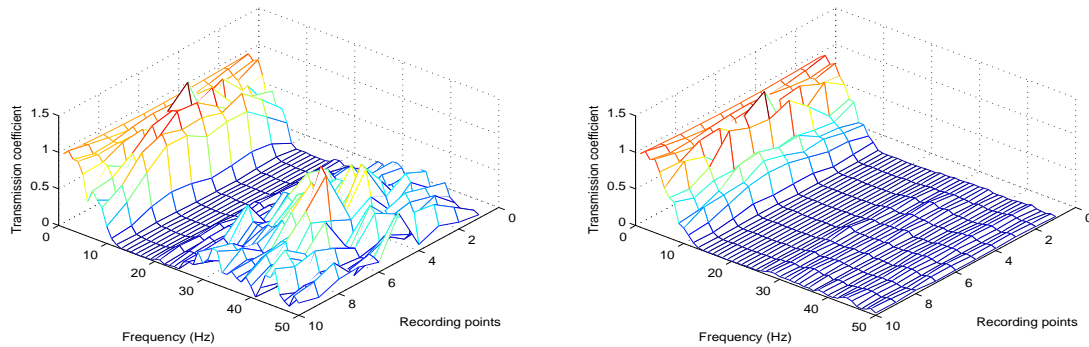


Figure 3: Wave propagating through periodic material (left); randomness added to the material (right)

As can be seen, in line with the conclusions made for 1D case, introducing Fibonacci-type geometrical randomness considerably increases the frequency range of the first stop band.

Acknowledgement We gratefully acknowledge the Leverhulme Trust for financial support under grant number F/00 120/CC. We are indebted to William J. Parnell (University of Manchester, UK) and Harm Askes (The University of Sheffield, UK) for the scientific input.

References

- [1] Y. Song, I.M. Gitman, W.J. Parnell and H. Askes The influence of random microstructure on wave propagation through heterogeneous media *International Journal of Fracture*.**204**: 115–120, 2017.
- [2] I.M. Gitman and Y. Song Fibonacci sequence for modelling stop bands in random microstructure *Journal of Applied Mathematics and Mechanics / Zeitschrift fr Angewandte Mathematik und Mechanik*, **98**: 270–276, 2018.

RECIPROCAL MASS MATRICES FOR ISOGEOMETRIC ANALYSIS VIA THE METHOD OF LOCALIZED LAGRANGE MULTIPLIERS

J. A. González^{1,*}, J. Kopačka², R. Kolman², S. S. Cho³ and K. C. Park⁴

¹Universidad de Sevilla, Seville, Spain; e-mail: japerez@us.es

²Institute of Thermomechanics AS CR, v.v.i., Prague, Czech Republic; e-mail: {kopacka,kolman}@it.cas.cz

³Korea Atomic Energy Research Institute, Daejeon, Republic of Korea; e-mail: sscho96@kaeri.re.kr

⁴University of Colorado, Boulder, CO, USA; e-mail: kcpark@colorado.edu

Keywords: reciprocal mass matrix, isogeometric analysis, Bézier extraction, localized Lagrange multipliers

A reciprocal mass matrix is an approximation of the mass matrix inverse that can be used to directly compute accelerations from a vector of applied forces. In this work, extension of our previous work [1] on the derivation of reciprocal mass matrices for classical finite element methods, it is presented a general framework for the computation of reciprocal mass matrices that can be employed in isogeometrical analysis methods with B-Splines, NURBS and Bézier elements.

The construction of these reciprocal mass matrices is based on a displacement-momentum-multiplier three-field mixed form of the Hamilton's principle,

$$H(\mathbf{u}, \mathbf{p}, \boldsymbol{\ell}) = \int_{t_1}^{t_2} \left\{ \int_{\Omega} \left(\frac{1}{2} \mathbf{p} \cdot \dot{\mathbf{u}} - \frac{1}{2} \boldsymbol{\varepsilon} : \boldsymbol{\sigma} + \mathbf{u} \cdot \mathbf{b} \right) d\Omega + \int_{\Gamma_b} \boldsymbol{\ell} \cdot (\mathbf{u} - \mathbf{u}_b) d\Gamma \right\} dt \quad (1)$$

that is discretized in space by using isogeometric interpolation functions for displacements \mathbf{u} , momenta \mathbf{p} and localized Lagrange multipliers $\boldsymbol{\ell}$. For this purpose, we carry out a standard IGA discretization with independent B-spline shape functions for the three fields. It is also explored the Bézier extraction technique, employed for transformation of isogeometric meshes into a standard finite element structure.

In particular, two different techniques are used for the construction of the reciprocal mass matrices. First, displacements and momenta in the mixed variational form (1) are approximated by dual space bases, simplifying the computation of the reciprocal matrix, that can be evaluated by simple element-by-element assembly operations. Second, a parametrization of the element mass matrix is introduced into the formulation with a combined consistent-lumped element mass matrix,

$$\mathbf{M}_e = (1 - \beta) \mathbf{M}_e^C + \beta \mathbf{M}_e^L \quad (2)$$

where parameter β can be optimized for high accuracy in certain conditions and frequency ranges. Optimal values for this parameter are obtained from dispersion analyses.

Other methods proposed for the same purpose [2, 3], require complicated modifications for the incorporation of inter patch compatibility and Dirichlet boundary conditions. Based on our previous work on reciprocal matrices [1], we bypass this difficulty by using localized Lagrange multipliers to apply natural boundary conditions and compatibility conditions between substructures or patches. This process is found to be computationally efficient, because the obtained matrices are sparse and only the factorization of a small submatrix associated with the constrained DOFs is required.

Diverse numerical experiments, like the one represented in Figure 1, are solved with the proposed methodology and investigated in order to validate its effectiveness and accuracy, specifically in vibration and transient analysis of structural elements like bars, beams, solids and plane stress problems.

In conclusion, it is demonstrated that the proposed reciprocal mass matrices outperform the lumped mass matrix inverse for all frequencies. Accuracy of the method is high for low-mid frequencies and the maximum frequencies of the structure are reduced around a 30%. This reduction in the maximum frequency allows to extend the critical time step for stability of explicit transient simulations.

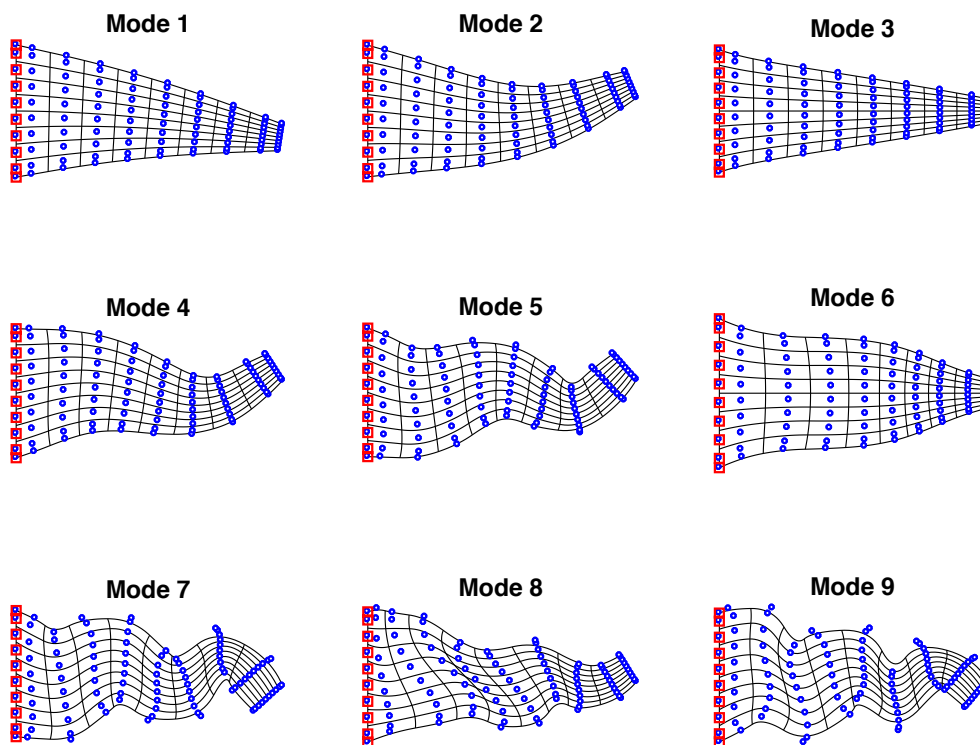


Figure 1: Representation of the 9 lowest vibration modes of a plate. Results correspond to the proposed reciprocal mass matrix with parameter $\beta = 2/5$ computed with quadratic B-splines.

Acknowledgement

The work of J. Kopačka and R. Kolman was supported by the Centre of Excellence for nonlinear dynamic behavior of advanced materials in engineering CZ.02.1.01/0.0/0.0/15 003/0000493 (Excellent Research Teams) in the framework of Operational Program Research, Development and Education, and the grant projects of the Czech Science Foundation, No. 17-22615S, No. 17-12925S and No. 16-03823S within institutional support RVO:61388998.

References

- [1] J. A. González, R. Kolman, S. S. Cho, C. A. Felippa and K. C. Park. Inverse Mass Matrix via the Method of Localized Lagrange Multipliers. *International Journal for Numerical Methods in Engineering* **113**: 277–295, 2017.
- [2] A. Schaeuble, A. Tkachuk and M. Bischoff. *Variationally consistent inertia templates for B-spline- and NURBS-based FEM: Inertia scaling and customization*. *Computer Methods in Applied Mechanics and Engineering*, **326**: 596–621, 2017.
- [3] A. Tkachuk, A. Schaeuble and M. Bischoff. Variational construction of reciprocal mass matrices for B-spline-based finite elements: multiparameter templates and customization. In *The 2nd International Conference on Advanced Modelling of Wave Propagation in Solids*, Prague, Czech Republic, September 17-21, 2018.

RITZ–RAYLEIGH APPROACH: NUMERICAL CALCULATION OF WAVES IN PLATES OF HIGH ANISOTROPY

Tomáš Grabec^{1,2,*}, Petr Sedlák¹, Hanuš Seiner¹ and Michal Landa¹

¹ Institute of Thermomechanics of the CAS, Prague, Czechia; e-mail: grabec@it.cas.cz

² Czech Technical University in Prague, Czechia

Keywords: Ritz-Rayleigh approach, numerical calculation, guided waves, anisotropic materials

A calculation of guided-wave propagation can turn into a cumbersome task when a higher-level anisotropy or a non-principal direction of propagation is considered. Time-domain numerical simulations are computationally demanding, which makes them inappropriate for inverse procedures, i.e. for determination of the sample's properties based on comparison experimental data and numerically obtained values. The Ritz–Rayleigh approach offers a fast calculation of the velocity of guided waves of various types, propagating in an arbitrary direction through a medium of any symmetry class.

The principle of the approach can be summarized into few steps. First, a computational domain with chosen material properties is defined. Boundary conditions imposed on the domain are set according to the investigated situation. Then, resonances of such domain are calculated using Hamilton's principle, i.e., by locating the stationary points of the Lagrangian energy of the body. To calculate this numerically, the displacement field is discretized into a functional basis of trigonometric functions in the direction of propagation, and Legendre polynomials in the direction into the depth of the domain. In the presented version, the solution in the third direction – i.e., perpendicular to the direction of propagation, is homogeneous. However, a more general case with discretization into Legendre polynomials in all three axes can be solved using the presented principle, as shown by Sedlák et al. [1] for calculations of resonance frequencies of a free-standing body. The approach thus allows a conversion of dealing with wave equation into a problem of searching for eigenvalues and eigenvectors, leading to a rather fast calculation even on an ordinary laptop. The resulting eigenvalues and eigenvectors determine the velocity and modal shape, respectively, of the corresponding wave mode. Therefore, it can be used advantageously to determine a development of velocity of the chosen mode, for example in a calculation of angular dispersion.

The same approach can be used for calculation of a broad spectrum of wave-related problems owing to the generality of the principle and variability in boundary conditions. Among a variety of possible guided-wave problems, the usefulness of the approach was already documented by Stoklasová et al. in [2] and by Grabec et al. in [3]. In the former, a problem of angular dispersion in velocity of Rayleigh waves propagating on a generally oriented plane of monocrystalline InP was described, while in the latter, a calculation of frequency dispersion of Rayleigh waves in a NiTi film on top of a Silicon substrate was shown. Both papers deal also with associated inverse problems – the former proving a capability of determining all 21 elastic constants of the sample, the latter showing a phase transition occurring in a micrometric film during thermal loading.

In the presented contribution, a use in another case of guided waves will be described, and namely in the case of waves in plates. It will be shown that the approach is a suitable tool for the calculation of frequency dispersion of Lamb modes. The transition from surface waves to waves in plates consists not only from a change of the boundary conditions but also from a slight, beneficial change of the functional basis decreasing the number of degenerated modes. Nevertheless, since the main principle of the approach remains, the calculation works equally for any arbitrary tensor of elastic coefficients, meaning that the dispersion of Lamb modes in any chosen material and orientations is feasible, while the computational time stays reasonable. The approach retains its ability to track individual modes in the calculation of dispersion. Furthermore, it allows calculating the corresponding group velocity, as well as the phase velocity. Therefore, it is suitable for a location of the zero-group-velocity point. As an example, the calculated dispersion of a thin plate of strongly anisotropic shape-memory material

will be presented.

Acknowledgement

This work was financially supported by the Czech Science Foundation (the AdMat project, No. 14-36566G).

References

- [1] P. Sedlák, H. Seiner, P. Zídek et al. Determination of all 21 independent elastic coefficients of generally anisotropic solids by resonant ultrasound spectroscopy: Benchmark examples. *Experimental mechanics*, **54**: 1073–1085, 2014.
- [2] P. Stoklasová, P. Sedlák, H. Seiner et al. Forward and inverse problems for surface acoustic waves in anisotropic media: a Ritz-Rayleigh method based approach. *Ultrasonics*. **56**: 381–389, 2015.
- [3] T. Grabec, P. Sedlák, P. Stoklasová et al. In-situ characterization of local elastic properties of thin shape memory films by surface acoustic waves. *Smart Materials and Structures*, **25(12)**, 2016.

ELASTIC WAVE PROPAGATION AND SCATTERING MODELLING ASSISTED NONDESTRUCTIVE TESTING AND MICROSTRUCTURED MATERIALS EVALUATION

Sigrun Hirsekorn

NDT Consultant, Rehbachstr. 126, Saarbrücken, Germany; e-mail: sigrun.hirsekorn@gmail.com

Keywords: analytical model, composite, defect, microstructure, ndt&e, polycrystal, scattering, simulation, theory, ultrasound

Ultrasonic techniques allow inspection and monitoring of diverse industrial components. The propagation properties of the sound waves, velocity and attenuation, may be exploited for materials characterization and evaluation while ultrasonic scattering and/or reflection at defects and impurities allow their detection and assessment. However, in microscopically inhomogeneous media as e.g. polycrystalline structures and fiber-reinforced materials, ultrasound is scattered also at grain and phase boundaries entailing velocity dispersion and additional sound attenuation along its propagation direction. These effects as well as scattering wave amplitudes may help with the assessment of such complex materials. Concomitant, scattering at the microstructure hampers defect detection and evaluation because the so-called structural noise superposes defect signals, and velocity dispersion corrupts defect positioning. Hence, ultrasonic signal evaluation has to take into account structural scattering, and the simulation of ultrasonic propagation and nondestructive testing and materials characterization procedures must comprise microstructural scattering phenomena.

To begin with, we consider measurements on two industrial components of different microscopically inhomogeneous materials. In car manufacturing, components of die-cast non-ferrous metals are used. Those parts show manufacturing caused pores and shrink holes, which may affect strength, tightness, and the surface roughness. Special attention has to be paid to surface-near zones up to about 2 mm depth because pores might be broached while machining the parts. High-frequency ultrasonic backscattering is applied for porosity detection, and the signal to grain noise ratio of the results is discussed. [1]

The two-phase anisotropic structure of typical composite materials, used e.g. in aircraft industry, implies a variety of challenges, not only structural scattering, but also beam skewing and sound field distortion, which complicates the localization, sizing, and characterization of defects. Inspections are required during the manufacturing stage, and additional tasks emerge once the composite ages, maybe by mechanical fatigue, chemical ageing, or irradiation. The characterization of composite materials based on ultrasonic methods allows monitoring the material properties along the whole life cycle of the parts. [2]

In the literature, comprehensive theoretical studies aiming for ensemble averaged intensities of scattering waves in microscopically inhomogeneous media arriving at a transducer attached to a sample surface for a given incident wave can be found, including effective sound velocity and attenuation calculations (e.g. [3-6] and references therein). Ensemble average means statistical average respective microscopic inhomogeneity reflecting the macroscopic materials behavior.

Numerical simulations of ultrasonic experiments and ndt&e procedures follow a different approach. A convenient microstructural scattering model capable to simulate ultrasonic time signals, e.g. A-scans (backscattering signals), flexibility in shape and macroscopic material inhomogeneity (e.g. microstructure variations, defects, etc.) of the considered component, and analytical scattering coefficient formulae allowing fast simulation algorithms are required. Statistically distributed single scatterers the ensemble averaged scattering energy flux densities of which reflect the structural noise in the test block may be used as grain scattering model [7]. The convenient numerical simulation procedure is then point source synthesis of the scattering waves stemming from the scatterers simulating structural noise and maybe also from defects and

impurities including possible reflections at the sample surfaces. At the half space surface of a semi-infinite microscopically inhomogeneous solid of macroscopic homogeneity, the point source synthesis will yield the scattering wave intensities well-known from the literature (e.g. [3-6] and references therein).

The solutions of the general equation of motion of inhomogeneous materials, which represent the ultrasonic displacement vectors in the considered medium, contain not only the incident ultrasonic wave and its propagation behavior, but also the scattering waves [3]. The scattering wave energy flux densities are formally derived from the infinite Born series presentation of these solutions. The energy flux densities are ensemble averaged respective the microscopic inhomogeneity and, to begin with, analytically evaluated for single-phase polycrystals in lowest non-zero order. The resultant directional and frequency dependent scattering wave amplitudes provide with the theoretical base for the simulation of ultrasonic propagation and nondestructive testing and materials characterization procedures and ultrasonic signal evaluation in polycrystalline materials [8]. The general elastodynamic equation of motion allows similar analytical evaluations for materials with different microstructural features.

Grain size distributions of single-phase polycrystals without texture determined by metallography are exploited for numerical realizations of proper statistical scatterer distributions. A 3D model is used to represent the arrangement of scatterers. Applying the analytical scattering coefficient formulae provided by the general theoretical approach [8], ultrasonic backscattering signals are numerically simulated [9, 10].

References

- [1] S. Hirsekorn, U. Rabe, D. Bruche, N. Grov, T. Kinzler, W. Arnold. High-frequency ultrasonic porosity testing of non-ferrous metal die castings. *CASTING Plant and Technology*, **4**, 28-33, 2007.
- [2] U. Rabe, T.B. Helfen, M. Weikert, S. Hirsekorn, H.-G. Herrmann, C. Boller, D. Backe, F. Balle, D. Eifler. Nonlinear Ultrasonic Testing of Carbon Fibre Reinforced Plastics in the Very High Cycle Fatigue Regime. XVII International Conference on Nonlinear Elasticity in Materials (ICNEM), Cefalù, Sicily, Italy, July 1-7, 2012. *Acoustical Society of America, Proceedings of Meetings on Acoustics (POMA)* **16**, 2012 <http://asadl.org/poma/resource/1/pmarew>.
- [3] S. Hirsekorn. The scattering of ultrasonic waves by multi-phase polycrystals. *J. Acoust. Soc. Am.*, **83**, 1231-1242, 1988.
- [4] J.A. Turner, R.L. Weaver. Time dependence of multiply scattered diffuse ultrasound in polycrystalline media. *J. Acoust. Soc. Am.*, **97**, 2639-2644, 1995.
- [5] F.J. Margetan, Linxiao Yu, R.B. Thompson. Computation of grain-noise scattering coefficients for ultrasonic pitch/catch inspections of metals. *Rev. Prog. QNDE*. D.O. Thompson and D.D. Chimenti (eds.). Plenum Press NY, **24**, 1300-1307, 2005.
- [6] O.I. Lobkis, L. Yang, J. Li, S.I. Rokhlin. Ultrasonic backscattering in polycrystals with elongated single phase and duplex microstructures. *Ultrasonics*, **56**, 694-705, 2012.
- [7] V. Dorval, F. Jenson, G. Corneloup, J. Moysan. Accounting for structural noise and attenuation in the modelling of the ultrasonic testing of polycrystalline materials. *Rev. Prog. QNDE*. D.O. Thompson and D.D. Chimenti (eds.). Plenum Press NY, **29**, 1309-1316, 2010.
- [8] S. Hirsekorn. Calculations on Ultrasonic Scattering in Polycrystalline Structures Aiming for Simulations on Nondestructive Materials Characterization and Defect Detection. ECNDT 2014, Prague, Czech Republic. *NDT.net issue*, **19** No.12, 2014.
- [9] D. Dobrovolskij, S. Hirsekorn, M. Spies. Simulation of Ultrasonic Materials Evaluation Experiments Including Scattering Phenomena due to Polycrystalline Microstructure. *Proceedings 2015 International Congress on Ultrasonics (ICU) Metz*, France, May 10-14, 2015.
- [10] S. Hirsekorn, D. Dobrovolskij, M. Spies. Modelling of Ultrasonic Scattering in Polycrystals Aiming for Tools to Simulate Experiments in NDT&E. *IXth Inter-national Workshop »NDT in Progress«, ed. Czech Society for NDT: 26-35*, 2017

ACOUSTIC EMISSION FROM FAST DISLOCATIONS IN 3D BCC IRON CRYSTALS

Petr Hora*, Anna Machová, Jan Červ and Alena Uhnáková

Institute of Thermomechanics AS CR, v.v.i., Prague, Czech Republic;
e-mail: hora@cdm.it.cas.cz, machova@it.cas.cz, cerv@it.cas.cz, uhnakova@it.cas.cz

Keywords: acoustic emission, dislocations, molecular dynamics

Acoustic emission and kinetics of dislocations emitted from a crack is studied via molecular dynamics (MD) utilizing nonlinear interatomic forces, [1] and [2]. 3D results indicate that edge dislocation segments in the middle of the crystal at the free sample surface can accelerate. The dislocations in MD penetrate the free surface in transonic or supersonic regime. Possible sources for such behaviour are discussed in the framework of continuum models. MD results comply with recent continuum analysis [3] of surface waves in anisotropic medium where supersonic regime of wave propagation at the free surface can exist unlike isotropic continuum.

Acknowledgement

The work was supported by the Institute Research Program RVO: 61388998 and by the projects of the Czech Science Foundation GACR 17-22615S and GACR 17-12925S. The work of P. Hora was supported by the European Regional Development Fund under Grant No.CZ.02.1.01/0.0/0.0/15_003/0000493 (Centre of Excellence for Nonlinear Dynamic Behavior of Advanced Materials in Engineering).

References

- [1] G.J. Ackland, D.J. Bacon, A.F. Calder and T. Harry. Computer simulation of point defect properties in dilute Fe-Cu alloy using a many-body interatomic potential. *Phil. Mag. A*, **75**: 713–732, 1997.
- [2] A. Machová and G.J. Ackland. Dynamic overshoot in α -iron by atomic simulations. *Modelling Simul. Mater. Sci. Eng.*, **6**: 521–542, 1998.
- [3] N. Favretto-Cristini, V. Komaditich, J. Garcione and F. Cavallini. Elastic surface waves in crystals, Part 1: Review of the Physics. *Ultrasonics*, **51**: 653–660, 2011.

WAVE DEVELOPMENT IN HIGH-PERFORMANCE YARNS UNDER TRANSVERSE IMPACT

Matthew Hudspeth^{1,2} and Wayne Chen^{2*}

¹Currently with Sandia National Laboratories, Albuquerque, NM, USA; e-mail: mhudspe@sandia.gov

²Purdue University, West Lafayette, IN, USA; e-mail: wchen@purdue.edu

Keywords: transverse impact, high-performance yarns, critical velocity

High-performance yarns are the basic construction materials for many soft body armors. It is not cost and time effective to test the performance of body armors by ballistic impact on the armors during the development stage. In this research we explore the wave propagation in a single yarn subject to transverse impact in the effort to identify the single-yarn behavior as indicators of body-army performance. The commonly accepted performance indicator for body armors is Cunniff parameter [1], whereas the single-yarn impact response was modeled by Smith equations [2]. In the experimental side of this research, we impacted single yarns in a transverse fashion to probe the characteristics of resulting stress and strain wave development. Longitudinal wave speeds were experimentally determined in efforts to directly measure the yarn tensile stiffness. Slight increase in the elastic moduli of Kevlar® KM2 and Dyneema® SK76 yarns were measured with increasing striking velocity. Furthermore, the load developed in AuTx® and Kevlar® KM2 yarns behind the longitudinal wave front was recorded, providing additional verification for the Smith relations. Predictions on the transverse wave by the Smith equations has were successfully verified via tracking transverse wave speeds in AuTx® yarns over a range of impacting velocities. Additional emphasis has been placed at understanding the transverse wave development around the yarn critical velocity, demonstrating that there is a velocity zone where partial yarn failure is detected. Above the critical velocity, the projectile cuts through without significantly deforming the yarn transversely. However, measurements of early time transverse wave speeds agreed with the Smith solution, though the wave speed quickly reduces in amplitudes due to the drop in tensile stresses resulting from filament rupture. Below the critical velocity, the yarn did not fail, but formed a tent shape with apex pushed by the projectile. The shape and the propagating speed are accurately predicted by the Smith equations. Finally, the Smith equations were simplified and compared to the Cunniff parameter, which bear a striking resemblance. Due to such a resemblance, it is suggested that yarn critical velocity experiments can be performed on trial yarn material. Based on the models of Smith equations and Cunniff parameter, the effect of modifying yarn mechanical properties on the ballistic impact performance is discussed [3].

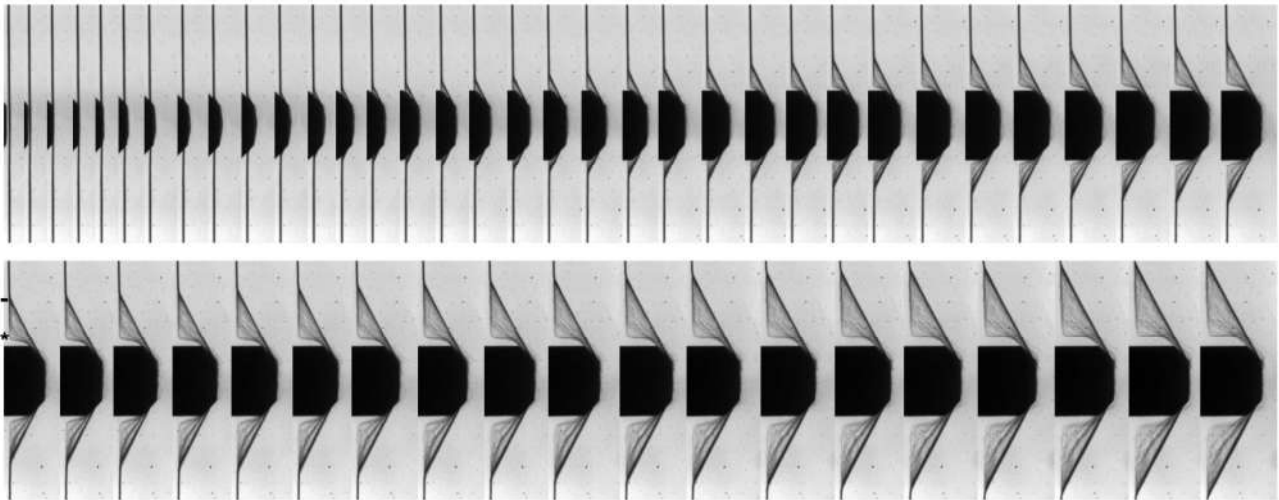


Figure 1: Transverse impact by an FSP on an AuTX® yarn near critical velocity.

Acknowledgement

This work was supported by a US National Defense Science and Engineering Fellowship to M.H. and by US Army PEO Soldier.

References

- [1] J.C. Smith, C.A. Fenstermaker, P.J. Shouse. Stress-Strain Relationships in Yarns Subjected to Rapid Impact Loading: Part X: Stress-Strain Curves Obtained by Impacts with Rifle Bullets. *Text. Res. J.*, **33**: 919–934, 1963.
- [2] P. Cunniff. Dimensionless Parameters for Optimization of Textile-Based Body Armor Systems. In *Proceedings of the 18th International Symposium on Ballistics*, San Antonio, TX, USA, Volume 2, pp. 1303–1310, 15–19 November 1999.
- [3] M. Hudspeth, E. Jewell, S. Horner, J. Zheng and W. Chen. Exploration of Wave Development during Yarn Transverse Impact. *Fibers*, **5**, 17; doi:10.3390/fib5020017, 2017.

WAVE PROPAGATION IN MEASUREMENT OF FLOW STRESS WITH HOPKINSON BAR TESTS AT HIGH STRAIN RATES

Hoon Huh^{1*}, Chunghee Park² and Geunsu Joo³

¹ Department of Mechanical Engineering, KAIST, Daejeon, Republic of Korea; e-mail: hhuh@kaist.ac.kr

² Launcher Structures & Materials Team, Korea Aerospace Research Institute; e-mail: chpark@kari.re.kr

³ Department of Mechanical Engineering, KAIST, Daejeon, Republic of Korea; e-mail: hijgs@kaist.ac.kr

Keywords: Wave propagation, Flow stress, Split Hopkinson pressure bar test, High strain rate

This paper is concerned with the effect of the stress wave on the strain hardening behaviour of materials at a wide range of strain rates ranging from 0.0001 s^{-1} to $4,000 \text{ s}^{-1}$. When the strain rate is beyond the quasi-static state, the stress wave is induced in the stress measuring devices inevitably, which causes inappropriate measurement of the flow stress because of wave dispersion. In measurement of the flow stress, it is necessary to consider the effect of the stress wave and its dispersion for reliable measurement results. Especially when the measurement needs to perform for a soft material such as PBX (Polymer-Bonded Explosives) simulants, it becomes critical to deal with the wave dispersion in SHPB (split Hopkinson pressure bar) tests. The experimental setup needs a noble device to induce the standard waves in the incident and reflected bars by controlling the wave dispersion in Hopkinson pressure bars [1].

The figure 1 and 2 demonstrate the stress wave induced in the incident bar when a projectile hits the end of the incident bar. When a projectile is aligned by guides as shown in Figure (a), the stress wave is induced in the incident bar improperly because of wave dispersion. The stress waves acquired from the strain gauge in the bar well demonstrate the essence and importance of the design of a projectile and its triggering devices.



Figure 1: Projectiles for Split Hopkinson Pressure Bar test: (a) jig 1; (b) jig 2.

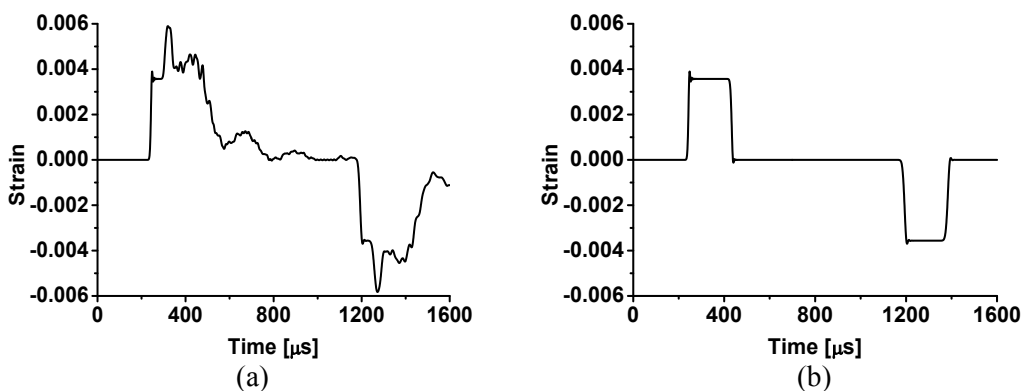


Figure 2: Stress Waves in the incident bar during Split Hopkinson Pressure Bar test: (a) jig 1; (b) jig 2.

Even when the strain rate is from the quasi-static state to intermediate strain rates ranging from 0.0001 s^{-1} to 100 s^{-1} , the measurement of flow stress needs to be carried out carefully in order to avoid the effect of

the stress wave and its dispersion [2, 3]. The figure 3 and 4 demonstrate the stress wave effect on the load measurement from the upper jig including the load cell during the intermediate tensile test of a high strength steel. It is noted from the figure 4 that the design of the upper jig has direct influence on the load–time curve.

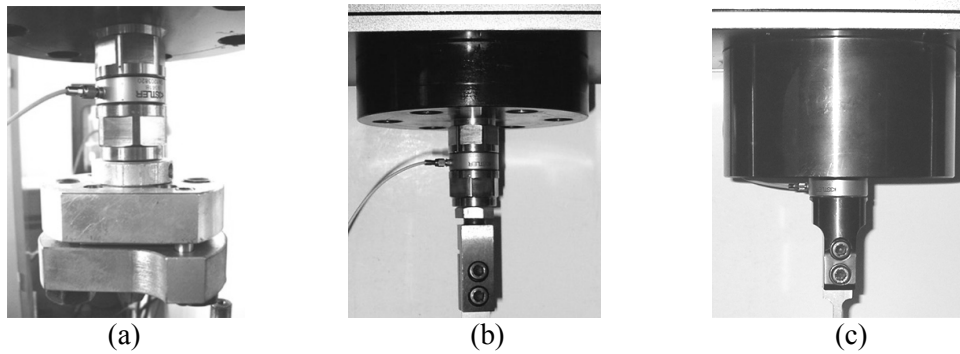


Figure 3: Upper gripping jigs for HSMTM: (a) jig 1; (b) jig 2; (c) jig 3.

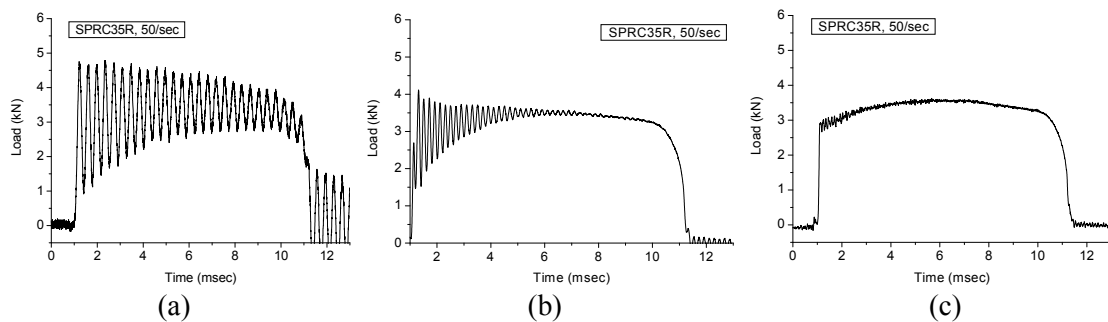


Figure 4: Load curves of SPRC35R at 50/sec with: (a) jig 1; (b) jig 2; (c) jig 3.

With the careful experiments for the stress wave effect, the stress–strain curves at a wide range of the strain rate has been obtained for the accurate simulation of plastic stress wave propagation in several practical application such as the launching of a warhead and the penetration of a warhead through the steel target in order to confirm the sustainability of the electronic fuse elements and other parts in a warhead.

Acknowledgement

This work was supported by the grant project from Poongsan Company.

References

- [1] C. Park, H. Huh, J. Park. Rate-Dependent Hardening Model for Polymer-Bonded Explosives with an HTPB Polymer Matrix Considering a Wide Range of Strain Rates, *Journal of Composite Materials*, **49-4**: 425–438, 2015.
- [2] H. Huh, S. Jeong, G.W. Bahng, K.S. Chae, C.G. Kim. Standard uncertainty evaluation for dynamic tensile properties of auto-body steel-sheets, *Experimental Mechanics*, **54**: 943–956, 2014.
- [3] M.K. Choi, H. Huh, S. Jeong, , C.G. Kim, K.S. Chae. Measurement Uncertainty Evaluation with Correlation for Dynamic Tensile Properties of Auto-body Steel Sheets, *Int. J. Mechanical Sciences*, **130**: 174–187, 2017.

ACOUSTIC BLACK HOLES: FROM GENERALIZATION TO REALIZATION

Wonju Jeon^{1*}

¹Korea Advanced Institute of Science and Technology, Daejeon, Republic of Korea; e-mail: wonju.jeon@kaist.ac.kr

Keywords: acoustic black holes, damping vibration, Archimedean spiral

This study starts with a simple question: can we efficiently reduce the vibration of plates or beams using a lightweight structure that occupies a small space? As an efficient technique to dampen vibration, we adopted the concept of an Acoustic Black Hole (ABH) with a simple modification of the geometry. The original shape of an ABH has a straight wedge-type profile with power-law thickness, with the reduction of vibration in beams or plates increasing as the length of the ABH increases [1]. However, in real-world applications, there exists an upper bound of the length of an ABH due to space limitations. Therefore, in this study, the authors propose a curvilinear shaped ABH using the simple mathematical geometry of an Archimedean spiral, which allows a uniform gap distance between adjacent baselines of the spiral [2].

In numerical simulations, the damping performance increases as the spiral length of the Archimedean spiral increases regardless of the curvature of the spiral in the mid- and high-frequency ranges. Adding the damping material to the ABH could strongly enhance the damping performance while not significantly increasing the weight.

In addition, the authors experimentally investigate the effect of curvatures of the curved ABH on the vibration damping performance. The curved ABHs studied in this work are divided into two cases: (1) the curved ABH with the baseline of constant curvature, i.e., a circular arc shape, (2) the curved ABH with the baseline of varying curvatures. After manufacturing the spiral ABH with high precision, the authors perform experiments to investigate the effect of curvatures on the damping performance of the circular arc shaped ABHs [3]. An Archimedean spiral ABH, a particular form of the curved ABH of slowly varying curvatures is also investigated experimentally in order to create the possibility of using the spiral ABH as a new and efficient method of damping vibration in real-world problems.

References

- [1] M.A. Mironov, Propagation of a flexural wave in a plate whose thickness decrease smoothly to zero in a finite interval. *Soviet Physics. Acoustics*, **34(3)**: 318–319, 1988.
- [2] J.Y. Lee, W. Jeon. Vibration damping using a spiral acoustic black hole. *Journal of the Acoustical Society of America*, **141(3)**: 1437–1445, 2017.
- [3] M. Kim, W. Jeon. An experimental study on vibration damping using curvilinear acoustic black holes, *INTER-NOISE and NOISE-CON Congress and Conference Proceedings*, InterNoise17, Hong Kong, pages 1004-1995, 1879-1883, 2017

TRANSITION WAVES IN RECONFIGURABLE MULTISTABLE SOFT STRUCTURES

Romik Khajehtourian^{1,5*}, Ahmad Rafsanjani^{2,5}, Katia Bertoldi^{2,3,5}, and Dennis Kochmann^{1,4,5}

¹Department of Mechanical and Process Engineering, ETH Zurich, 8092 Zurich, Switzerland;

² John A. Paulson School of Engineering and Applied Sciences, Harvard University,
Cambridge, Massachusetts 02138, USA;

³ Kavli Institute, Harvard University, Cambridge, Massachusetts 02138, USA;

⁴Division of Engineering and Applied Science, California Institute of Technology, Pasadena, CA 91125, USA;

⁵ Email: kromik@ethz.ch, rafsanjani@seas.harvard.edu, bertoldi@seas.harvard.edu, dmk@ethz.ch

Keywords: tunable metamaterials, phase transitions, nonlinear waves, nonconvex energy, instability

Transition waves are a unique class of evolution event propagating through a domain and converting a concerned system from one stable state to another. These waves can explain phenomena such as dislocation motion, ferromagnetic domain wall motion, ferroelectric domain switching, among others (see [1] and references therein). Unfortunately, these phenomena emerge at the microscopic and atomic scales and are hard to observe or control. In this study, we focus on mechanical analogs, multistable mechanical metamaterials, that obey the same principles and allow full control over their design and operation, hence, enabling to establish a theory for the underlying phenomena and regulate the design to receive the desired dynamical response of the system. Our studies of 1D and 2D systems with one degree of freedom (DoF) per node have shown that providing a nonsymmetric bistable energy potential, elements can snap between two states and initiate sustainable transition waves through the system with constant speed. These systems follow a universal scaling law describing the energy transport, relating transition wave speed, elastic energy release, and dissipation through mechanical damping [2, 3]. However, considered systems in these studies are not reconfigurable, i.e., switch between states keeping a constant size.

We consider networks of bistable elements changing their geometry between two stable configurations forming 1D and 2D systems respectively with one and two DoFs per node. We model these systems by attaching multistable elements – consisted of point mass m , springs with stiffnesses of k_1 and k_2 forming a bistable energy potential ψ , and viscous dashpots with dissipation η – on a periodic lattice in 1D, and a hexagonally packed lattice in 2D. We label each bistable element with the multi-index integer $\mathbf{n} \in \mathbb{R}^2$ and characterize by the lattice basis vectors $e_1 = (1, 0)$ and $e_2 = (1/2, \sqrt{3}/2)$. Each element is connected to its set of nearest neighbors and represented by the displacement $\mathbf{q}_{n_1, n_2}(t) = (u_{n_1, n_2}(t), v_{n_1, n_2}(t))$ from the static equilibrium situated at position $\mathbf{p} = a(n_1 e_1 + n_2 e_2)$ where a is the lattice spacing.

In the case of 1D discrete system, we consider a nonconvex energy density of ψ similar Fig. 1a and we derive the equation of motion

$$m\ddot{u}_{n_1} + \eta\left(\frac{-\dot{u}_{n_1-1} + 2\dot{u}_{n_1} - \dot{u}_{n_1+1}}{a}\right) + \psi'\left(\frac{u_{n_1} - u_{n_1-1}}{a}\right) - \psi'\left(\frac{u_{n_1+1} - u_{n_1}}{a}\right) = 0. \quad (1)$$

which upon taking its limit $a \rightarrow 0$ using Taylor expansion of $u_{n_1 \pm 1}$ and the correct scaling of the system parameters, we obtain

$$\rho\ddot{u} - \eta\dot{u}_{xx} - \psi''(u_x)u_{xx} = 0, \quad (2)$$

where $\rho = m/a$ is the mass density.

We present a theoretical description of the strongly-nonlinear transition waves propagating in the media and in the case of significant damping, $|\rho\ddot{u}| \ll |\eta\dot{u}_{xx}|$, we recover the energy transport scaling law

$$\frac{E}{v} = \frac{\Delta\psi}{2\eta}. \quad (3)$$

where E is the total relative kinetic energy per density ρ transported by the transition wave with speed v (Fig. 1).

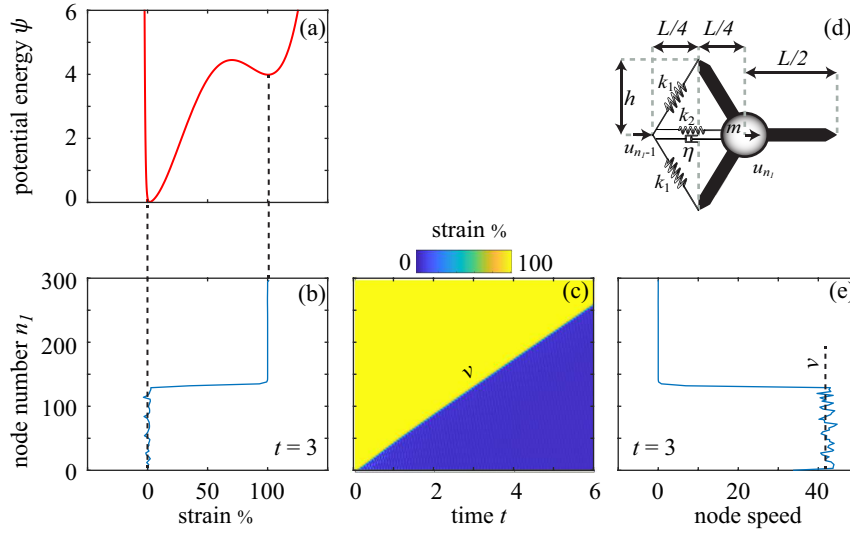


Figure 1: Example of moving transition wave. (a) energy landscape corresponding to bistable element (d); (b) state of strain at $t = 3$; (c) contour plot of the wave propagation in x - t form. The phase boundary moves at a constant velocity; (e) state of wave speed at $t = 3$.

In the case of 2D system, we assume a predominant volumetric deformation is the source of bistability, and define the energy density $\psi = \psi_b(\theta) + \psi_d(\mathbf{e})$, with the bistable energy share of $\psi_b(\theta)$ and the deviatoric strain energy share of $\psi_d(\mathbf{e})$. The energy density is a function of hydrostatic and deviatoric strains with respectively $\theta = \varepsilon_{ii}/d$ and $\mathbf{e} = \text{dev}\boldsymbol{\varepsilon} = \boldsymbol{\varepsilon} - \theta\mathbf{I}$ in d dimensions. The balance of linear momentum in absence of body forces and inertial effects reads $\nabla \cdot \boldsymbol{\sigma} = \mathbf{0}$, which upon substitution of $\boldsymbol{\sigma} = \boldsymbol{\sigma}_e + \boldsymbol{\sigma}_v$ with the elastic stresses $\boldsymbol{\sigma}_e = \partial\psi/\partial\boldsymbol{\varepsilon}$ and viscous stresses $\boldsymbol{\sigma}_v = \eta\dot{\boldsymbol{\varepsilon}}$, the governing equation of the system becomes

$$\frac{\psi''(\theta)}{d} \nabla \theta + \mu \text{div} \mathbf{e} + \eta \text{div} \dot{\boldsymbol{\varepsilon}} = \mathbf{0}. \quad (4)$$

We solve (4) numerically and verify our scaling law experimentally for a variety of systems.

Acknowledgement

This work was supported by the ARO grant 2-71534-17.

References

- [1] D. M. Kochmann and K. Bertoldi. Exploiting Microstructural Instabilities in Solids and Structures: From Metamaterials to Structural Transitions. *Applied Mechanics Review*, **69**: 050801, 2017.
- [2] N. Nadkarni, C. Daraio, R. Abeyaratne, and D. M. Kochmann. Universal energy transport law for dissipative and diffusive phase transitions. *Physical Review B*, **93**: 104109, 2016.
- [3] M. J. Frazier and D.M. Kochmann. Atomimetic mechanical structures with nonlinear topological domain evolution kinetics. *Advanced Materials*, **29**: 1605800, 2017.
- [4] Rafsanjani and D. Pasini. Bistable auxetic mechanical metamaterials inspired by ancient geometric motifs. *Extreme Mechanics Letters*, **9**: 291–296, 2016.

REPRESENTATION THEOREM FOR VISCOELASTIC WAVES WITH A NON-SYMMETRIC STIFFNESS MATRIX

Luděk Klimeš

Department of Geophysics, Faculty of Mathematics and Physics, Charles University,
Ke Karlovu 3, 121 16 Praha 2, Czech Republic, <http://sw3d.cz/staff/klimes.htm>

Keywords: viscoelastic media, stiffness tensor, wave propagation, Green function, representation theorem, reciprocity relation

The $3 \times 3 \times 3 \times 3$ complex-valued frequency-domain stiffness tensor (elastic tensor, tensor of elastic moduli) $c^{ijkl} = c^{ijkl}(x^m, \omega)$ is symmetric with respect to the first pair of indices, $c^{ijkl} = c^{jikl}$, and with respect to the second pair of indices $c^{ijkl} = c^{ijlk}$. It is thus frequently expressed in the form of the 6×6 stiffness matrix which lines correspond to the first pair of indices and columns to the second pair of indices.

In an elastic medium, it was proved that the stiffness tensor is symmetric with respect to the exchange of the first pair of indices and the second pair of indices, $c^{ijkl} = c^{klij}$. The 6×6 stiffness matrix is thus symmetric in an elastic medium.

However, the above mentioned proof does not apply to a viscoelastic medium. Analogously to [5], we thus consider viscoelastic waves with a *non-symmetric stiffness matrix*, $c^{ijkl} \neq c^{klij}$. The *frequency-domain ray theory* in question is described in [4]. Here we derive the corresponding representation theorem. Refer to [3] for more details. For the sake of better correspondence, the equations are labelled here according to [3].

Viscoelastodynamic equation in the frequency domain

The anisotropic viscoelastodynamic equation for the displacement in the frequency domain reads

$$[c^{ijkl}(\mathbf{x}, \omega) u_{k,l}(\mathbf{x}, \omega)]_{,j} + \omega^2 \rho(\mathbf{x}) u_i(\mathbf{x}, \omega) + f^i(\mathbf{x}, \omega) = 0 \quad . \quad (9)$$

The Einstein summation over repetitive lower-case Roman indices is used hereinafter. If the definition volume for viscoelastodynamic equation (9) is not infinite, we assume homogeneous boundary conditions according to [1], box 2.4.

The frequency-domain Green function for a viscoelastic medium is the solution of equation

$$[c^{ijkl}(\mathbf{x}, \omega) G_{km,l}(\mathbf{x}, \mathbf{x}', \omega)]_{,j} + \omega^2 \rho(\mathbf{x}) G_{im}(\mathbf{x}, \mathbf{x}', \omega) + \delta_m^i \delta(\mathbf{x} - \mathbf{x}') = 0 \quad , \quad (10)$$

analytical with respect to the inverse Fourier transform. The partial derivatives are related to variable \mathbf{x} .

Representation theorem

Analogously to [2], eq. 12, we define *complementary medium* $\tilde{c}^{ijkl}(\mathbf{x}, \omega) = c^{klij}(\mathbf{x}, \omega)$ corresponding to the transposed stiffness matrix.

We define the frequency-domain *complementary Green function* $\tilde{G}_{km}(\mathbf{x}, \mathbf{x}', \omega)$ as the frequency-domain Green function in the complementary medium,

$$[c^{klij}(\mathbf{x}, \omega) \tilde{G}_{km,l}(\mathbf{x}, \mathbf{x}', \omega)]_{,j} + \omega^2 \rho(\mathbf{x}) \tilde{G}_{im}(\mathbf{x}, \mathbf{x}', \omega) + \delta_m^i \delta(\mathbf{x} - \mathbf{x}') = 0 \quad . \quad (13)$$

We first derive the *provisional representation theorem* as the relation between the frequency-domain wave field $u_i(\mathbf{x}, \omega)$ in the given medium and the frequency-domain complementary Green function $\tilde{G}_{im}(\mathbf{x}, \mathbf{x}', \omega)$. We consider volume V which is the subset of the definition volume for viscoelastodynamic equation (9) and need not contain the support of force density $f^i(\mathbf{x}, \omega)$. We multiply equation

(13) for the frequency–domain complementary Green function by $u_i(\mathbf{x}, \omega)$, subtract the product of the frequency–domain viscoelastodynamic equation (9) with $\tilde{G}_{im}(\mathbf{x}, \mathbf{x}', \omega)$, integrate over volume V , and after simple conversions arrive at [3]

$$u_m(\mathbf{x}', \omega) = \int_V d^3\mathbf{x} \left\{ \tilde{G}_{im}(\mathbf{x}, \mathbf{x}', \omega) f^i(\mathbf{x}, \omega) - [\tilde{G}_{im,j}(\mathbf{x}, \mathbf{x}', \omega) c^{ijkl}(\mathbf{x}, \omega) u_k(\mathbf{x}, \omega)]_{,l} + [\tilde{G}_{im}(\mathbf{x}, \mathbf{x}', \omega) c^{ijkl}(\mathbf{x}, \omega) u_{k,l}(\mathbf{x}, \omega)]_{,j} \right\} . \quad (16)$$

We apply the divergence theorem to the integral of the gradients and obtain the provisional representation theorem [3],

$$u_m(\mathbf{x}', \omega) = \int_V d^3\mathbf{x} \tilde{G}_{im}(\mathbf{x}, \mathbf{x}', \omega) f^i(\mathbf{x}, \omega) + \oint_{\partial V} d^2\mathbf{x} \left[\tilde{G}_{im}(\mathbf{x}, \mathbf{x}', \omega) n_j(\mathbf{x}) c^{ijkl}(\mathbf{x}, \omega) u_{k,l}(\mathbf{x}, \omega) - \tilde{G}_{im,j}(\mathbf{x}, \mathbf{x}', \omega) c^{ijkl}(\mathbf{x}, \omega) u_k(\mathbf{x}, \omega) n_l(\mathbf{x}) \right] , \quad (17)$$

where $n_i(\mathbf{x})$ is the unit normal to the surface ∂V of volume V pointing outside volume V .

For $f^i(\mathbf{x}, \omega) = \delta_n^i \delta(\mathbf{x} - \mathbf{x}'')$, the above equation yields $u_m(\mathbf{x}', \omega) = G_{mn}(\mathbf{x}', \mathbf{x}'', \omega)$. Integrating over the whole definition volume, we obtain *reciprocity relation*

$$G_{mn}(\mathbf{x}', \mathbf{x}'', \omega) = \tilde{G}_{nm}(\mathbf{x}'', \mathbf{x}', \omega) \quad (18)$$

between the frequency–domain Green function and the frequency–domain complementary Green function.

We now insert reciprocity relation (18) into provisional representation theorem (17), and obtain the final version of the *representation theorem*:

$$u_m(\mathbf{x}', \omega) = \int_V d^3\mathbf{x} G_{mi}(\mathbf{x}', \mathbf{x}, \omega) f^i(\mathbf{x}, \omega) + \oint_{\partial V} d^2\mathbf{x} \left[G_{mi}(\mathbf{x}', \mathbf{x}, \omega) n_j(\mathbf{x}) c^{ijkl}(\mathbf{x}, \omega) u_{k,l}(\mathbf{x}, \omega) - G_{mi,j}(\mathbf{x}', \mathbf{x}, \omega) c^{ijkl}(\mathbf{x}, \omega) u_k(\mathbf{x}, \omega) n_l(\mathbf{x}) \right] . \quad (19)$$

The integral over volume V represents the wave field corresponding to the sources situated inside volume V . The integral over the surface ∂V of volume V represents the wave field corresponding to the sources situated outside volume V , and is zero if all sources are situated inside volume V .

Acknowledgement

The research has been supported by the Grant Agency of the Czech Republic under contract 16-05237S, and by the members of the consortium “Seismic Waves in Complex 3–D Structures” (see “<http://sw3d.cz>”).

References

- [1] K. Aki, P. Richards. *Quantitative Seismology*. W.H. Freeman & Co, San Francisco, 1980.
- [2] E.O. Kamenetskii. Nonreciprocal microwave bianisotropic materials: Reciprocity theorem and network reciprocity. *IEEE Trans. Antennas Prop.*, **49**: 361–366, 2001.
- [3] L. Klimeš. Representation theorem for viscoelastic waves with a non–symmetric stiffness matrix. *Seismic Waves in Complex 3–D Structures*, **27**: 93–96, 2017, online at “<http://sw3d.cz>”.
- [4] L. Klimeš. Frequency–domain ray series for viscoelastic waves with a non–symmetric stiffness matrix. *Stud. geophys. geod.*, **62**: 421–431, 2018.
- [5] C.J. Thomson. Complex rays and wave packets for decaying signals in inhomogeneous, anisotropic and anelastic media. *Stud. geophys. geod.*, **41**: 345–381, 1997.

GEOMETRIC RAY TRACING APPLIED TO TIME REVERSED ACOUSTICS

Jan Kober^{1*}, Milan Chlada¹ and Radovan Zeman^{1,2}

¹Institute of Thermomechanics AS CR, v.v.i., Prague, Czech Republic; e-mail: kober@it.cas.cz

²Faculty of Nuclear Sciences and Physical Engineering, The Czech Technical University, Prague, Czech Republic;

Keywords: time reversed acoustics, ray tracing, wave propagation

Time reversed acoustics (TR) allows focusing of elastic waves in time and space based on recorded forward propagation response [1]. The method takes advantage of complicated wave propagation including reflections and scattering in order to direct backpropagating waves to their original source. Apart from FEM simulations commonly used for wave propagation simulations, ray based approach allows us to have “a look under the hood” and trace each partial contribution to TR reconstruction individually. This is especially useful when analyzing general principles of TR.

The theory of TR is using Green functions to describe the wave propagation from the source to a sensor. When considering that the wave propagation takes place along a certain wave paths – rays, the Green function degenerates to a sum of delta functions with delays corresponding to arrival times of particular rays. In this work a simple geometric method was used to compute the arrival times of rays. Our method is applicable only for rectangular (or cuboid) geometry and acoustic waves but that does not compromise its usability for TR analysis, since the principles of TR are independent of those restrictions. The way in which are the arrival times computed, is sketched in Fig. 1a. The whole procedure is based on a construction of a grid of virtual sensors which are mirror images of the real sensor with respect to the edges of the specimen. The model is used to explain the temperature effects on TR focusing or time reversal of continuous sources.

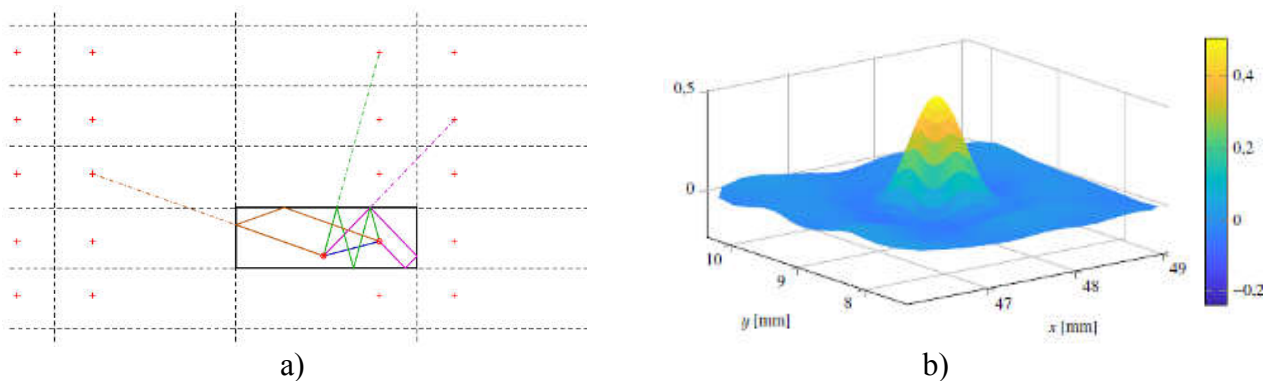


Figure 1: a) Ray construction by creating a grid of virtual sensors. b) An example of resulting TR focusing.

Acknowledgement

This work was supported by the grant project GACR 17-22615S of the Czech Grant Agency and by Institute of Thermomechanics CAS under support RVO: 61388998.

References

- [1] M. Fink, D. Cassereau, A. Derode, et al., Time-reversed acoustics, *Reports Prog. Phys.* 63: 1933–1995, 2000
- [2] Z. Prevorovsky, J. Kober, Some factors affecting time reversal signal reconstruction, *Phys. Procedia* from ICU Metz, 2015.

A LOCAL TIME STEPPING FOR DISCONTINUOUS WAVE PROPAGATION IN A HETEROGENEOUS BAR

Radek Kolman^{1,*}, Sang Soon Cho², K.C. Park³, José A. González⁴,
Arkadi Berezovki⁵, Petr Hora⁶ and Vítězslav Adámek⁷

¹Institute of Thermomechanics, The Czech Academy of Sciences, Prague, Czech Republic; e-mail: kolman@it.cas.cz

²Korea Atomic Energy Research Institute, Daejeon, Korea; e-mail: sscho96@kaist.ac.kr

³University of Colorado at Boulder, Boulder, Co, USA; e-mail: kcpark@colorado.edu

⁴Universidad de Sevilla, Sevilla, Spain; e-mail: japerez@us.es

⁵Tallinn University of Technology, Tallinn, Estonia; e-mail: arkadi.berezovski@cs.ioc.ee

⁶Institute of Thermomechanics, CAS, v.v.i., Pilsen, Czech Republic; e-mail: hora@cdm.it.cas.cz

⁷New Technologies for the Information Society, University of West Bohemia, Pilsen, CZ; e-mail: vadamek@kme.zcu.cz

Keywords: wave propagation, heterogeneous and functionally graded bars, explicit time integration, finite element method, local time stepping, spurious oscillations.

At this time, additive technology is acceptable as a technology for manufacturing of complex bodies with complicated shapes and various and advanced properties as smart materials, where conventional technologies are not possible to use for manufacturing. One could find applications of 3D printed bodies in mechanical, biomechanical or aerospace engineering and in many others. For that reason, understanding to wave processes in heterogeneous, layered and functionally graded materials is important issue [1]. Based on this knowledge, heterogeneous bodies under dynamic and shock loading can be designed to hold optimal properties for real applications with respect to utilization, termo-mechanical behaviours, lifetime, cost and so on.

Wave propagation problems in graded elastic bars has been studied in [2]. The accurate modelling of discontinuous wave propagation in elastic heterogeneous bodies is still an open problem in numerical methods. In the context of the numerical modelling, complications arise from spurious stress oscillations, different wave speed in each material point, varying local stability conditions with obvious consequences on the discretization scheme, and dispersion errors. The numerical methods currently used comprise the finite volume method [3], spectral methods, higher order discontinuous Galerkin formulation, the graded finite element method [4] and many others. In this paper, we adopted the Park's scheme with pullback time integration presented in [5]. In this method, the local stepping algorithm with respect to local wave speed and local stability condition at each material point is employed [6].

1 Wave propagation in graded bar with linear distribution of elastic modulus

We study discontinuous wave propagation in a graded bar with the linear distribution of elastic modulus and constant mass density. The analytical solution of the problem can be found in [7]. The length of the bar is $L = 1$ m. In this test, the mass density is chosen as $\rho = 1$ kg/m³. The elastic modulus on the left side of the bar is $E_1 = 1$ Pa and on the right side it is set as $E_2 = 0.25$ Pa. The bar is loaded on the left side by the Heaviside pulse with the stress amplitude as $\sigma_0 = 1$ Pa. Results of numerical solution of the elastic wave propagation problem in the graded elastic bar are presented in Fig. 1 for time $T = 0.75$ s obtained by the analytical solution [7], semi-analytical solution with the numerical inverse Laplace transformation [8], the finite volume method [3], the finite element method with explicit time integration by the central difference method, the finite element method with the Park's method with and without the local time stepping [6]. For FEM and FVM, the time step size was set as a minimum value of local stable time steps over all elements/cells.

In the numerical test, the presented explicit scheme with local time stepping produces results with improving spurious oscillations in the finite element method. We observed only cusps on wavefront of stress discontinuities. Further, the improvement of stress spurious oscillations is evident with comparison of the scheme with and without local time stepping, because the local stepping time process respects local critical time step size at each material point.

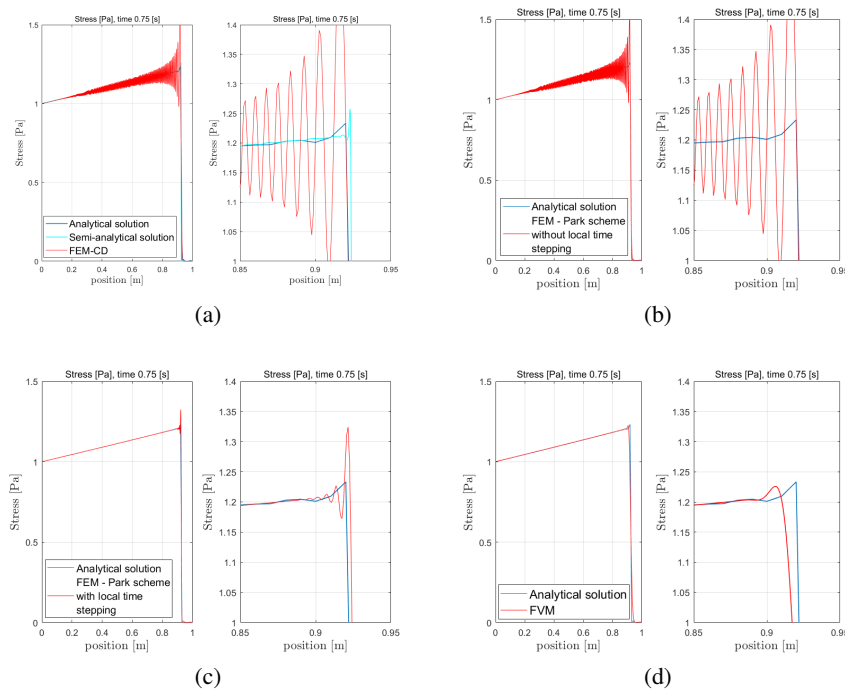


Figure 1: Stress distributions in a graded bar obtained by a) FEM with the central difference method (CD), b) FEM with the Park method without local time stepping, c) FEM with the Park method with local time stepping, and d) FVM.

Acknowledgement The work of was supported by the Centre of Excellence for Nonlinear Dynamic Behaviour of Advanced Materials in Engineering CZ.02.1.01/0.0/0.0/15_003/0000493 (Excellent Research Teams) in the framework of Operational Programme Research, Development and Education, and also by the grant project with No. 17-22615S of the Czech Science Foundation (CSF) within institutional support RVO: 61388998.

References

- [1] F. Ebrahimi, *Advances in Functionally Graded Materials and Structures*. InTech, 2016.
- [2] T.-C. Chiu, F. Erdogan. One-dimensional wave propagation in a functionally graded elastic medium. *Journal of Sound and Vibration*, **222**: 453–487, 1999.
- [3] A. Berezovski, J. Engelbrecht, G.A. Maugin. *Numerical Simulation of Waves and Fronts in Inhomogeneous Solids*, World Scientific Pub Co Inc., 2008.
- [4] J.-H. Kim, G. H. Paulino. Isoparametric graded finite elements for nonhomogeneous isotropic and orthotropic materials. *Journal of Applied Mechanics*, **69**:502–514, 2002.
- [5] K.C. Park, S.J. Lim, H. Huh. A method for computation of discontinuous wave propagation in heterogeneous solids: basic algorithm description and application to one-dimensional problems. *International Journal of Numerical Methods and Engineering*, **91**(6): 622–643, 2012.
- [6] R. Kolman, S.S. Cho, K.C. Park, J.A. González, A. Berezovski, P. Hora, V. Adánek. A method with local time stepping for computation of discontinuous wave propagation in heterogeneous solids: Application to one-dimensional layered problems and unstructured meshes. To appear *International Journal for Numerical Methods in Engineering*, 2018.
- [7] R. Brepta R, I. Huněk. *Pohyb pulzu v tenké tyči s proměnlivým modulem pružnosti*. Technická zpráva Z1032/87, Ústav termomechaniky ČSAV, 1987.
- [8] V. Adánek, F. Valeš, J. Červ. Numerical Laplace inversion in problems of elastodynamics: Comparison of four algorithms. *Advances in Engineering Software*, **113**: 120–129, 2017.

ACOUSTIC ENERGY FOCUSING IN ROBOCAST CERAMIC SCAFFOLDS

Martin Koller^{1,2,*}, Alena Kruisová³, Hanuš Seiner⁴, Petr Sedlák⁵, Benito Román-Manso⁶,
Pilar Miranzo⁷, Manuel Belmonte⁸ and Michal Landa⁹

¹Institute of Thermomechanics of the CAS, v.v.i., Prague, Czech Republic; e-mail: koller@it.cas.cz

²Faculty of Nuclear Sciences and Physical Engineering, Czech Technical University in Prague, Czech Republic

³Institute of Thermomechanics of the CAS, v.v.i., Prague, Czech Republic; e-mail: alena@it.cas.cz

⁴Institute of Thermomechanics of the CAS, v.v.i., Prague, Czech Republic; e-mail: hseiner@it.cas.cz

⁵Institute of Thermomechanics of the CAS, v.v.i., Prague, Czech Republic; e-mail: psedlak@it.cas.cz

⁶School of Engineering and Applied Sciences, Harvard University, Cambridge, MA, USA;
e-mail: romanmanso@seas.harvard.edu

⁷Institute of Ceramics and Glass (ICV-CSIC), Madrid, Spain; e-mail: pmiranzo@icv.csic.es

⁸Institute of Ceramics and Glass (ICV-CSIC), Madrid, Spain; e-mail: mbelmonte@icv.csic.es

⁹Institute of Thermomechanics of the CAS, v.v.i., Prague, Czech Republic; e-mail: ml@it.cas.cz

Keywords: ceramic scaffolds, robocasting, acoustic energy focusing, phononic crystals, frequency band gaps

The use of additive manufacturing (AM) has rapidly grown in the recent years, as the AM techniques are capable of the fabrication of samples with complex geometries. Robocasting is an AM method, in which ceramic scaffolds consisting of thin ceramic rods are produced by layer-by-layer printing of the corresponding ceramic-based pseudoplastic ink. The ceramic powder is mixed with water and organic additives to create a printable ink with highly shear-thinning behavior, and this ink is then extruded through a nozzle following a predefined printing pattern. After drying and burning-out of the organic additives, the ceramic scaffolds are densified by using the spark plasma sintering (SPS) technique, leading to the structure consisting of well-interconnected fully sintered ceramic rods.

In this work, the acoustic properties of different patterned robocast silicon carbide (SiC) scaffolds are studied. All of them had a parallel orientation of the ceramic rods in the same layer, and they differed in mutual orientation of the rods in the neighboring layers, leading to several types of material symmetry. For tetragonal scaffolds, the rods in each layer were perpendicular to the rods of the neighboring layers, and for hexagonal scaffolds, the angle between the orientations of the rods of the neighboring layers was 60°. Moreover, two orthorhombic scaffolds were produced, one had two different in-plane spacings between the rods, and the other had the rods inclined of 46° angle to the rods in the neighboring layers.

The acoustic properties of the ceramic scaffolds were obtained by utilizing finite element method (FEM) modeling [1]. For each scaffold, a computational unit cell with the geometric parameters of the sintered scaffolds was designed. Then, tensile and shear straining modes were applied, and the full set of elastic coefficients was determined by FEM. The distributions of phase velocity, slowness vector, and group velocity vector were obtained from the Christoffel's equation.

The tetragonal scaffolds were shown to focus the acoustic energy along the rods, as the group velocity vector lies along the rods for the most of the wave propagation directions in the plane parallel to the orientation of the rods. The acoustic energy focusing is more pronounced for the sample with higher in-plane spacing between the rods. Similar effect was observed also for the orthorhombic scaffold with two different in-plane spacings between the rods, having the higher group velocity in the direction with denser arrangement of the rods.

On the other hand, the hexagonal scaffolds exhibited in-plane isotropy due to their highest level of macroscopic material symmetry among the studied scaffolds. Nevertheless, the calculation of velocity distribution was made from the set of elastic coefficients by the assumption of a homogeneous medium with an effective density given by the scaffold geometry. Therefore, these results correspond to a low-frequency limit, where the wavelengths are much higher than the principal dimensions of the scaffolds. When the wavelengths become comparable to the spacings between the rods, some level of acoustic energy focusing can be expected. Thus, the FEM model was also utilized for dynamic calculations of the wave vector dependence on the wave frequency. It is shown that the acoustic energy becomes more focused along the ceramic rods with increasing frequency even in the hexagonal scaffolds.

The robocast ceramic scaffolds also exhibited phononic crystal behavior, as it was shown in [2]. The transmission of longitudinal waves was measured through the robocast scaffolds placed between piezoelectric transducers. The longitudinal pulses with nominal frequencies from 1 to 12 MHz were sent along one of the directions of the ceramic rods and the amplitudes of the received signal were analyzed. Moreover, FEM modeling was also utilized to calculate eigenfrequencies for a given set of wave vectors, in order to identify eigenmodes with dominant longitudinal component. The frequency band gaps calculated by FEM, e.g. the frequencies where there is no eigenmode with dominant longitudinal components, very well correspond to the frequencies, at which the measured amplitudes of the transmitted longitudinal wave signal were very low. Thus, it is shown that these robocast SiC scaffolds exhibit frequency band gaps in MHz range.

Acknowledgement

This work was supported by Czech Science Foundation grant No. 17-01618S, and by Spanish Project MAT2015-67437-R (MINECO, FEDER, UE).

References

- [1] A. Kruisová, H. Seiner, P. Sedlák, M. Landa, B. Román-Manso, P. Miranzo, M. Belmonte. Acoustic metamaterial behavior of three-dimensional periodic architectures assembled by robocasting. *Applied Physics Letters*, **105**: 211904, 2014.
- [2] A. Kruisová, M. Ševčík, H. Seiner, P. Sedlák, B. Román-Manso, P. Miranzo, M. Belmonte, M. Landa. Ultrasonic bandgaps in 3D-printed periodic ceramic microlattices. *Ultrasonics*, **82**: 91–100, 2018.

TEMPORAL-SPATIAL DISPERSION ERRORS IN FEM MODELLING OF WAVE PROPAGATION AND IMPLICIT TIME INTEGRATION

Alena Kruisová^{1,*}, Radek Kolman¹ and Jiří Plešek¹

¹Institute of Thermomechanics AS CR, v.v.i., Prague, Czech Republic; e-mail: {alena;kolman;plesek}@it.cas.cz

Keywords: dispersion errors, finite element method, implicit time integration

The dispersion of propagated waves is a dependency of a phase velocity on its frequency or wavenumber. The finite element method (FEM) [1] shows this dispersive behaviour [2]. The phenomenon originates from the replacement of continuous variables with their discrete counterparts. During the modelling of elastic wave propagation in solids by the finite element method, the solution is influenced by both the spatial and temporal dispersion errors caused by discretizations in space and in time, see e.g. [2].

Here the regular two-dimensional mesh assembled from four-noded bilinear and eight-noded quadratic serendipity square elements was studied with the size of an element H for plane strain condition. The spatial dispersion errors of such elements are studied in [3] with results, that the difference between the calculated phase velocity and theoretical one in continuum is less than 2% in the case when the wavelength λ is modelled by at least three quadratic elements, i.e. $H/\lambda < 1/3$, or by ten bilinear elements, i.e. $H/\lambda < 1/10$.

Additional dispersion errors are caused by the temporal discretization during the direct time integration. The error estimation for explicit time integration method is given in [4]. Similarly the dispersion errors for the implicit time integration methods are established here. The most well known implicit time integration methods are those from the Newmark family, [5]. The work is limited to method without numerical damping with the parameter $\gamma = 1/2$, namely the average acceleration method with the parameter $\beta = 1/4$, the linear acceleration method with $\beta = 1/6$ and Fox-Goodwin method with $\beta = 1/12$. The dispersion properties were determined in the similar way as in [4]. The non-dimensional angular wave velocity $\bar{\omega}_i$ of the propagated wave is [6]

$$\bar{\omega}_i = \frac{2}{C} \arcsin \sqrt{\frac{\Lambda_i C^2 c_0^2}{4\beta \lambda_i C^2 c_0^2 + 4c_1^2}}, \quad i = 1, 2, \dots, N_c \quad (1)$$

where $C = \Delta t c_1 / H$ is the Courant number representing the non-dimensional time step size, Δt is the time step size, c_0 is the wave speed in a bar, c_1 is the wave speed of the longitudinal wave for plane strain condition, and Λ_i are the eigenvalues for grid dispersion computations, see ([4]). N_c is the number of dispersion branches. During assembling the matrices for the eigenvalue problem the consistent mass matrix was employed.

For the average acceleration method with $\gamma = 1/2$ and $\beta = 1/4$, the dispersion errors of the numerical phase velocity are depicted in polar diagrams in Fig. 1. For different Courant numbers, the dispersion errors of the phase velocity of the shear wave (red line) and longitudinal wave (blue line) modes are given for bilinear (left) and quadratic (right) elements. For quadratic elements some spurious optical modes appear. Black lines show the values of the phase velocity of the shear (smaller circle) and longitudinal (bigger circle) waves in continuum. The dispersion polar diagrams for the linear acceleration method are shown in Fig. 2. The plots shown in Fig. 1 and 2 enable us to estimate the dispersion errors during the transient dynamic calculations.

Acknowledgement

This work was supported by the grant project 17-22615S of the Czech Grant Agency within the institutional support RVO: 61388998 and by the Centre of Excellence for Nonlinear Dynamic Behaviour of Advanced Materials in Engineering CZ.02.1.01/0.0/0.0/15_003/0000493 (Excellent Research Teams) in the framework of Operational Programme Research, Development and Education.

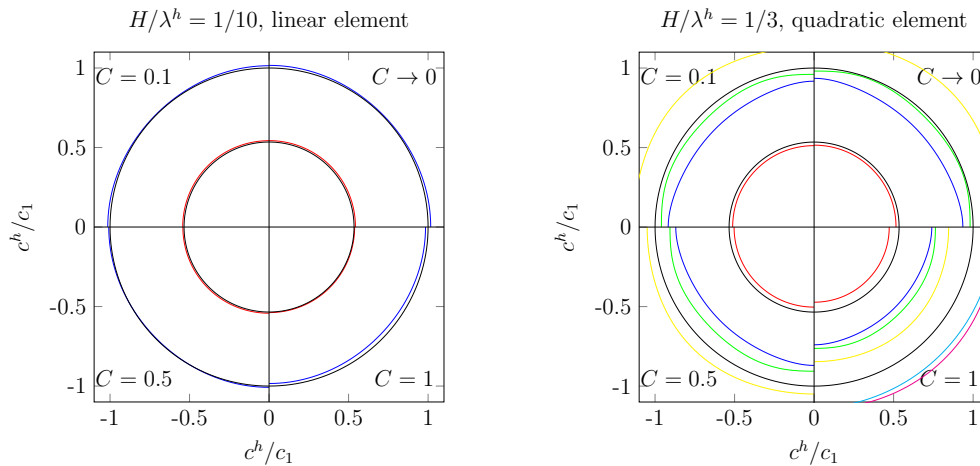


Figure 1: Dispersion errors on the phase velocity for the average acceleration method.

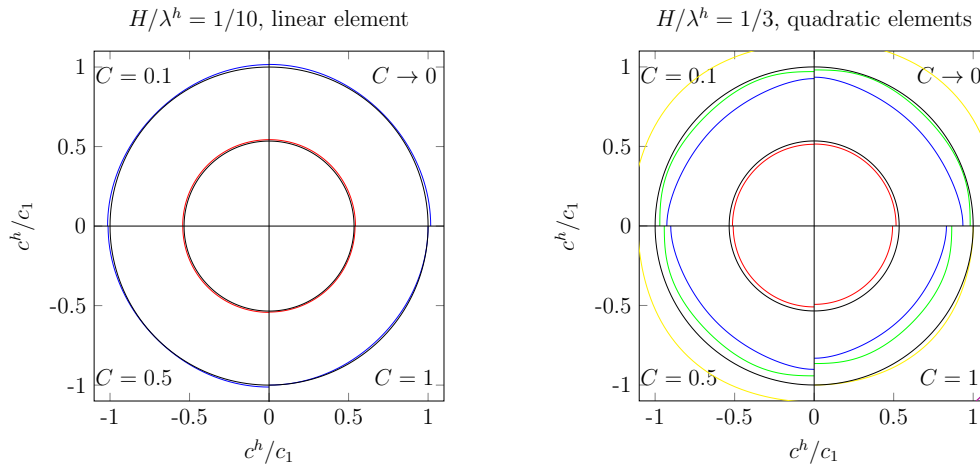


Figure 2: Dispersion errors on the phase velocity for the linear acceleration method.

References

- [1] T.J.R. Hughes. *The Finite Element Method: Linear Static and Dynamic Finite Element Analysis*. Dover Publications, New York, 2000.
- [2] R. Mullen and T. Belytschko. Dispersion analysis of finite element semidiscretizations of the two-dimensional wave equation. *International Journal for Numerical Methods in Engineering*, **18**: 11–29, 1982.
- [3] R. Kolman et al. Grid dispersion analysis of plane square biquadratic serendipity finite elements in transient elastodynamics. *International Journal for Numerical Methods in Engineering*, **96**: 1–28, 2013.
- [4] R. Kolman et al. Temporal-spatial dispersion and stability analysis of finite element method in explicit elastodynamics. *International Journal for Numerical Methods in Engineering*, **106**: 113–128, 2016.
- [5] N. Newmark. A method of computation for structural dynamics. *Journal of the Engineering Mechanics Division*, **85**: 67–94, 1966.
- [6] A. Krusova et al. Temporal-spatial dispersion of finite element method in implicit elastodynamics. *International Journal for Numerical Methods in Engineering*, under preparation

EIGENFREQUENCY ANALYSIS OF ELASTIC STRUCTURES UNDER HEAVY FLUID LOADING BY MEANS OF THE BI-ORTHOGONALITY RELATIONS

L.S. Ledet¹, S.V. Sorokin^{2*}

¹Department of Materials and Production, Aalborg University, Fibigerstraede 16, Aalborg, 9220, Denmark; e-mail: lsl@mp.aau.dk

²Department of Materials and Production, Aalborg University, Fibigerstraede 16, Aalborg, 9220, Denmark; e-mail: svl@mp.aau.dk

Keywords: bi-orthogonality relations, multi-modal waveguides, eigenfrequencies

The bi-orthogonality relations [1-2] are known as a robust tool for solving forcing problems for infinite and semi-infinite waveguides, which support infinitely many free waves. The canonical examples are the Rayleigh-Lamb problem for a semi-infinite elastic layer exposed to the edge excitation [3] and formulation of Green's matrix for a cylindrical shell filled with a compressible inviscid fluid [4]. These relations allow to find the modal amplitudes independently upon each other and to control convergence very easily. Such an efficiency is achieved due to exploiting the oddness/evenness properties of generalised displacements and forces, which are, following [2,4,5], divided into the Class A and Class B functions.

Remarkably, the bi-orthogonality relations, although formulated for free waves in unbounded symmetric waveguides, can be used for accurate prediction of eigenfrequencies of finite structures, and this is the subject of intended presentation. In the cases, when boundary conditions are formulated consistently with the Class properties, eigenfrequencies may be found directly from the inspection of dispersion diagrams. In the cases of an 'inconsistent' formulation of boundary conditions (i.e., then functions belonging to different Classes are involved) a simple method is proposed to accelerate convergence of numerically found eigenfrequencies to their exact values.

The technicalities of eigenfrequency analysis by means of the bi-orthogonality relations are illustrated in elementary examples, where exact solutions are available. Then two advanced problems (the eigenfrequency analyses of a finite membrane backed by a layer of compressible fluid and of a finite segment of a thin elastic cylindrical shell filled with a compressible fluid) are solved and the differences between the cases of 'consistent' and 'inconsistent' boundary conditions are highlighted and explained.

References

- [1] W.B. Fraser. Orthogonality relation for the Rayleigh-Lamb modes of vibration of a plate. *Journal of Acoustical Society of America*, **59**: 215-216, 1976.
- [2] S.V. Sorokin. On the bi-orthogonality conditions for multi-modal elastic waveguides. *Journal of Sound and Vibration* **332**: 5606-5617, 2013.
- [3] B. Karp. Generation of symmetric Lamb waves by non-uniform excitations *Journal of Sound and Vibration* **312**: 195-209, 2008.
- [4] L.S. Ledet, S.V. Sorokin. Bi-orthogonality relations for fluid-filled elastic cylindrical shells: Theory, generalisations and application to construct tailored Green's matrices. *Journal of Sound and Vibration* **417**: 315-340, 2018.
- [5] D. Mead. Wave propagation and natural modes in periodic systems: II. Multi-coupled systems with and without damping. *Journal of Sound and Vibration* **40**: 19-39, 1975.

NUMERICAL SIMULATION OF ULTRASONIC TIME REVERSAL ON DEFECTS IN CARBON FIBRE REINFORCED POLYMER

Martin Lints^{1,*}, Andrus Salupere², Serge Dos Santos³

¹Tallinn University of Technology, Tallinn, Estonia; e-mail: martin.lints@cens.ioc.ee

²Tallinn University of Technology, Tallinn, Estonia; e-mail: salupere@ioc.ee

³INSA CVL Blois, France; e-mail: serge.dossantos@insa-cvl.fr

Keywords: contact acoustic nonlinearity, time reversal, ultrasonics

This work considers detection of defects in reinforced polymer materials by using nonlinear ultrasonic spectroscopy. Carbon Fibre Reinforced Polymer (CFRP) is increasingly used in safety-critical applications, where its performance needs to be closely monitored. In contrast, the monitoring can be difficult due to its complex internal structure. Furthermore, its possible defect models are disadvantageous to ultrasonic Non-Destructive Testing (NDT). Therefore novel signal processing methods need to be used to detect smaller than wavelength defects in CFRP.

We are using the Time Reversal – Nonlinear Elastic Wave Spectroscopy (TR-NEWS) [2, 7] and delayed TR-NEWS [5] signal processing methods to detect the sources of nonlinearities, such as contact acoustic nonlinearities [1, 4, 6], by focusing the ultrasonic wave energy into the defect to “activate” the nonlinearity. The studies use finite element method simulations, which analyse the wavefield at sensors and inside the material. The parameters are chosen to simulate physical experiments of ultrasonic TR-NEWS for NDT of CFRP.

TR-NEWS is a reciprocal time reversal method: the transmitting and receiving sensors are dedicated and do not switch roles. Figure 1 shows the simulation model, which is a 2D model of a CFRP plate with one transmitting shear wave transducer and one receiving plane wave transducer. The left and right sides of the model have absorbing boundary conditions to simulate a large plate where the wave energy is not contained. The defect is situated between the transmitter and receiver but not in close proximity of either. This simulates an NDT test of a CFRP plate where the location of the defect is unknown.

The goal is to analyse the applicability of the TR-NEWS and delayed TR-NEWS methods for detecting nonlinearities in the global sense, i.e. detecting a defect which is not directly under the ultrasonic transducer, but somewhere else in the object. To do this, the nonlinear signature of the defect needs to be detected in the received TR-NEWS signal and then used to focus the ultrasonic wave energy on the defect [3]. Thus the suitability of the TR-NEWS signal processing method is studied for possible applications in NDT and structural health monitoring.

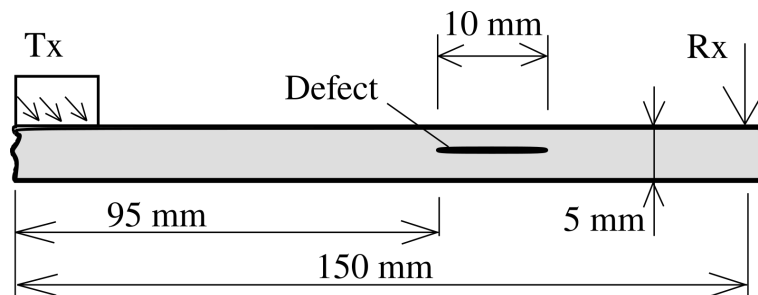


Figure 1: Schematic of the carbon fibre reinforced polymer plate in the 2D simulation.

References

- [1] P. P. Delsanto, editor. *Universality of Nonclassical Nonlinearity: Applications to Non-Destructive Evaluations and Ultrasonics*. Springer, 2006.
- [2] S. Dos Santos, Z. Dvořáková, M. Caliez, and Z. Převorovský. Nonlinear time reversal signal processing techniques applied to acousto-mechanical imaging of complex materials. *J. Acoust. Soc. Am.*, 138(3):1835–1835, 2015.
- [3] T. Goursolle, S. Dos Santos, O. Bou Matar, and S. Callé. Non-linear based time reversal acoustic applied to crack detection: Simulations and experiments. *Int. J. Non-Linear. Mech.*, 43(3):170 – 177, 2008. 11th International Workshop on Nonlinear Elasticity in Materials.
- [4] M. Griffa, B. E. Anderson, R. A. Guyer, T. J. Ulrich, and P. A. Johnson. Investigation of the robustness of time reversal acoustics in solid media through the reconstruction of temporally symmetric sources. *J. Phys. D: Appl. Phys.*, 41(8):085415, 2008.
- [5] M. Lints, S. Dos Santos, and A. Salupere. Solitary Waves for Non-Destructive Testing Applications: Delayed Nonlinear Time Reversal Signal Processing Optimization. *Wave Motion*, 71:101–112, 2017.
<http://dx.doi.org/10.1016/j.wavemoti.2016.07.001>.
- [6] I. Y. Solodov, N. Krohn, and G. Busse. CAN: an example of nonclassical acoustic nonlinearity in solids. *Ultrasonics*, 40(1):621–625, 2002.
- [7] T. J. Ulrich, A. M. Sutin, R. A. Guyer, and P. A. Johnson. Time reversal and non-linear elastic wave spectroscopy (TR NEWS) techniques. *Int. J. Non-Linear Mech.*, 43(3):209–216, 2008.

PARALLEL TDNNS-FEM FOR ELASTODYNAMICS OF THIN-WALLED STRUCTURES

Dalibor Lukáš^{1,*}, Lukáš Malý¹, Erika Straková¹, and Joachim Schöberl²

¹VŠB-Technical University of Ostrava, Czech Republic; e-mails: {dalibor.lukas,lukas.maly,erika.strakova}@vsb.cz

²Vienna University of Technology, Austria; e-mail: joachim.schoeberl@tuwien.ac.at

Keywords: TDNNS mixed finite elements, elastodynamics, shear locking, spectral elements, domain decomposition

When modelling elasticity of thin-walled structures, the standard finite element method (FEM) suffers from the shear locking effect meaning that convergence deteriorates when refining the discretization. The reason is a bad aspect ratio of the geometry under consideration. Besides other methods such as various plate and shell models a remedy is the mixed finite element method searching simultaneously for displacements u and stresses σ . It relies on a weak setting of the Hellinger-Reissner formulation

$$\begin{cases} \int_{\Omega} A^{-1} \sigma : \tau + \int_{\Omega} \operatorname{div} \tau \cdot u = 0 & \forall \tau, \\ \int_{\Omega} \operatorname{div} \sigma \cdot v - \rho \int_{\Omega} \frac{\partial^2 u}{\partial t^2} \cdot v = 0 & \forall v, \end{cases} \quad (1)$$

where ρ is the density, $:$ stands for the Frobenius inner product and $\tau(x), v(x)$ denote the stress and displacement test functions, respectively, where $\tau_n(x) = 0$ on $\partial\Omega$. The first equation in (1) represents the Hooke's law, the second equation describes the Newton (force equilibrium) law. The key point is choosing proper regularity of the stresses and displacements. In the standard mixed setting one lets the displacements piecewise discontinuous and the stresses are symmetric tensors with continuous normal components. However, a known stable finite element discretization over tetrahedra [1] leads to 162 DOFs per element. Here we follow another approach of Joachim Schöberl and Astrid Pechstein (born Sinwel) [2, 3] who chose tangential-continuous displacements and normal-normal-continuous stresses, which leads to a tetrahedral finite element of only 36 DOFs. The method is referred to as TDNNS.

In [3] prismatic anisotropic elements allowing for discretizations of thin structures are proposed and analyzed. In [4] we propose novel prismatic hexahedral elements with 2 DOFs per edge, 4 DOFs per vertical face and 2 (bubble) DOFs per element as far as displacements are considered. Concerning stresses we have 9 DOFs per face and 70 (bubble) DOFs per element. We can get rid of the large amount of stress bubbles by hybridization so that the (face, normal-normal) continuity of stresses is broken and reinforced again by Lagrange multipliers, which act as normal displacements. Therefore we end up in the following purely displacement finite element:

- 2 DOFs per edge representing tangential displacements,
- 4 DOFs per vertical face representing tangential displacements,
- and 9 DOFs per (both vertical and horizontal) face representing normal displacements.

By means of solution to a quasiperiodic eigenvalue problem on a single layered-element we confirm that the finite element convergence rate is independent of the thickness. At the same time a very few (often one) layers of elements in the thickness direction suffices to cover all elastic guided waves up to ultrasonic frequencies, see Fig. 1.

In this paper we propose parallel solution methods to the arising linear systems of ordinary differential equations. We employ two methods: spectral finite elements [5] and domain decomposition. The former makes use of the tensor-product structure and employs L^2 -orthogonal basis so that the mass matrix in an explicit time stepping scheme is diagonal. However, the number of time steps can be large. This is why we also employ implicit time schemes and improve bad conditioning of the arising

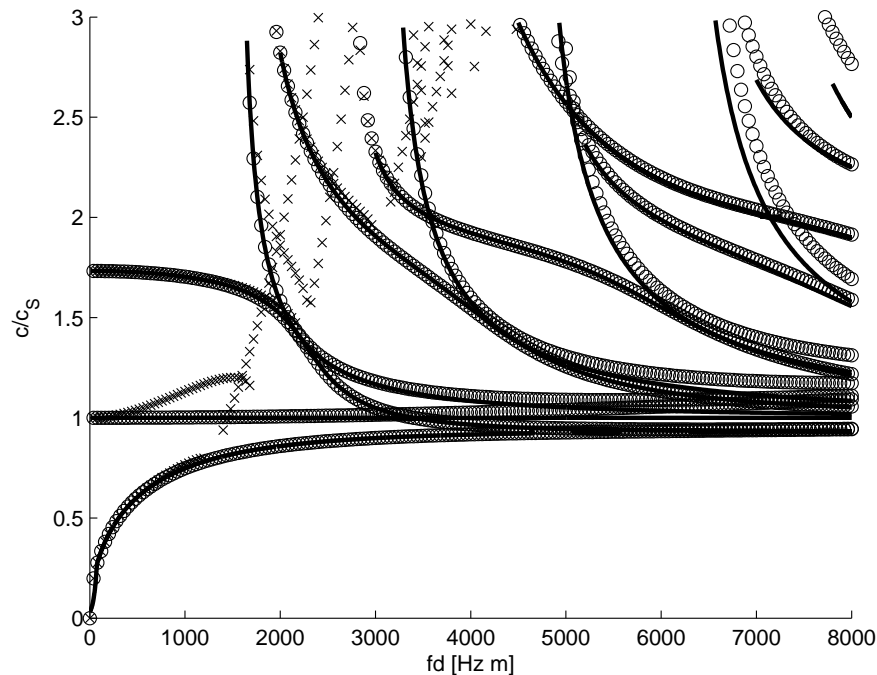


Figure 1: Dispersion analysis (dependence of velocity on the frequency-times-thickness) of elastic guided waves in a 1 mm thin aluminium plate discretized into 5 layers of elements. Analytical theory (solid lines), discretization step $h := 1$ mm (crosses) and $h := 0.1$ mm (circles).

systems by means of domain decomposition methods. We are experienced with Schur complement methods [6], where we solve local problems on subdomains, local problems on pairs of subdomains, and a global coarse problem. Iterative solution to such preconditioned systems leads to number of iterates that are only logarithmically dependent on the number of elements per subdomain interface.

Acknowledgement

This work was supported by the Czech Science Foundation under the project 17-22615S.

References

- [1] S. Adams, B. Cockburn. A mixed finite element method for elasticity in three dimensions. *Journal of Scientific Computing* **25**(3):515–521, 2005
- [2] A. Pechstein, J. Schöberl. Tangential-displacement and normal-normal-stress continuous mixed finite elements for elasticity. *Mathematical Models and Methods in Applied Sciences* **21**(8):1761–1782, 2011
- [3] A. Pechstein, J. Schöberl. Anisotropic mixed finite elements for elasticity. *International Journal for Numerical Methods in Engineering* **90**(2):196–217, 2012
- [4] D. Lukáš, J. Schöberl, L. Malý. Dispersion analysis of displacement-based and TDNNS mixed finite elements for thin-walled elastodynamics. Submitted.
- [5] D. Komatitsch, J.-P. Vilotte. The spectral element method: An efficient tool to simulate the seismic response of 2d and 3d geological structures. *Bulletin of the Seismological Society of America* **88**(2):368–392, 1998
- [6] D. Lukáš, J. Bouchala, P. Vodstrčil, L. Malý. 2-dimensional primal domain decomposition theory in detail. *Applications of Mathematics* **60**(3):265–283, 2015

INFLUENCE OF TEMPERATURE IN COMPUTATIONAL TIME REVERSAL METHOD

Michal Mračko^{1,*}, Radek Kolman¹, Jan Kober¹, Zdeněk Převorovský¹ and Jiří Plešek¹

¹Institute of Thermomechanics of the CAS, v. v. i., Dolejšková 1402/5, 182 00, Praha 8, Czech Republic
e-mail: {mracko, kolman, kober, zp, plesek}@it.cas.cz

Keywords: Time reversal method, elastic wave propagation, temperature influence

Time reversal (TR) method uses backward wave propagation for refocusing and reconstruction of the original source, see e.g. [2] or [3]. This method can be employed in non-destructive testing (NDT) for localization of cracks, imperfections or defects in materials. The TR process, from the perspective of NDT, consists of two steps. In the first step – the Frontal task, a real body is loaded at the given place with the defined loading signal and a response is recorded in a prescribed position of the body. In the second step – the Reversal task, this responding signal is reversed in time and loaded into the computational model so as to locate so called scatterers (e.g. cracks). In computational TR method, both steps are performed numerically. Nonetheless, here we focus on refocusing and reconstruction of the original source.

For numerical solution, we use the linear finite element method, see [1], with the lumped mass matrix and one-point Gauss integration rule. For direct integration in time the explicit central difference scheme is employed. This integration scheme is conditionally stable and reversible in time, see [3].

In this paper, we model a situation when temperature changes around several degrees of Celsius in between the frontal and the reversal problem. Even though the change in shape can be neglected, the change in elastic parameters plays an important role, see e.g. [4], and this small temperature variation has to be taken into account in real applications of TR, because the local wave speed changes. We simulate the change of temperature by modifying Young’s modulus E to make our study dependent only on one parameter. The change of E reflects in the change of the longitudinal wave speed as $c_L = \sqrt{\frac{E}{(1-\nu^2)\rho}}$. In the Table 1, the values of c_L and E for particular tasks are presented.

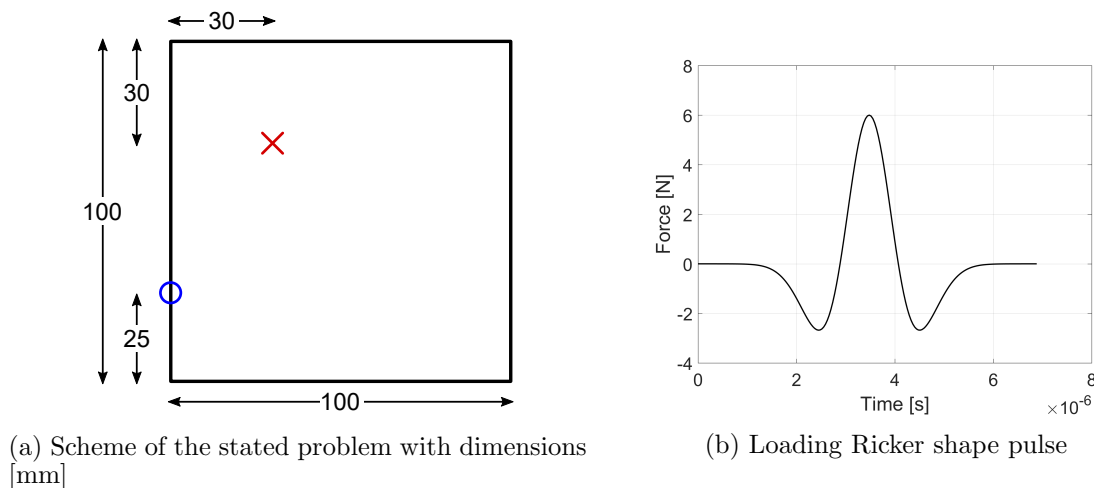


Figure 1: Scheme of the problem and the loading pulse

We consider a two-dimensional domain under a plane stress condition with stress-free boundary conditions. Dimensions of the domain of interest are depicted in Figure 1a. In the Frontal task, the position "X" shows the location of the loading signal and the position "O" shows the place of recording of the response. In the Reversal task, these points are swapped. Figure 1b shows the loading signal.

Number of task	Decrease of c_L in %	c_L [ms^{-1}]	E [Pa]
Reversal task 0	0.00	5 291.265	$2.0000 \cdot 10^{11}$
Reversal task 1	0.01	5 290.735	$1.9996 \cdot 10^{11}$
Reversal task 2	0.02	5 290.206	$1.9992 \cdot 10^{11}$
Reversal task 3	0.05	5 288.619	$1.9980 \cdot 10^{11}$
Reversal task 4	0.08	5 287.032	$1.9968 \cdot 10^{11}$
Reversal task 5	0.10	5 285.974	$1.9960 \cdot 10^{11}$

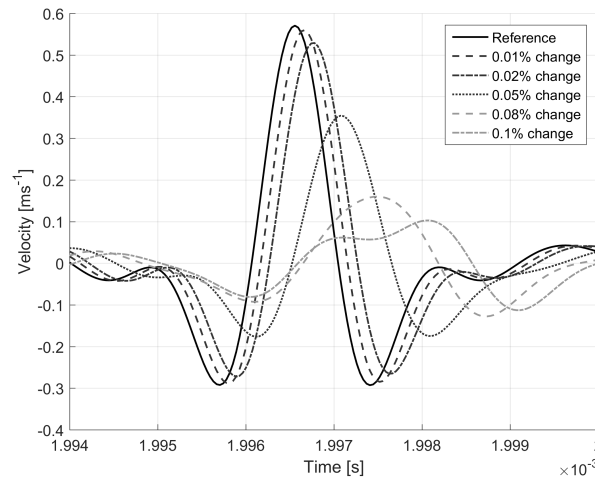
Table 1: Change of longitudinal wave speed c_L and Young’s modulus E in case studyFigure 2: Reconstruction of the original pulse for decreased longitudinal velocities c_L

Figure 2 shows the reconstructed pulses for particular decreased longitudinal wave speeds. It is apparent that for values over 0.05% of c_L decrease, the reconstructed signal becomes hardly distinguishable. Roughly estimated, a 0.1% decrease of c_L corresponds to an increase of temperature for 15 °C.

Acknowledgement

The work of M. Mračko and J. Plešek was supported by the European Regional Development Fund under Grant No. CZ.02.1.01/0.0/0.0/15 003/0000493 (Centre of Excellence for Nonlinear Dynamic Behaviour of Advanced Materials in Engineering). The work of J. Kober, R. Kolman and Z. Převorovský was supported by the grant project CSF with No. 17-22615S within institutional support RVO:61388998.

References

- [1] K.-J. Bathe. *Finite Element Procedures*, Prentice Hall, 2012.
- [2] M. Fink, D. Cassereau, A. Derode, C. Prada, P. Roux, J.-L. T. Tanter, F. Wu. Time-reversed acoustics. *Reports on Progress in Physics*, **63**: 1933–1995, 2000.
- [3] D. Givoli, E. Turkel. Time reversal with partial information for wave refocusing and scatterer identification. *Computer Methods in Applied Mechanics and Engineering*, **213**: 223–242, 2012.
- [4] Z. Převorovský, J. Kober. Some Factors Affecting Time Reversal Signal Reconstruction. *Physics Procedia*, **70**: 604–608, 2015.

DEFECT INDUCED METASTABILITY AND POWER UNIVERSALITY OF WAVE FRONTS IN SHOCKED CONDENSED MATTER

Oleg Naimark

Institute of Continuous Media Mechanics UB RAS, Russia; e-mail: naimark@icmm.ru

Keywords: nonlinear defects kinetics, metastability, power universality, shock wave fronts

Metastable states in condensed matter with defects. Defects kinetics is analyzed as specific type of the criticality in out-of-equilibrium system “condensed matter with defects” – the structural-scaling transition [1]. Theoretical and experimental study is devoted to mechanisms of structural relaxation caused by different types of metastable states in condensed matter with defects, strain instability and damage-failure transition in a wide range of load intensities. It is shown that the "decomposition" of the metastable states is accompanied by the origin of multi-scale collective modes of mesodeflects ensembles (microshears, microcracks) described by the kinetics of two structural variables - defect density tensor having a sense of deformation due to defects, and structural scaling parameter, which characterizes the current susceptibility of material to the defect initiation and growth and represents the mean ratio of the spacing between defects and the size of defects. Defect induced mechanisms of structural relaxation are linked to the generation of different types of the collective modes of defects, that have the nature of self-similar solutions: auto-solitary waves providing the multiscale plastic strain localization and blow-up dissipative structures responsible for the damage localization kinetics. Dynamics of excitation and evolution of collective modes are linked to the mechanisms of instability and failure in condensed matter with defects and used to explain the original experiments.

Universality of wave fronts in shocked condensed matter. The subjection of the mechanisms of defect induced structural relaxation to solitary wave self-similar solution in the metastability area allowed the explanation of the power universality of plastic wave fronts [2]. Such a front propagates without changing its form (in the self-similar coordinates) due to a stable balance between competitive processes governed by nonlinearly of stress-strain dependence and dissipative (viscous) properties of a medium [3].

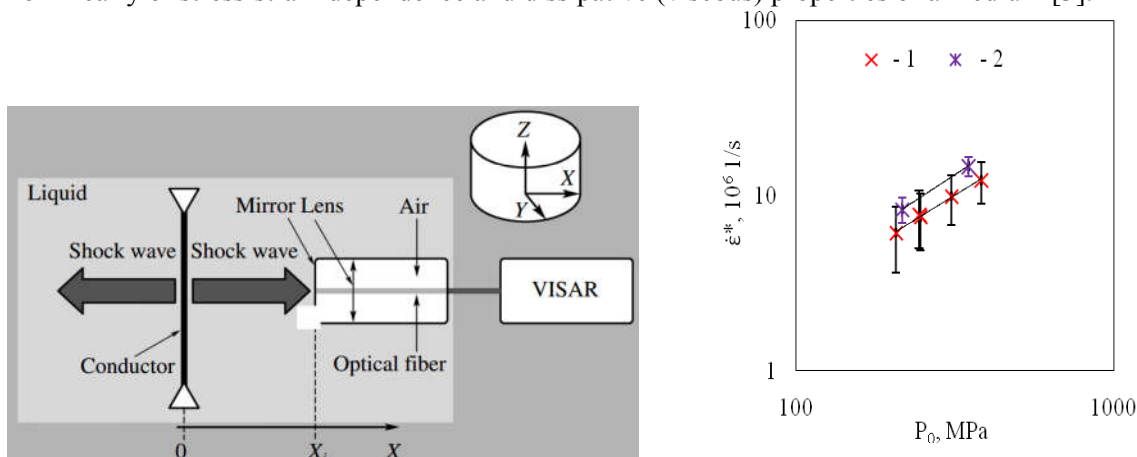


Figure 1: Explosive wire initiation of shock wave in liquids (a). Strain rate versus pressure amplitude at shock wave front (b) (1 - silicone oil; 2 - transformer oil, 18 °C).

The self-similarity of wave fronts was studied in shock-loaded liquids [4]. A copper wire was exploded in a cylindrical chamber to initiate a compression wave in liquid. The mass velocity at different distances from the wire was measured using the VISAR system with a fiber optic gage. It was found that the dependence

$\dot{\epsilon}^*(P_0)$ has a power-law form with an exponent equal to 3.2, which turned out to be close to the values established for metals, and points to the self-similar character of the shock front profile.

These results allow us to justify the assumption that in the range of strain rates (10^5 – 10^7 1/s), non-Newtonian behavior can be associated with the mechanisms of momentum transfer characteristic for plastic flow. Power law of the shock wave rise in liquid are analogous to plastic wave fronts in solids [2,3] and reflect the self-similar character of the momentum transfer in this range of load intensities. This confirms the assumption concerning the mechanisms of momentum in the range of strain rates 10^5 – 10^7 1/s due to "coordinated motion of groups of molecules" [5, 6] that is kinematically the equivalent to the plastic shears.

These data make it possible to conclude that the fluids under corresponding pressure range have relaxation times $\tau > \dot{\epsilon}^{*-1} \sim 10^{-5}$ s that differ by 6 orders of magnitude from the molecular (diffusion) relaxation times, the evaluation of which can be obtained on the basis of the Einstein formula $\tau_D = \Delta^2 / 6D_{sd} \sim 10^{-11}$ s, where Δ is the distance between particles, D_{sd} is the self-diffusion coefficient [7].

Acknowledgement

This work was supported by the RFBR grant n.17-0100867_a.

References

- [1] O.B.Naimark. Defect Induced Transitions as Mechanisms of Plasticity and Failure in Multifield Continua. In *Advances in Multifield Theories of Continua with Substructure*, G. Capriz and P. Mariano (eds), Birkhäuser, Boston, 75-114, 2004.
- [2] O.B.Naimark. Some regularities of scaling in plasticity, fracture and turbulence. *Physical Mesomechanics*, **19**: 307-318, 2016.
- [3] J.W Swegle. and D.E. Grady. Shock viscosity and the prediction of shock wave rise times, *J. Appl. Phys.*, **58**: 692–701, 1985.
- [4] I.A Bannikova et al. An experimental study of non-Newtonian properties of water under electroexplosive loading, *Technical Physics Letters*. **40**: 766-768, 2014.
- [5] Ya.I.Fraenkel. *Kinetic Theory of Liquid*, Nauka, Leningrad, 1975.
- [6] A.D. Sakharov, R.M. Zaydel, V.N. Mineev, A.G. Oleinik. Experimental study of the stability of shock waves and mechanical properties of substances at high pressures and temperatures. *Soviet Physics-Doklady*, **9**: 1091-1094, 1965
- [7] O.B Naimark. Defect-Induced Instabilities in Condensed Media. *JETP Lett.*, **67**: 751–757, 1998.

NUMERICAL SIMULATION OF PLASMA DYNAMICS AND SHOCK-INDUCED RESIDUAL STRESSES IN THE LASER SHOCK PROCESSING OF METALLIC MATERIALS

José L. Ocaña¹, Angel García-Beltrán¹, Ignacio Angulo¹, Francisco Cordovilla¹

¹ UPM Laser Centre. Polytechnical University of Madrid. C/ Alan Turing, 1. 28031 Madrid. SPAIN.
e-mail: jlocana@etsii.upm.es

Keywords: Laser Shock Processing, Plasma Dynamics, Shock Waves, Material Behaviour Models, Residual Stresses

Laser Shock Processing is based on the application of a high intensity pulsed laser beam ($I > 1 \text{ GW/cm}^2$; $t < 50 \text{ ns}$) at the interface between the metallic target and the surrounding medium (a transparent confining material, normally water) forcing a sudden vaporization of the metallic surface into a high temperature and density plasma that immediately develops inducing a shock wave propagating into the material.

When its peak pressure is greater than the dynamic yield limit of the material, the shock wave is engineered to induce plastic deformation and a residual stress distribution in the target material. The material is also heated by the thermal flux generated upon laser material interaction and by the plastic deformation work. This can produce a deleterious effect due thermal stress relaxation and tensile stresses generation in a narrow layer under the target free surface which can be of a critical importance from the point of view of the mechanical behaviour of the treated target [1].

The appropriate description of the LSP process must obtain the pressure and the heat source pulses applied at the target surface from the complex laser–plasma interaction process in the first steps of the treatment.

Provided the large amount of physical phenomena arising in the considered processes, the corresponding modelling, including the formation of a vapour/plasma phase, the generally far from equilibrium ionization-recombination processes in this plasma, its thermos-fluid-dynamic behaviour under extreme pressure and temperature conditions (typically leading to pressure/shock waves) and other related effects, require a deep understanding of the physics underlying their development, and appears as absolutely needed for the reliable predictive assessment of the material evolution under irradiation.

The appropriate description of the LSP process requires a three level description providing the adequate interconnection of the data obtained in each phase in a self-consistent way from the physical point of view. The referred three-level description includes:

- i) Analysis of the plasma electronic population dynamics, including consideration of breakdown phenomenology in dielectric media,
- ii) Simulation of the hydrodynamic phenomenology arising from plasma expansion between the confinement layer and the base material
- iii) Analysis of the propagation and induction of permanent structural changes by shock wave evolution in bulk material

A simulation model (SHOCKLAS), dealing with the main aspects of LSP modelling in a coupled way, has been developed by the authors [1,2]. A scheme with the different codes and their relations with input and output variables is shown in Fig. 1 (adapted from [2]).

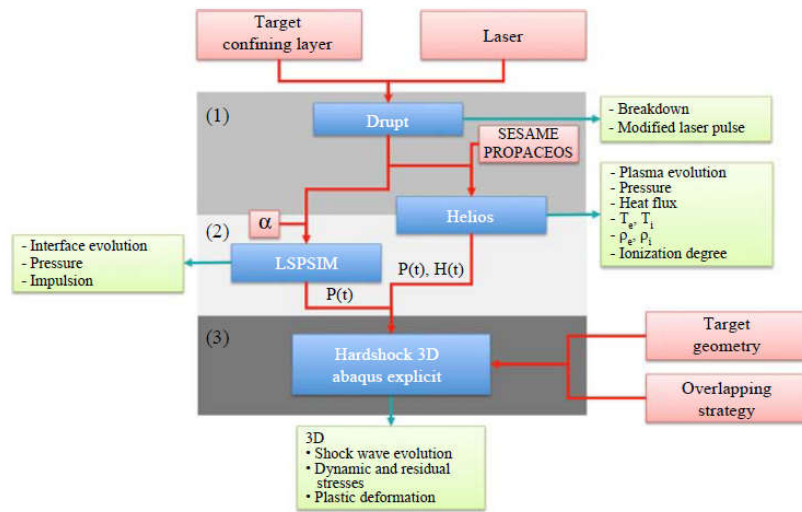


Fig. 1. Calculational scheme of the developed system SHOCKLAS

For the description of the Laser-Plasma Interaction, the 1-D HELIOS radiation-hydrodynamics code [2] is used to simulate the evolution of the plasma density, temperature, hydrodynamic velocity and ionization degree in order to obtain the temporal evolution of the pressure and thermal waves applied to the treated solid material.

For the analysis of the behaviour of the solid target material subject to these waves, a FEM based solid behaviour model (HARDSHOCK 3D) with fitted material dependent deformation and hardening constants is applied. The code solves the shock propagation problem into the solid material, with specific consideration of the material response to alterations induced by the thermal and mechanical interaction (i.e. effects as elastic-plastic behaviour). The temperature evolution is also computed in a consistent way.

With the aid of the SHOCKLAS calculational system, key results have been obtained on the parametric evaluation of experimental conditions to be applied for a successful induction of compressive residual stresses fields in technologically relevant materials as different Al and Ti alloys and several stainless steels. In the application of the code, involving the consideration of deformation rates exceeding 10^6 s^{-1} , the provision for the appropriate material behaviour constants has also needed to be accomplished.

In the present contribution, characteristic results of the application of the SHOCKLAS calculational system are presented showing its appropriateness for the proper modelling of LSP treatments along with new developments in the modelling of the materials behaviour at the involved extremely high deformation rates.

Acknowledgement

Work partially supported by MINECO (Spain; Project MAT2015-63974-C4-2-R)

References

- [1] M. Morales, J.A. Porro, M. Blasco, C. Molpeceres, J.L. Ocaña: Numerical simulation of plasma dynamics in laser shock processing experiments. *Applied Surface Science*, **255**, 5181–5185 (2009)
- [2] M. Morales, C. Correa, J.A. Porro, C. Molpeceres, J.L. Ocaña: Thermomechanical Modelling of Stress Fields in Metallic Targets subject to Laser Shock Processing. *International Journal of Structural Integrity*, **2**, 51-61 (2011)

TOWARD NUMERICAL REALIZATION OF SPLIT-HOPKINS PRESSURE BAR: A FONDEST HOPE BY A COMPUTATIONAL MECHANICIAN

K. C. Park

University of Colorado, Department of Aerospace Engineering Sciences and Center for Aerospace Structures,
Boulder, CO 80309; e-mail: kcpark@colorado.edu

Keywords: wave propagation, dynamic material properties, numerical split-Hopkins bar

This talk presents an overview of recent advances in capturing wave front tracking simulation capabilities and leverage them in paving a way toward realization of numerical split-Hopkins bar. To this end, we first identify prerequisites for a numerical split-Hopkins bar, and survey several notable advances in high-fidelity numerical simulation of tracking discontinuous waves propagating through linear and nonlinear materials. We have found that a numerical split-Hopkins bar must employ a judicious combination of nano , micro and continuum-scale wave treatment strategies. In particular, accurately capturing energy exchanges among vastly different wave lengths constitute a key element for the successful development of a numerical split-Hopkins bar.

Research needs for realizing numerical split-Hopkins bar are listed in a hierarchical levels and this presenter's sincere hope is that this community addresses research issues identified in the present study.

References

- [1] https://en.wikipedia.org/wiki/Split-Hopkinson_pressure_bar
- [2] H.Kolsky, An Investigation of the Mechanical Properties of Materials at Very High Rates of Loading, Proc. Phys. Soc. London, B62, (1949), p.676.

ON EQUIVALENCE OF THE STRESS AND DISPLACEMENT FORMULATION OF THE RAYLEIGH WAVES PROPAGATION PROBLEM IN TWO-DIMENSIONAL COMPOSITE MATERIAL

Slavomír Parma^{1,*}, Jan Červ¹ and Jiří Plešek¹

¹Institute of Thermomechanics of the CAS, Prague, Czech Republic; e-mail: {parma, cerv, plesek}@it.cas.cz

Keywords: Wave Propagation, Rayleigh Waves, Secular Equation, Anisotropic Media

There are two frequently used approaches suitable to solve *Rayleigh waves* propagation problem in two-dimensional anisotropic elastic media—the *stress formulation*, which yields an *explicit* secular equation, and the *displacement formulation*, which yields an *implicit* secular equation. In this work, however, the displacement formulation is used and the explicit secular equation is obtained. Further, an equivalence between the stress and displacement formulation is shown.

Let us suppose that material and body axes of two-dimensional orthotropic linear elastic medium are denoted by X_1, X_2 and x_1, x_2 , respectively. The third axis $x_3 = X_3$ is perpendicular to the x_1 – x_2 plane and constitutes an axis of possible rotation of principal material axes X_1, X_2 from body axes x_1, x_2 by the angle ϑ , as shown in Fig. 1. Material obeys Hooke's law in the form

$$\begin{bmatrix} \sigma_{11} \\ \sigma_{22} \\ \sigma_{12} \end{bmatrix} = \begin{bmatrix} C_{11} & C_{12} & C_{16} \\ C_{12} & C_{22} & C_{26} \\ C_{16} & C_{26} & C_{66} \end{bmatrix} \begin{bmatrix} \epsilon_{11} \\ \epsilon_{22} \\ 2\epsilon_{12} \end{bmatrix}, \quad (1)$$

where σ_{ij} are the stress components, ϵ_{ij} are the strain components, and C_{ij} are the elastic stiffness components. As material and body axes do not coincide, a general stiffness matrix is considered [1]. The strain components are given by

$$2\epsilon_{ij} = (u_{i,j} + u_{j,i}) \quad (i, j = 1, 2), \quad (2)$$

where u_i are displacement components. Neglecting body forces, the equation of motion reduces to

$$\sigma_{ij,j} = \rho u_{i,tt} \quad (i, j = 1, 2), \quad (3)$$

where t is the time and ρ is the density of material. The solution of Eq. (3) may be assumed in the form

$$u_i(x_1, x_2, t) = U_i \exp[ik(x_1 - px_2 - vt)] \quad (i, j = 1, 2), \quad (4)$$

where k is a positive wave number, v is the velocity, and $p = iq/k$, where q is a complex-valued attenuation factor. Substituting Eq. (4) into Eq. (3), a non-trivial solution is obtained if and only if

$$\begin{aligned} & [k^2 C_{11} - 2ikqC_{16} - q^2 C_{66} - k^2 \rho v^2] [k^2 C_{66} - 2ikqC_{26} - q^2 C_{22} - k^2 \rho v^2] - \\ & [k^2 C_{16} - ikq(C_{12} + C_{66}) - q^2 C_{26}] [k^2 C_{16} - ikq(C_{12} + C_{66}) - q^2 C_{26}] = 0, \end{aligned} \quad (5)$$

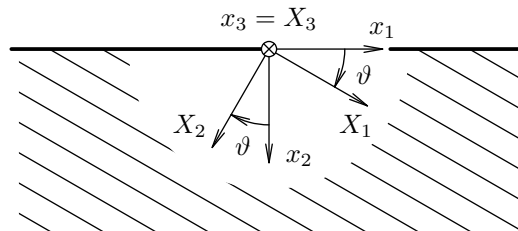


Figure 1: Coordinates defined in a thin semi-infinite orthotropic medium.

which may be rearranged in the form

$$Ap^4 + Bp^3 + Cp^2 + Dp + E = 0, \quad (6)$$

where A , B , C , D , and E are real-valued parameters dependent on ρv^2 and C_{ij} , and that can be found in [2].

As Rayleigh waves are expected to attenuate with depth of media, the displacement field (4) has to obey the *Dirichlet boundary condition* in the form

$$\begin{aligned} \lim_{x_2 \rightarrow +\infty} u_1(x_1, x_2, t) &= 0, \\ \lim_{x_2 \rightarrow +\infty} u_2(x_1, x_2, t) &= 0. \end{aligned} \quad (7)$$

Boundary conditions (7) impose restrictions on the roots of Eq. (6). It can be seen that the fulfilment of Eq. (7) can only be guaranteed by the roots with $\text{Im}(p) < 0$. Let us consider that p_2 and p_4 are such roots of Eq. (6).

The *Neumann boundary condition* for the stress free edge $x_2 = 0$ reads

$$\begin{aligned} \sigma_{22} &= C_{12}\epsilon_{11} + C_{22}\epsilon_{22} + C_{26}2\epsilon_{12}, \\ \sigma_{12} &= C_{16}\epsilon_{11} + C_{26}\epsilon_{22} + C_{66}2\epsilon_{12}. \end{aligned} \quad (8)$$

In paper [2], Eqs. (1)–(8) are used to obtain an implicit secular equation and the equation is solved numerically. In this work, however, it is shown that this system may be used to obtain an explicit secular equation.

Eqs. (1)–(8) yield a system of algebraic equations in variables p_2 , p_4 , and ρv^2 . Employing substitutions $\xi = p_4 p_2$ and $\chi = p_4 + p_2$, after very long algebra one obtains an explicit secular equation in the form

$$ax^4 + bx^3 + cx^2 + dx + e = 0, \quad (9)$$

where $x = \rho v^2$ and coefficients a , b , c , d , and e depend on elastic stiffness components C_{ij} .

Eq. (9) is equivalent to that one obtained by making use of Stroh formalism and reported by Destrade [3]. Thus, this equivalence reveals certain relation between both the stress and displacement formulation.

Acknowledgement

This work was supported by the European Regional Development Fund under Grant No. CZ.02.1.-01/0.0/0.0/15.003/0000493 (Centre of Excellence for Nonlinear Dynamic Behaviour of Advanced Materials in Engineering) and by the Czech Science Foundation under grant No. GA17-22615S.

References

- [1] J. Červ, V. Adámek, F. Valeš and S. Parma. Numerical solution of a secular equation for Rayleigh waves in a thin semi-infinite medium made of a composite material. 22nd International Conference ENGINEERING MECHANICS 2016, Svratka, Czech Republic, May 9–12, 2016.
- [2] J. Cerv and J. Plešek. Implicit and explicit secular equations for Rayleigh waves in two-dimensional anisotropic media. *Wave Motion*, **50**(7): 1105–1117, 2013.
- [3] M. Destrade. Rayleigh waves in symmetry planes of crystals: explicit secular equations and some explicit wave speeds. *Mechanics of Materials*, **35**(9): 931–939, 2003.

CONTROL OF NONLINEAR STRAIN WAVES IN DI-ATOMIC CRYSTALLINE MEDIA

Alexey Porubov^{1,2,*}, Ilya Antonov^{1,2}

¹ Institute of Problems in Mechanical Engineering, Saint Petersburg, Russia
e-mail:alexey.porubov@gmail.com

² Peter the Great St. Petersburg Polytechnic University (SPbPU),
Polytechnicheskaya st., 29, Saint Petersburg, Russia

Keywords: nonlinear wave, control, crystalline lattice

Understanding of the behavior of localized nonlinear strain waves is important from the point of view of durability of materials. Also application of such waves is promising for nondestructive testing provided that these waves keep their form and velocity on propagation. It is known that some balances, like a balance between nonlinearity and dispersion, allow us to support stable propagation of localized waves. Breaking of the balances results in the wave delocalization.

Recently, a method of control of nonlinear waves has been developed [1–3]. The algorithm of a distributed feedback control allows us to achieve the desired profile of a localized wave and its stable propagation with a permanent shape and velocity. According to the method, an extra term is added to the equation under study that provides a tendency to a target function. This function does not necessarily correspond to an analytical solution to the equation.

A natural question arises about the reason of such additional term. For this purpose, a mechanical system has been revealed in [3] where the control terms in the equation for the strain waves in a layer are caused by an external loading of its lateral surfaces. It was found that the form of the control terms depends on kind of the waves to be localized, longitudinal or shear.

The aim of the present study is to find out a similar system for a waveguide whose material has diatomic crystalline structure. The governing equations are obtained in the continuum form using the expression for the strain energy developed in [4]. Then the layer is considered subjected to an external loading. As a result, the coupled nonlinear wave equations are obtained for the functions responsible for a macro-strain and variations in an internal structure. The loading gives rise to the terms that play the role of the feedback control. It is known, that the equations possess localized traveling wave solutions. However, due to a coupling, stable propagation of the localized waves strongly depend not only on the equations coefficients but also on the relative position of the waves for macro-strain and variations in the internal structure. The control allows us to provide the stable propagation of the localized strain waves even in the cases where analytical solution to the coupled equations without control don't exist.

Acknowledgement

The work was performed in IPME RAS, supported by the Russian Science Foundation (grant 14-29-00142).

References

- [1] A.V. Porubov, I.D. Antonov, A.L. Fradkov, and B.R. Andrievsky, Control of localized non-linear strain waves in complex crystalline lattices. *Intern. J. of Non-Linear Mech.*, **86**, 174 - 184, 2016.
- [2] A.V. Porubov, I.D. Antonov, Control of coupled localized nonlinear wave solutions, *Journal of Physics Conference Series*, **788(1)**, 012029, 2017.
- [3] A.V. Porubov, I.D. Antonov, D.A. Indeitsev, and A.L. Fradkov, Mechanical system allowing distributive control with feedback, *Mech. Res. Commun.*, <http://dx.doi.org/10.1016/j.mechrescom.2017.07.014>, 2017.

- [4] A.V. Porubov, Two-Dimensional Modeling of Diatomic Lattice, In: Advances in Mechanics of Microstructured Media and Structures, F. dell'Isola et al. (eds.), Advanced Structured Materials 87, Springer International Publishing AG, part of Springer Nature, 263–272, 2018

ACOUSTIC SOURCE LOCATION BY TIME REVERSAL SIGNAL TRANSFER FROM EXPERIMENT TO NUMERICAL MODEL (DIGITAL TWIN)

Zdenek Prevorovsky^{1*}, Michal Mracko¹, Jan Kober¹, Josef Krofta¹, Radek Kolman¹

¹Institute of Thermomechanics AS CR, v.v.i., Prague, Czech Republic; e-mail: zp@it.cas.cz

Keywords: Elastic waves modelling, time reversal signal transfer, acoustic emission source location

Reliable and relatively precise location of Acoustic Emission (AE) sources is one of the most important inverse problems in nondestructive testing (NDT) and structural health monitoring (SHM) of engineering structures. Standard AE source location procedures often fail in a case of more complicated structures with wave dispersion, propagation velocity or geometry changes, etc. Difficult is also precise location of continuous AE sources like leakage noise. Very effective tool in such situations became some years ago time reversal (TR) signal processing [1]. Time reversal procedure consists of forward propagation, when a source excites the medium and a complex wave field is created, and followed by backpropagation, which results in space time wave focusing and source reconstruction. TR operation can also substantially enhance signal to noise ratio (SNR) and enables planar source location with only one transducer for burst, and two transducers for continuous AE sources [2]. Advantages of TR based source location are in its high precision and elimination of problems connected with dispersion, attenuation, reflections, etc. in relatively simple way. Some complicated signal processing and knowledge of structure geometry and wave celerity is there not necessary.

Disadvantage of that method consists in necessity of detailed scanning the structure surface for searching location of the best source reconstruction (signal maximum). Such scanning can be performed under e.g. by scanning laser interferometer or mechanical scanner. However, more effective solution is TR transfer of detected signal from the real structure onto its numerical model (“digital twin”) and source location in the model [3].

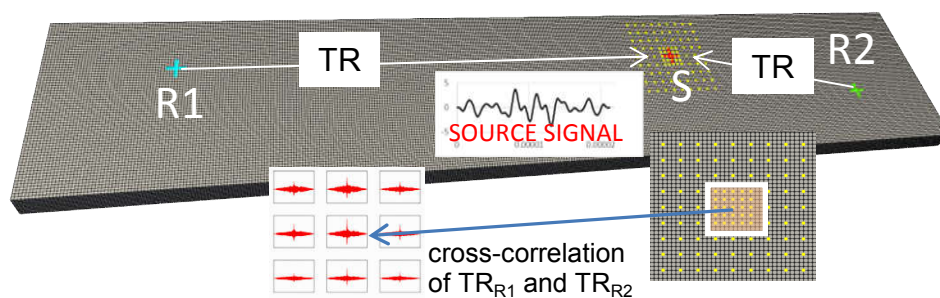


Figure 1: Simulation of continuous AE source location on metallic structure.

Effectivity of such procedure is illustrated in Fig. 1. Simulated continuous AE source (random noise) excites surface of thin metallic stripe (142x24x3 mm) using piezoelectric AE transducer acting as a transmitter (source S). Another two similar transducers are placed on the stripe as signal receivers (R1 and R2). Signals received by transducers R1 and R2 are time-reversed and rebroadcast into the model. Maximum of their cross-correlation define position of the source S.

FEM numerical wave propagation model is used for TR signals transfer from experiments. A proper calibration of numerical model is essential in order to achieve good transferability of signals. Computer model allows better and easier analysis of AE sources and related defects, which has special importance at inaccessible structures like flying aircrafts, satellites, nuclear power plants, etc.

Acknowledgement

This work was supported by the grant project GACR 17-22615S of the Czech Grant Agency and by Institute of Thermomechanics CAS under support RVO: 61388998.

References

- [1] Z.Prevorovsky, J.Krofta, M. Chlada, Z. Farova, V. Kus: Progressive Approaches to Localization and Identification of AE Sources. 30th European Conf. on AE Testing & 7th Internat. Conf. on AE, Granada, Spain, 2012, CD Proc., www.ndt.net/EWGAE-ICAE 2012.
- [2] Z. Prevorovsky, J. Krofta , J. Kober, M. Chlada: Time Reversal Localization of Continuous and Burst Acoustic Emission under Noise Background. Proc. of the 14th Internat. Conf. of the Slovenian Society for NDT “Application of Contemporary NDT in Engineering”, Bernardin, Slovenia, Sept. 4-6, 2017, keynote, pp.3-14.
- [3] Kober J., Dvorakova Z., Prevorovsky Z., Krofta J.: Time reversal transfer: Exploring the robustness of time reversed acoustics in media with geometry perturbations. J. Acoust. Soc. Am., Vol. 138 (1), 2015, EL 49- 53; Doi: 10.1121/1.4922623.

THE GENERALIZATION OF THE MPSM ALGORITHM IN CASE OF C-SCAN FOR THE IMAGE RECONSTRUCTION OF THE DELAMINATION DEFECT IN COMPOSITES

Rejani Sofia^{1*}, Khamlichi Abdellatif² and El Hajjaji Abdellah³

¹Faculty of Sciences, 93000, Tetouan, Morocco; e-mail: sofia.rejjani@gmail.com

²Faculty of Sciences, 93000, Tetouan, Morocco; e-mail: khamlichi7@yahoo.es

³Faculty of Sciences, 93000, Tetouan, Morocco; e-mail: abelhajjaji@yahoo.fr

Keywords: CND, Delamination, composite, C-scan, SAFT, MPSM

The CFR composites that use the carbon fibred as the primary structural components have particular characteristics that make them among the most used for both structural applications and components, in all aircraft and spacecraft. [1] The principal damage of those materials by which defects are created throughout use is impact damage. Distinctive imperfections are produced by this damage are matrix cracking, fiber fractures, and delamination. Therefore it is necessary to inspect such defects before propagating and giving rise to serious accident using nondestructive evaluation by ultrasound.

UT is a sensitive technique and the most successful nondestructive evaluation technique for the inspection of composites materials, the aim objective of this technique is to obtain images having the best possible spatiotemporal resolution. Imaging by ultrasonic testing allows a potential to easily distinguish defects, a closer inspection of the region of interest with high resolution and a specific value in defects diagnosis, evaluation and accuracy. [2]

Considering a C-scan strategy which is conducted over composite panels with the elements fully coupled to the test medium, one of the challenging problems nowadays is producing high resolution images of the scanned parts. This allows by using adequate technique in post-processing of data to perform sizing of a flaw by means of the collected defect indication. For large defects, various methods have been introduced in order to report the size of the flaw.

Considering our case the inspection of delamination defect in composite panels. And the ultrasonic synthetic aperture technique elaborated in frequency domain as the adequate method enabling high resolution imaging at large distances. Especially the algorithm MPSM (Multi-layer phased shift migration) which use the Fourier transform and C-scan matrix in order to obtain the focused image. In this work, the inspection using C-scan strategy is applied followed by the simulation on MATLAB software of the application of the MPSM algorithm to reconstruct the delamination defect in the composite panel. A comparison with simulation of MPSM based on B-scan strategy and simulation of MPSM based on C-scan strategy is adopted.

References

- [1] U.G. Student, Mechanical, B.V.Bhoomaraddi. *Composite Materials in Aerospace Applications*. International Journal of Scientific and Research Publications, Volume 4, Issue 9, September 2014 1 ISSN 2250-3153.
- [2] Li S., Chu T.P. *Super-resolution image reconstruction for ultrasonic nondestructive evaluation*. IEEE Transactions on ultrasonics, ferroelectrics, and frequency control, Volume 60, 2575 - 2585, 2013

HOMOGENIZATION AND BLOCH ANALYSIS OF WAVE DISPERSION IN HETEROGENEOUS FLUID SATURATED POROUS MEDIA

Eduard Rohan^{1,*}, Vu-Hieu Nguyen², Salah Naili²

¹NTIS – New Technologies for Information Society, Faculty of Applied Sciences, University of West Bohemia, Pilsen, Czech Republic; e-mail: rohan@kme.zcu.cz

²Laboratoire Modélisation et Simulation Multi Echelle, Université Paris Est Creteil, MSME UMR 8208 CNRS, Créteil cedex, France

Keywords: Poroelasticity, Biot model, Bloch waves, wave dispersion, homogenization

The mathematical model governing the wave propagation in fluid-saturated porous media (FSPM) made of an elastic solid skeleton whose pores constitute a connected pore network was first proposed by Biot [1]. It is well known that, in (mesoscopically) homogeneous media in \mathbb{R}^n , there are $n + 1$ principle modes of plane waves propagating as the $n - 1$ shear waves (S), fast quasi-compressional waves (P1) and slow quasi-compressional waves (P2), cf. [5], where the homogenization based approach was reported. In this paper, we consider FSPM governed by the Biot model relevant to a mesoscopic scale whereby the material coefficients oscillate with a given spatial period. To analyze the wave propagation in such media, as an alternative to the homogenization based approach, we have derived a formulation based on the Bloch wave decomposition (BWD) which yields a quadratic eigenvalue problem for complex wave numbers within the first Brillouin zone associated with the periodic structure. Using an abstract matrix notation, for a given frequency $\omega \in \mathbb{R}$, the wave numbers \varkappa and generalized polarizations $\mathbf{q} \neq \mathbf{0}$ must satisfy the dispersion equation,

$$[\mathbf{A} + \varkappa^2 \mathbf{S} - \varkappa \mathbf{P} + i\varkappa \mathbf{R} - (i\omega)^{-1} \mathbf{C} - \omega^2 \mathbf{M}] \mathbf{q} = \mathbf{0}, \quad (1)$$

where the matrix $\mathbf{H} := \mathbf{A} + \varkappa^2 \mathbf{S} - \varkappa \mathbf{P} + i\varkappa \mathbf{R}$ and \mathbf{M} are Hermitean (all depending on ω). However, due to the permeability represented by the term $(i\omega)^{-1} \mathbf{C}$, all the wavenumbers are complex.

It turns out that especially the P2 modes are strongly damped, so that is cumbersome to identify them easily using the BWD approach giving dispersion diagrams with many P2-closed modes of different attenuation ratios. Therefore, we suggest to use the homogenized model obtained in [2], further referred to as the simple-porosity (SP) model, as a guide to compare and to identify the particular propagative modes within the dispersion curves computed using the BWD approach. Due to the reconstruction based on the corrector results of the homogenization with fixing a finite characteristic size of the mesoscopic structure (say ε), the wave responses computed by the two approaches can be compared.

For media with high contrasts in the permeability and other poroelastic coefficients, as associated with the two components, the homogenization leads to a double-porosity (DP) model with frequency dependent effective macroscopic parameters [3]. This property amplifies dispersion phenomena [5]. In paper [4], we compared the two above mentioned models (the SP and DP models) with direct finite element simulations of the plane wave propagation in a half-space occupied by the heterogeneous Biot medium. In the present study, an analogous comparison is proposed with respect to the BWD analysis. While the wave responses computed by BWD approach and using the DP models (if the high contrasts are considered) depend on a particular size of the mesoscopic heterogeneities, the SP homogenized model response is invariant with respect to ε , unless the mesoscopic field are to be reconstructed. For illustration, in Fig. 1 we display the phase velocities and the corresponding quality factors computed by the two approaches to the analysis of plane wave propagation in the FSPM (a 2D problem with plane strain conditions). The mesoscopic structure is constituted by the sandstone elliptic inclusions periodically distributed in a rock matrix. The considered characteristic size of the mesoscopic inclusions $\ell = 1\text{mm}$ indicates that the Bloch wave analysis relevant to the first Brillouin zone holds for frequencies below 10^5Hz , whereas it fails for frequencies higher than 0.5MHz (Note that

$v_{\text{ph}} \approx 10^3$ m/s for the P2 wave, which yields the wavelengths $\lambda \approx \ell$ for the frequencies $f \approx 1$ MHz.

In this paper devoted to the dispersion phenomena in the FSPM, we discuss several issues related to the mesoscopic structure, such as presence of two fluids, the role of the stiffness and permeability contrasts, anisotropy and the size effect.

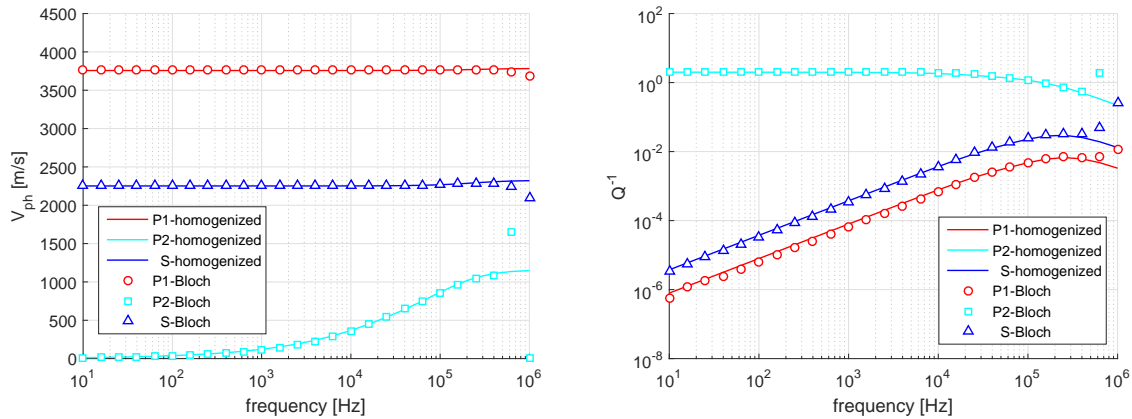


Figure 1: Phase velocities of P1,P2, and S-waves (left) and the corresponding quality factor. Comparison of the BWD approach with the response of the homogenized SP model.

Acknowledgement The research and the conference attendance was supported by the grant projects GACR 17-01618S the Czech Scientific Foundation and, in part, by project LO 1506 of the Czech Ministry of Education, Youth and Sports. A part of the work was done during the Rohan’s stay at the University of Paris-Est with the support of the “Université Paris-Est Créteil” (UPEC).

References

- [1] M.A. Biot. Theory of propagation of elastic waves in a fluid-saturated porous solid. I. Low-frequency range. *J. Acoust. Soc. Am.*, **28** (2): 168–178, 1956
- [2] A. Mielke and E. Rohan. Homogenization of elastic waves in fluid-saturated porous media using the Biot model. *Math. Models and Meth. in Appl. Sci.*, **23**: 873–916, 2013.
- [3] E. Rohan, S. Naili, and V.-H. Nguyen. Wave propagation in a strongly heterogeneous elastic porous medium: Homogenization of biot medium with double porosities. *Comptes Rendus Mecanique*, **344** (6):569–581, 2016.
- [4] E. Rohan, V.-H. Nguyen, and S. Naili. Numerical modelling of waves in double-porosity Biot medium, *Computers & Structures* (In Press), <https://doi.org/10.1016/j.compstruc.2017.09.003>. (2017),
- [5] Eduard Rohan, Vu Hieu Nguyen, and Salah Naili. Dynamics and wave dispersion of strongly heterogeneous fluid-saturated porous media. *Procedia Engineering*, **199**:1507 – 1512, 2017. ISSN 1877-7058. X International Conference on Structural Dynamics, EUROLYN 2017.

INVERSION OF P-WAVE VSP TRAVELTIMES IN ANISOTROPIC MEDIA

Bohuslav Růžek^{1,*}, and Ivan Pšenčík²

¹Institute of Geophysics AS CR, v.v.i., Prague, Czech Republic; e-mail: b.ruzek@ig.cas.cz

²Institute of Geophysics AS CR, v.v.i., Prague, Czech Republic; e-mail: ip@ig.cas.cz

Keywords: anisotropy, inversion, P wave, VSP experiment

Success of traveltimes inversion in anisotropic media depends strongly, among other effects as configuration of an experiment, amount and quality of data, on the selection of the parametrization of the medium and on an efficient forward modelling scheme. We react to these requirements by using the so-called anisotropy parameters, and by using the forward modelling scheme based on the weak-anisotropy approximation. In this approximation, P and S waves are separated and can be treated independently. P-wave attributes are then specified by only 15 anisotropy parameters instead of 21 parameters, which are required when we deal with P and S waves together. We test the proposed inversion scheme on a synthetic VSP (vertical seismic profiling) experiment. From the traveltimes obtained for the VSP configuration, we try to recover the complete set of 15 P-wave anisotropy parameters. From them, we can later estimate the type of the anisotropy, its orientation and values of the parameters in the natural coordinate system, in which anisotropy symmetry elements coincide with coordinate planes and lines.

Anisotropy parameters, which we are using represent a generalization of Thomsen (1986) parameters, which were designed for the parametrization of VTI (transverse isotropy with vertical axis of symmetry) anisotropy. Anisotropy parameters can be used for the specification of anisotropy of arbitrary symmetry, strength and orientation. They represent an alternative to elements of elastic stiffness tensor or to elastic parameters in the Voigt notation. For the definition and more details on anisotropy parameters, see Pšenčík et al., (2018).

For the inversion of P-wave traveltimes, we use an approximate velocity formula based on the first-order weak-anisotropy approximation, whose earlier tests indicated that it provides results of high accuracy even for anisotropy stronger than 20%. Růžek and Pšenčík (2016) showed that the formula is an appropriate choice for the traveltimes inversion of noisy data.

We solve the inverse problem in two ways. In the first, simplified way, the VSP experiment is situated in a homogeneous anisotropic medium. This leads to a linear problem, in which quantities containing the observed data are linearly related to anisotropy parameters. The solution is explicit, one seeks 15 P-wave anisotropy parameters with no need for an iterative solution. Some promising results have already been obtained in this respect, see Růžek and Pšenčík (2016), Pšenčík et al., (2018). In the second way, the VSP experiment is situated in an inhomogeneous anisotropic medium. This leads to a significantly more complicated problem. The problem is non-linear. Instead of one set of 15 P-wave anisotropy parameters as in the previous case, sets of 15 P-wave anisotropy parameters must be sought in a system of grid points.

An example of results of the traveltimes inversion in the VSP experiment situated in a homogeneous orthorhombic medium is shown in Figure 1. The model is a tilted version of orthorhombic medium proposed by Schoenberg and Helbig (1997). We consider the VSP configuration with 4 receivers situated in a borehole at depths of 0.1, 0.4, 0.7 and 1.0 km. There are 50 sources distributed randomly on the surface in the circle of the radius of 1 km around the borehole. “Observed” synthetic P-wave traveltimes are generated by the program package ANRAY (Gajewski and Pšenčík, 1990). Random Gaussian noise of 5% is imposed on the calculated traveltimes. The goal of the inversion is the determination of all 15 P-wave anisotropy parameters, and an approximate reconstruction of the P-wave phase-velocity surface from these parameters. The phase-velocity surface reconstructed from inverted anisotropy parameters is shown in the right plot of Figure 1. The quality of the inversion can be checked by comparison with the phase-velocity surface determined from exact anisotropy

parameters inserted to the same formula (left). Of course, realization of a similar experiment in an inhomogeneous anisotropic medium is considerably more complicated task.

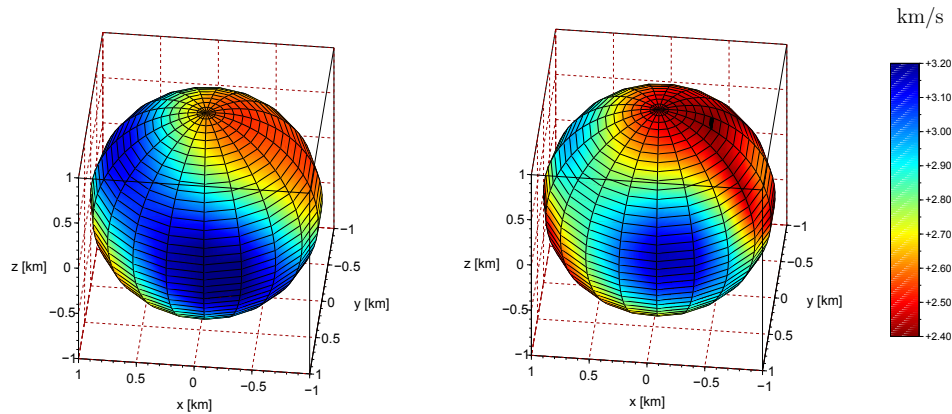


Figure 1: P-wave phase-velocity surfaces calculated from first-order weak-anisotropy approximation of phase-velocity formula. Exact anisotropy parameters are used in the left plot, anisotropy parameters estimated from the inversion are used in the right plot.

Acknowledgement

We are grateful to the Research Project 16-05237S of the Grant Agency of the Czech Republic and the project "Seismic waves in complex 3-D structures" (SW3D) for support.

References

- [1] D. Gajewski, I. Pšenčík. Vertical seismic profile synthetics by dynamic ray tracing in laterally varying layered anisotropic structures. *Journal of Geophysical Research*, **95**: 11301–11315, 1990.
- [2] I. Pšenčík, B. Růžek, T. Lokajíček, T. Svitek. Determination of rock-sample anisotropy from P- and S-wave traveltimes inversion. *Geophysical Journal International*, submitted.
- [3] B. Růžek, I. Pšenčík. P-wave VSP traveltimes inversion in weakly and moderately anisotropic media. *Seismic Waves in Complex 3-D Structures*, **26**: 17–59, 2016, online at <http://sw3d.cz>.
- [4] M. Schoenberg, K. Helbig. Orthorhombic media: Modeling elastic wave behavior in a vertically fractured earth. *Geophysics*, **62**: 1954–1974, 1997.
- [5] L. Thomsen. Weak elastic anisotropy. *Geophysics*, **51**: 1954–1966, 1986.

2D DISCRETE SPECTRAL ANALYSIS AND EMERGENCE OF SOLITONIC STRUCTURES

Andrus Salupere* and Mart Ratas

Department of Cybernetics, School of Science,
Tallinn University of Technology, Tallinn, Estonia; e-mail: salupere@ioc.ee

Keywords: 2D discrete spectral analysis, solitonic structures, KPI equation

Authors of the paper have demonstrated earlier that in case of 1D models of wave propagation the discrete spectral analysis is very helpful tool in order to analyze the space-time behavior of different wave structures [1, 2, 3]. Here the method proposed in [1] is generalized to 2D case. The KPI equation

$$(u_t + \alpha_1 u u_x + \alpha_2 u_{xxx})_x - \alpha_3 u_{yy} = 0, \quad (1)$$

is applied as a model equation. Here α_1 , α_2 and α_3 can be called as the nonlinear coefficient, the dispersion coefficient and the transverse perturbation coefficient, respectively. For numerical integration the pseudospectral method is applied. We demonstrate application of 2D spectral characteristics for analysis of complicated wave structures that can be formed from different banded initial pulses in case of the KPI equation, see [4] for details. Temporal periodicity, temporal symmetry recurrence phenomenon and solitonic character of the solution will be discussed in the presentation.

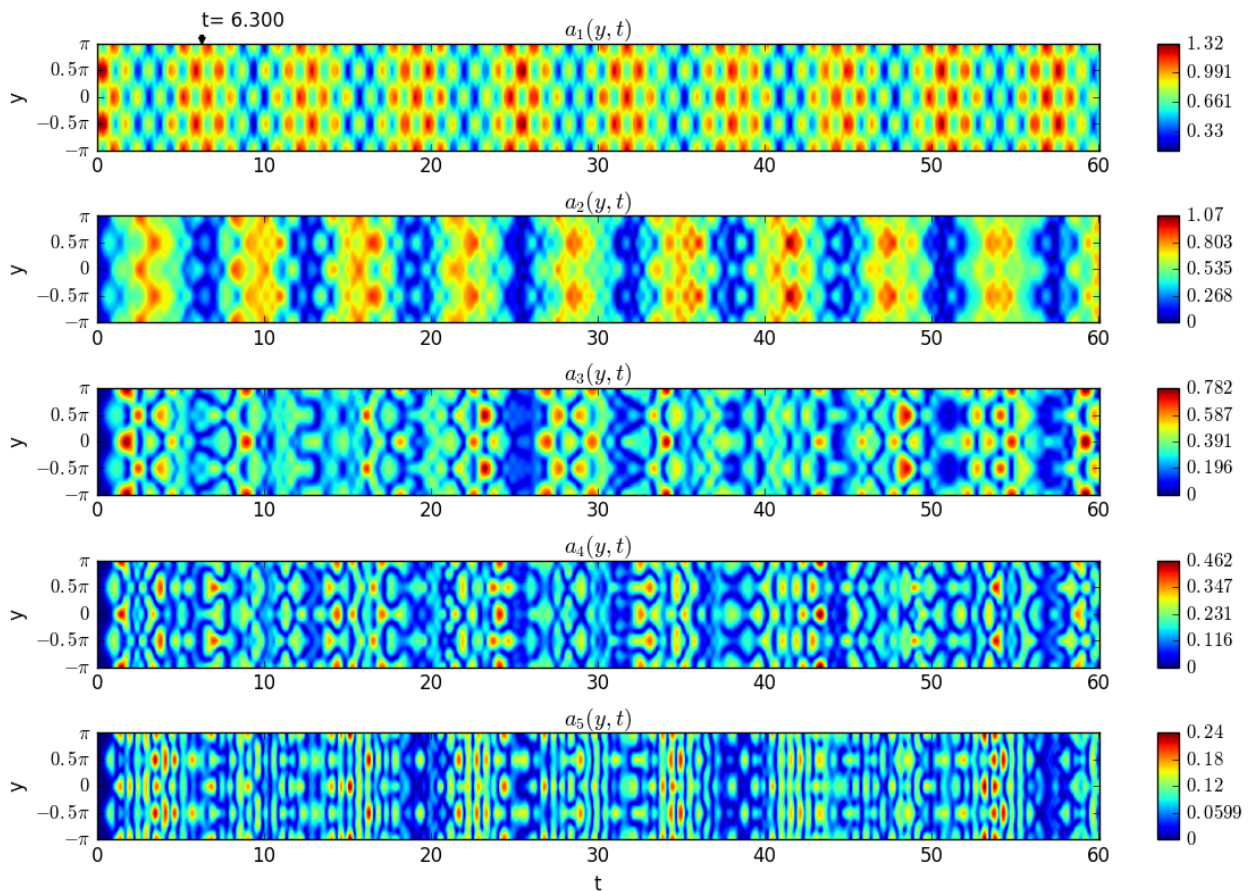


Figure 1: Example of 2D spectral amplitudes.

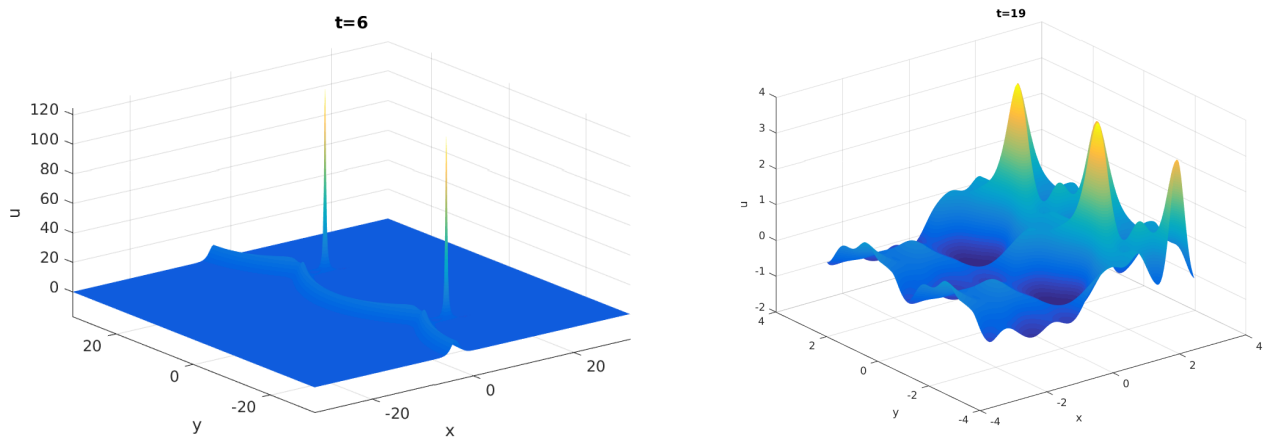


Figure 2: Solitonic structures formed from bended initial pulses: $u(x, y, 0) = 12 \sinh^2[x + \beta \cos(\delta y)]$ in the right panel and $u(x, y, 0) = \sin[\gamma x + \beta \cos(\delta y)]$ in the left panel.

Acknowledgement

This research was supported by the Estonian Research Council (project IUT 33-24).

References

- [1] A. Salupere, The pseudospectral method and discrete spectral analysis. In *Applied Wave Mathematics: Selected Topics in Solids, Fluids, and Mathematical Methods*, E. Quak, T. Soomere (eds.), Springer, Heidelberg, 301–333, 2009.
- [2] A. Salupere, M. Lints, J. Engelbrecht, On solitons in media modelled by the KdV equation. *Archive of Applied Mechanics*, **84**: 1583–1593, 2014.
- [3] A. Salupere, M. Ratas, On solitonic structures and discrete spectral analysis. In *Book of Abstracts: The Ninth IMACS International Conference on Nonlinear Evolution Equations and Wave Phenomena: Computation and Theory, Athens, Georgia, April 1-4, 2015*, G. Biondini, T. Taha (Eds.), Athens, University of Georgia, 30, 2015.
- [4] M. Ratas, A. Salupere, *2D spectral analysis of the KPI equation*, Research Report, Institute of Cybernetics at Tallinn University of Technology, Tallinn, 2017.

VARIATIONAL CONSTRUCTION OF RECIPROCAL MASS MATRICES FOR B-SPLINE-BASED FINITE ELEMENTS: MULTIPARAMETER TEMPLATES AND CUSTOMIZATION

Anton Tkachuk^{1,*}, Anne-Kathrin Schaeuble¹ and Manfred Bischoff¹

¹Institute for Structural Mechanics, University of Stuttgart, 70550 Stuttgart, Germany;
e-mail: {tkachuk,schaeuble,bischoff}@ibb.uni-stuttgart.de

Keywords: reciprocal mass matrices, multiparameter template, customization, dispersion

In this contribution, variational multiparameter templates for reciprocal mass matrices in case of B-spline-based finite elements are proposed and their customization for low grid dispersion error is performed. The variational templates used in the derivation employ a three-field parametrized functional with primary variables for displacement, velocity and linear momentum and it naturally includes free parameters. Later, these parameters are defined in the customization procedure. Finally, the limits on accuracy for homogeneous and heterogeneous material are discussed for practically relevant scenarios.

Recently, several formulations for the scalar wave equation and structural dynamics were proposed that compute the nodal accelerations from the total force vector by multiplying it with a non-diagonal sparse matrix also called here reciprocal mass matrix. This idea can be traced back to the dispersion-corrected method for bilinear quadrilateral elements by Krenk [4] with the equation of motion

$$\mathbf{D}\dot{\mathbf{V}} + \mathbf{K}\mathbf{U} = \mathbf{F}, \quad (1)$$

$$\mathbf{D}\dot{\mathbf{U}} = 0.5(\mathbf{D} + \mathbf{M})\mathbf{V}, \quad (2)$$

where \mathbf{U} and \mathbf{V} are the displacement and velocity vectors, \mathbf{K} and \mathbf{F} are the stiffness matrix and the force vector, \mathbf{D} and \mathbf{M} are the diagonalized and consistent mass matrices. This formulation implies the matrix $0.5\mathbf{D}^{-1}(\mathbf{D} + \mathbf{M})\mathbf{D}^{-1}$ as a directly constructed sparse inverse of the mass matrix. Later, a similar formulation was used for structural dynamics with low-order elements in [3]. Unfortunately, a naïve generalization of the approach given in equation (2) with the weighted sum of the diagonalized and consistent mass matrices to B-spline-based elements neither yields satisfactory accuracy nor provides enough customization parameters. Therefore, a systematic approach extending the ideas of templates [1, 6] is discussed in this contribution.

The three-field parametrized functional uses a modified kinetic energy inside Hamilton's principle

$$T^\circ(\dot{\mathbf{u}}, \mathbf{v}^{(\alpha)}, \mathbf{p}, C_{2,\alpha}) = -\frac{1}{2} \int_{\Omega} \rho^{-1} \mathbf{p} \cdot \mathbf{p} \, d\Omega + \int_{\Omega} \dot{\mathbf{u}} \cdot \mathbf{p} \, d\Omega + \sum_{\alpha=1}^{n_p} \frac{C_{2,\alpha}}{2} \int_{\Omega} \rho^{-1} (\mathbf{p} - \rho \mathbf{v}^{(\alpha)})^2 \, d\Omega, \quad (3)$$

where ρ is the density, \mathbf{u} and \mathbf{p} are displacement and linear momentum, respectively. $C_{2,\alpha}$ and $\mathbf{v}^{(\alpha)}$ are the free parameters and the velocity field for $(\alpha) = 1, 2, \dots, n_p$. The number of free parameters n_p can be chosen depending on the order of the B-spline basis p and the spatial dimension [5]. The modified kinetic energy is discretized using independent ansatz functions for the fields

$$\mathbf{u} \approx \mathbf{N}\mathbf{U}, \quad \mathbf{v}^{(\alpha)} \approx \boldsymbol{\Psi}^{(\alpha)}\mathbf{V}^{(\alpha)}, \quad \mathbf{p} \approx \boldsymbol{\chi}\mathbf{P}, \quad (4)$$

where \mathbf{P} is the vector of the nodal linear momentum. A special instance of the template can be obtained in case of biorthogonality between displacement \mathbf{N} and linear momentum $\boldsymbol{\chi}$ ansatz functions. Then, after static condensation of velocity parameters $\mathbf{V}^{(\alpha)}$ the equation of motion reduces to

$$\dot{\mathbf{P}} + \mathbf{K}\mathbf{U} = \mathbf{F}, \quad (5)$$

$$\dot{\mathbf{U}} = \mathbf{C}^\circ(C_{2,\alpha})\mathbf{P}, \quad (6)$$

with $\mathbf{C}^\circ(C_{2,\alpha})$ being a reciprocal mass matrix depending on the parameters $C_{2,\alpha}$. Such a discretization is optimized for low grid dispersion error for a uniform infinite patch, see [5]. It results in low-frequency accuracy with order $2p + 2$ for homogeneous materials, where p is the order of the B-spline basis.

This contribution does not cover all issues of the approach. Reciprocal mass matrices for isogeometric elements that avoid explicit expressions for the dual basis for the linear momentum and also include elements with Bezier extraction are presented in the contribution [2].

Acknowledgment

This work was supported by the grant project Deutsche Forschungsgemeinschaft (DFG) – Projekt-nummer 279006948 and Projektnummer 326748051 (TK 63/1-1).

References

- [1] C. A. Felippa. A survey of parametrized variational principles and applications to computational mechanics. *Computer Methods in Applied Mechanics and Engineering*, 113(1–2):109–139, Mar. 1994.
- [2] J. A. González, J. Kopačka, R. Kolman, S. Cho, and K. Park. Reciprocal mass matrices for isogeometric analysis via the method of localized lagrange multipliers. In *The 2nd International Conference on Advanced Modelling of Wave Propagation in Solids*, Prague, Czech Republic, Sept. 2018.
- [3] A. Idesman and D. Pham. Finite element modeling of linear elastodynamics problems with explicit time-integration methods and linear elements with the reduced dispersion error. *Computer Methods in Applied Mechanics and Engineering*, 271:86–108, Apr. 2014.
- [4] S. Krenk. Dispersion-corrected explicit integration of the wave equation. *Computer Methods in Applied Mechanics and Engineering*, 191(8-10):975–987, Dec. 2001.
- [5] A.-K. Schaeuble, A. Tkachuk, and M. Bischoff. Variationally consistent inertia templates for B-spline-and NURBS-based FEM: Inertia scaling and customization. *Computer Methods in Applied Mechanics and Engineering*, 326:596–621, 2017.
- [6] A. Tkachuk and M. Bischoff. Direct and sparse construction of consistent inverse mass matrices: general variational formulation and application to selective mass scaling. *Int. J. Numer. Meth. Engng*, 101(6):435–469, Oct. 2015.

EXPLOSION WAVE PROPAGATION IN MASS OF SOLID PARTICLES TO CREATION EXTINGUISHING WHIRLY FOR FAST, EFFECTIVE REMOTE CONTROL OF LARGE, POWER FIRES

Vladimir Zakhmatov^{1,2*}, Michail Chernyshov³, Oldrich Kwech⁴ and Victoria Bojko²

¹University of State Fire Service, Sankt-Petersburg, Russia; e-mail: zet.pulse@gmail.com

²Science Firm "PulsTECH", Tallinn, Estonia; e-mail: pulstech@wiswpuls.com

³Baltic Technical university "Voenmech" Sankt-Petersburg, Russia; e-mail: mvcher@mail.ru

⁴Firm "InterTrade", Praha, Czech; e-mail: ok@intertradeas.cz

Keywords: explosion wave, wave penetration in mass, extinguishing whirly, thin, pulse pulverization, large scale, remote control, safety of firemans.

Impulse, shock wave firefighting systems potentially exceed all other fire extinguishing systems by the quality of creating localizing jets and flows - their dimensions, kinetic energy, directivity of action and degree of dispersion of the sprayed extinguishing agents, natural materials. This determines the effectiveness and scale of the functional impact, in turn. It is shown that the efficiency of the functional impulse action is mainly determined by the process of motion of the vortex front and its parameters - density, size, velocity and angle of encounter with the target surface, and not by the completeness of the uniform distribution of the localizing composition over the target, compositions by a narrow jet or several jets. It is important that the scale of the motion of the vortex front is equal to or comparable to the total scale of the surface of the source of the damaging effect, which for the first time makes it possible to determine with sufficient accuracy the main parameters of quenching: the time, the consumption of the extinguishing composition, depending on the number of vortices and the time of their creation, so that the edges of the vortices block the entire area of the hearth.

Experiments on the study of two-phase flow behind a shock tube section were carried out on a detonation plant. The installation barrel consists of two parts: the slow combustion to detonation transition channel and the research block on which the pressure sensors and powder dispensers were placed. On the flange of the research unit and on its barrel were installed two pressure sensors, the response time of which determined the speed of the wave. Changing the volume of air and a detonating mixture, the regime corresponding to the velocity of the shock wave $M = 1.3$ was chosen [1].

Since the late 40-ies of the twentieth century, methods of extinguishing fires with the help of rockets, shells, and bombs, equipped instead of charging explosive with extinguishing powder agents, are actively being developed, however such use of munitions was ineffective for extinguishing real fires and was accompanied by large areas of destructive and damaging effects. Therefore, from the mid-1960s, special barrel, powder spray guns were shot and devices of spherical and hemispherical spraying with an explosion were developed. Such fire extinguishing systems are called pulsed-vortex [2] or shock-wave systems [2]. By the power [3] and the effectiveness of fire extinguishing, they potentially many times exceed the most advanced samples of traditional pneumatic and hydraulic fire engines. Since 1980 the mini-extinguisher was used at the Moscow Olympics-80, modules for preventing fires and explosions during explosive cutting and welding of gas and oil pipelines; Since May 1986, suspended, water bombs have been used to extinguish fires in the "Red Forest"; since 1983. multi-barrel modules (MM) on the trolley were used in the Metallic Mines (Sverdlovsk) and Coal Mines (Karaganda); in 1988. MM extinguished the bush of burning wells on the offshore platform, Oil Rocks, the Caspian Sea; since 1984. MM extinguished fires in artillery warehouses; since 1985. mini-modules for extinguishing fires on the production lines of explosives (explosives) and ammunition; In 1992-94 the "Impulse-3" installation was put into practice [3], 15 such units are successfully operated at nuclear power plants (Chernobyl, Balakovo), oil and gas and chemical facilities in the territories of Russia and Ukraine.

The author describes the implementation of protective technologies: - prevention of volumetric explosions of dust-gas or vapor-air mixtures, - localization of radioactive dusts by means of large-scale,

fine-dispersed spraying of viscous and sticky compounds; - deposition of toxic clouds by remote creation of large-scale squalls of finely-dispersed water; - localization and neutralization of oil and oil products spills by large-scale and long-distance spraying of sorbents, very sensitive, powdery gases and detonation products destroyed at high temperatures and pressures of shock waves; - Creation of large-scale squalls, eddies and hurricanes, imitating natural and flexibly controlled kinetic energy front for guaranteed non-lethal effects. It achieved a number of positive results in approaching the technology of explosive, shock-wave directional spraying of special agents and environmentally friendly materials for practical quenching.

These modules are of great importance, they can be used in combination with the above-mentioned well-known, pneumatic-pulse-spray and gun-powder-pulse-spray technique:

- No limits for the use of fire-explosive able plants,
- No limits for usage because of orders for gun-powder and explosive,
- Effective spray & pulverization of extinguishing liquids, gels, powders,
- Long period of waiting, reliable, high-effective acting,
- Compact modules can be installed at various chemical industries, oil-refinery shops, pumping stations, offshore oil-wells platform, oil and gas tanks, sea-ports oil terminals, petroleum & liquids gas fitting stations, oil & gas pumping stations, machine-halls at nuclear power stations,
- Fast recharging, simple technical service, no need high-qualified service,
- Cheap production at civil plants, wide diapason of elements for assembly.

References

- [1] V. D. Zakhmatov, A. S. Kozhemyakin, V. L. Tsikanovskii. Jetting of extinguishing powders from trunks. *Physics of combustion and explosion*, **34**(1): 106–109, 1998.
- [2] X. Rogue, G. Rodriguez, H. F. Haas, R. Sourel. Experimental and numerical investigation of the shock-induced fluidization of a particles bed. *Physics of combustion and explosion*, **38**(1): 29–45, 1998.
- [3] V. D. Zakhmatov. Shock-Wave Mechanisms of Impulse Fire-Quenching. In *Sat. reports 3rd Int. colloquium on the physics of shock waves, combustion and detonation*, A. V. Lykov (ed). Minsk: Institute of Heat and Mass Transfer, 100–101, 2013.

SHOCK WAVES. WHAT MAY BE LEARNT FROM THEIR PROPAGATION THROUGH SOLIDS?

Eugene Zaretsky^{1*}, Nahum Frage² and Louisa Meshi²

¹Department of Mechanical Engineering; e-mail: zheka@bgu.ac.il

²Department of Materials Engineering; Ben-Gurion University of the Negev, Beer-Sheva, Israel
e-mail: nfrage@bgu.ac.il

Keywords: elastic precursor decay, Peierls stress, point obstacle strength

It is generally accepted that depending on the level of the acting shear stress or rate of deformation two different modes of inelastic behavior of metals or alloys may be discerned. At low stress insufficient for overcoming different obstacles (Peierls barriers, foreign atoms, etc.) by moving dislocations and characteristic for routine quasi-static loading conditions, the rate of plastic deformation is controlled by thermal fluctuations whose help is required for maintaining dislocations in motion. The flow stress in this regime decreases with temperature while its dependence on strain rate is weak. As soon, as the shear stress τ acting in the material exceeds some threshold value τ^* the regime of plastic deformation, actually the mode of dislocation motion, changes drastically. The dislocation glide becomes an over-barrier one and the control of the dislocation motion is passed to the interaction of the dislocation core with lattice phonons, so-called phonon viscous drag [1]. An additional outcome of the transition from thermally activated to over-barrier glide is an abrupt increase, by factor of 5 – 6, of the material strain rates sensitivity. In pure BCC metals the transition stress τ^* is equal to the material's Peierls stress τ_P [2] whose normalized on shear modulus value τ_P/G is of about 10^{-3} [3]. Due to low value of Peierls stress, $\tau_P/G \sim 10^{-5}$, such transition cannot be observed in pure FCC metals [2 and the references herein] but it can be observed in alloys based on FCC metals, such as, e.g., brass where either solid solution or short range order strengthening make the transition observable and, respectively, the stress τ^* corresponding to these types of strengthening measurable.

The technique employed for such measurements is so-called planar impact test in which plane-parallel sample of the studied material is shock loaded by also plane-parallel impactor. High planarity of the impact provides accurately determined unidimensional loading conditions. Since the material compressibilities in elastic and plastic states are different the input stress pulse is split on elastic precursor wave of relatively low amplitude σ_{HEL} (Hugoniot elastic limit) propagating through the sample with velocity close to the longitudinal speed of sound c_l and the plastic wave whose amplitude is greater than σ_{HEL} while the propagation velocity is of about bulk speed of sound $c_b < c_l$. Propagation of elastic precursor wave through the sample is accompanied by conversion of the shear stress excess into plastic strain γ . As result, the amplitude of the precursor, σ_{HEL} , decays with propagation distance h so, that [4]

$$\frac{d\sigma_{HEL}}{dh} = -\frac{4}{3} \frac{G}{c_l} \dot{\gamma}. \quad (1)$$

The experimentally obtained dependences $\sigma_{HEL}(h)$ are fit reasonably well by power functions of the type $\sigma_{HEL}(h) = \sigma_0(h/h_0)^{-\alpha}$ ($h_0 = 1\text{mm}$). When the factor controlling the dislocation motion is PD, the value of exponent α may vary between 0.35 and 0.7 [2, 5]. As soon as the control of the decay mechanism is passed from PD to TA, the value of α drops to ~ 0.1 or less [2, 5]. The stress τ^* at which the PD-TA transition occurs characterizes the strength of the obstacles.

In the case of pure BCC metals (Ta, V, Mo, Nb, Fe, W, Cr were studied) such obstacle is the Peierls barrier. Measuring the transition stress τ^* at different temperatures allows obtaining the $\tau_P(T)$ dependence unobtainable by any other technique.

This technique was found to be applicable for quantitative determination of strengthening produces by special types of thermal treatment of FCC-based alloys. In particular, the technique made it possible to

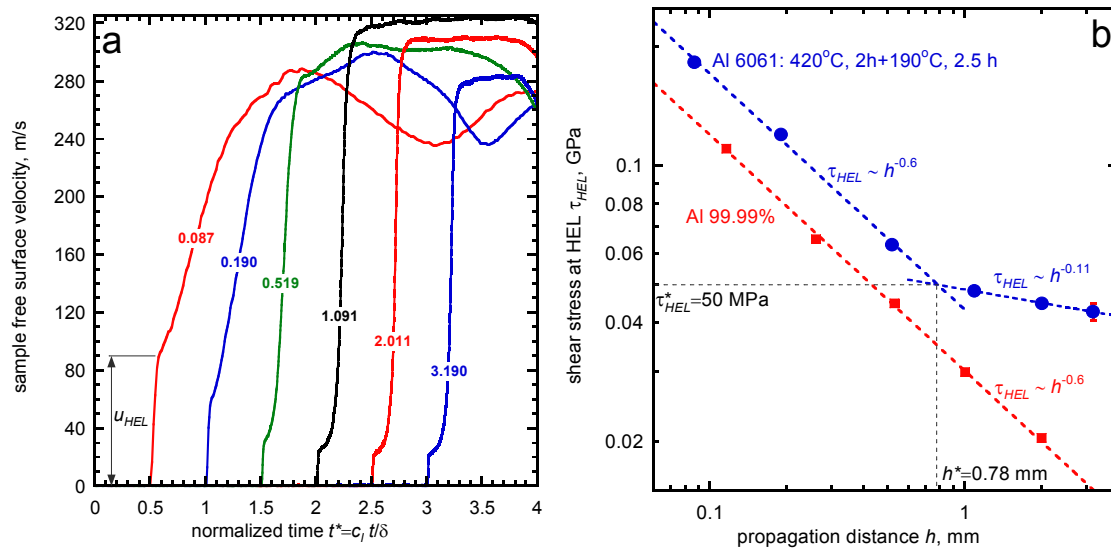


Figure 1. (a) Velocity histories recorded with peak-aged Al6061 samples of different thickness (given in mm directly on the curves). The value of u_{HEL} used for estimating τ_{HEL} is shown by arrow. (b) Presently obtained values of u_{HEL} of peak-aged samples (filled circles) as a function of propagation distance h . Error bar displays typical uncertainty of τ_{HEL} determination. Dashed lines correspond to power fits $\tau_{HEL}(h) = \tau_0(h/h_0)^{-\alpha}$ of experimental data. Point ($\tau_{HEL}^* = 50$ MPa, $h^* = 0.78$ mm) corresponds to the change of the mechanism controlling the dislocation motion.

quantify the interaction of solute Zn atom with dislocation in the cartridge brass (Cu+30%Zn) and to determine the effect of the short range order on this interaction [5].

Strengthening of aluminum alloy 6061 is caused by Guinier-Prestone (GP) zones, monoatomic layers of solute atoms of nanometer transversal dimensions whose periodicity is equal to that of aluminum lattice.

The results of testing of 6061 alloy aged to the maximum GP strengthening are shown in Fig. 1. The change of the regime of the elastic precursor decay takes place at the propagation distance $h^* = 0.78$ mm and shear stress $\tau_{HEL}^* = 50$ Mpa. For the propagation distances less than h^* the decay rate virtually coincides with that found for pure aluminum [6], $\tau_{HEL} \sim h^{-0.6}$, pointing to the over-barrier dislocation glide controlled by the phonon viscous drag. Beyond h^* the decay exponent is much smaller, $\tau_{HEL} \sim h^{-0.11}$ and the decay is governed by the overcoming of the GP zones by moving dislocations. Estimating the activation volume associated with passage (cutting) the obstacle by dislocation gives $V_a \approx 0.84 \times 10^{-27}$ m³. Taking into account that the "thickness" and the height of the GP zone cut by dislocation are of about of $b = 0.286$ nm (aluminum Burgers vector) the average cut width is of about 10 nm.

The above said proves that the shock wave experiment is an effective tool for studying microscopic processes responsible of plastic deformation of crystalline solids.

References

- [1] A.D. Brailsford, Anharmonicity contributions to dislocation drag, *J. Appl. Phys.*, 43, 1380 (1972).
- [2] E. B. Zaretsky, and G. I. Kanel, The high temperature impact response of tungsten and chromium, *J. Appl. Phys.*, 122, 115901 (2017).
- [3] J.N. Wang, Prediction of Peierls stresses for different crystals, *Mater. Sci. Eng.*, A206, 259- 269 (1996).
- [4] G.E. Duvall. Propagation of plane shock waves in a stress-relaxing medium. In: *Stress Waves in Anelastic Solids*, edited by H. Kolsky and W. Prager, pp. 20-32, Springer-Verlag, Berlin, 1964.
- [5] E. B. Zaretsky, and G. I. Kanel, Abnormal temperature effects on the dynamic yield stress of alpha-brass, *J. Appl. Phys.*, 124, 045902 (2018).
- [6] E. B. Zaretsky and G. I. Kanel, Effect of temperature, strain, and strain rate on the flow stress of aluminum under shock-wave compression, *J. Appl. Phys.*, 112, 073504, 2012.

LIST of REGISTERED PARTICIPANTS

Mustafa Abuziarov

Research institute of mechanics
Nizhnii Novgorod State university
Gagarine Ave 23 bl.6
Nizhnii Novgorod
603090
Russia
E-mail: abouziar@mech.unn.ru
Page: 21

Ruben Acevedo

Institute of Thermomechanics, AS CR, v.v.i.
Dolejškova 1402/5
Praha
182 00
Czech Republic
E-mail: ruben.acevedo@rocketmail.com
Page: 23

Vítězslav Adámek

NTIS - New Technologies for the Information Society
University of West Bohemia
Technická 8
Pilsen
301 00
Czech Republic
E-mail: vadamek@kme.zcu.cz
Page: 25

Xavier Arnoult

HiLASE Centre, Institute of Physics, AS CR, v.v.i.
Na Slovance 1999/2
Prague
18221
Czech Republic
E-mail: arnoult@fzu.cz
Page:

Benny Bar-On

Ben Gurion University of the Negev
P.O.Box 653
Beer Sheva
84105
IL
E-mail: bbo@bgu.ac.il
Page: 27

Hajar Benzeroual

National School of Applied Sciences
Mhaneche II, Avenue Palestine B.P. 2117 Tetouan
Tetouan
93000
Morocco
E-mail: benzeroual.hajar@gmail.com
Page: 29

Arkadi Berezovski

Tallinn University of Technology
Akadeemia tee 21
Tallinn
12618
Estonia
E-mail: arkadi.berezovski@cs.ioc.ee
Page: 41

Marc Bonnet

CNRS
828 boulevard des Maréchaux
Palaiseau
91120
France
E-mail: mbonnet@ensta.fr
Page: 33

Anne-Sophie Bonnet-Ben Dhia

CNRS
828 Boulevard des Maréchaux
Palaiseau
91120
France
E-mail: Anne-Sophie.bonnet-Bendhia@ensta-paristech.fr
Page: 29

Stéphanie Chaillat

CNRS
828 Boulevard des Maréchaux
Palaiseau
91120
France
E-mail: stephanie.chaillat@ensta-paristech.fr
Page: 35

Wayne Chen

Purdue University
701 West Stadium Avenue
West Lafayette
47907-2045
USA
E-mail: wchen@purdue.edu
Page: 61

Martin Colvez

CNRS, CentraleSupélec, Université Paris-Saclay
3 rue Joliot-Curie
Gif-sur-Yvette
91190
France
E-mail: martin.colvez@centralesupelec.fr
Page: 37

Regis Cottereau

CNRS, CentraleSupélec, Université Paris-Saclay
3 rue Joliot-Curie
Gif-sur-Yvette
91190
France
E-mail: regis.cottereau@centralesupelec.fr
Page: 37, 39

Jüri Engelbrecht

Tallinn University of Technology
Akadeemia tee 21
Tallinn
12618
Estonia
E-mail: je@ioc.ee
Page: 41

Tomáš Fíla

Czech Technical University in Prague
Faculty of Transportation Sciences
Konviktská 20
Prague
110 00
Czech Republic
E-mail: fila@fd.cvut.cz
Page: 43

Marc Fivel

Univ. Grenoble Alpes / CNRS
101 Rue de la Physique
Grenoble
38402
France
E-mail: Marc.Fivel@simap.grenoble-inp.fr
Page: 45

Marek Foglar

Czech Technical University in Prague
Faculty of Mechanical Engineering
Technická 4
Praha 6
16607
Czech Republic
E-mail: marek.foglar@fsv.cvut.cz
Page: 47

Dušan Gabriel

Institute of Thermomechanics, AS CR, v.v.i.
Dolejšková 1402/5
Prague
18200
Czech Republic
E-mail: gabriel@it.cas.cz
Page: 23, 49

Inna Gitman

The University of Sheffield
Dept. Mechanical Engineering
Sir Frederick Mappin building, Mappin Street
Sheffield
S1 3JD
Great Britain
E-mail: i.gitman@sheffield.ac.uk
Page: 51

José A. González

Universidad de Sevilla
Avda. de los Descubrimientos s.n.
Seville
41092
Spain
E-mail: japerez@us.es
Page: 49, 53

Tomáš Grabec

Institute of Thermomechanics, AS CR, v.v.i.
Dolejškova 1402/5
Prague
18200
Czech Republic
E-mail: grabec@it.cas.cz
Page: 55

Sigrun Hirsekorn

NDT&E Consultant
Rehbachstraße 126, Dudweiler
Saarbrücken
66125
Germany
E-mail: sigrun.hirsekorn@gmail.com
Page: 57

Petr Hora

Institute of Thermomechanics, AS CR, v.v.i.
Velešlavínova 11
Pilsen
30100
Czech Republic
E-mail: hora@cdm.it.cas.cz
Page: 59

Hoon Huh

KAIST
291 Daehak-ro, Yuseong-gu
Daejeon
34141
Korea
E-mail: hhuh@kaist.ac.kr
Page: 63

Wonju Jeon

KAIST
291 Daehak-ro, Yuseong-gu
Daejeon
34141
Korea
E-mail: wonju.jeon@kaist.ac.kr
Page: 65

Romik Khajetourian

ETH Zürich
Leonhardstr. 21, LEE N205
Zurich
8092
Switzerland
E-mail: kromik@ethz.ch
Page: 67

Luděk Klimeš

Faculty of Mathematics and Physics
Charles University in Prague
Ke Karlovu 3
Praha
121 16
Czech Republic
E-mail: klimes@seis.karlov.mff.cuni.cz
Page: 69

Jan Kober

Institute of Thermomechanics, AS CR, v.v.i.
Dolejšková 1402/5
Praha
182 00
Czech Republic
E-mail: Kober@it.cas.cz
Page: 71, 85, 97

Martin Koller

Institute of Thermomechanics, AS CR, v.v.i.
Dolejšková 1402/5
Praha
182 00
Czech Republic
E-mail: koller@it.cas.cz
Page: 75

Radek Kolman

Institute of Thermomechanics, AS CR, v.v.i.
Dolejšková 1402/5
Prague
18200
Czech Republic
E-mail: kolman@it.cas.cz
Page: 23, 49, 53, 77, 85, 97

Alena Kruisová

Institute of Thermomechanics, AS CR, v.v.i.
Dolejšková 1402/5
Prague
18200
Czech Republic
E-mail: alena@it.cas.cz
Page: 75, 77

Martin Lints

Tallinn University of Technology
Akadeemia tee 21
Tallinn
12618
Estonia
E-mail: martin.lints@cens.ioc.ee
Page: 79

Bruno Lombard

CNRS
4 impasse Nikola Tesla
Marseille
13453 Cedex 13
France
E-mail: lombard@lma.cnrs-mrs.fr
Page: 31

Dalibor Lukáš

Technical University of Ostrava
Faculty of Electrical Engineering and Computer Science
17. listopadu 15/2172
Ostrava
70833
Czech Republic
E-mail: dalibor.lukas@vsb.cz
Page: 83

Michal Mračko

Institute of Thermomechanics, AS CR, v.v.i.
Dolejšková 1402/5
Praha
182 00
Czech Republic
E-mail: mracko@it.cas.cz
Page: 85, 97

Oleg Naimark

ICMM UB RAS
Koroleva str, 1
Perm
614013
Russia
E-mail: naimark@icmm.ru
Page: 87

Jose L. Ocaña

Universidad Politécnica de Madrid
Jose Gutierrez Abascal, 2
Madrid
28006
Spain
E-mail: jlocana@etsii.upm.es
Page: 89

K. C. Park

University of Colorado
1111 Engineering Way
Boulder
80309-0429
USA
E-mail: kcpark@colorado.edu
Page: 53, 91

Slavomír Parma

Institute of Thermomechanics, AS CR, v.v.i.
Dolejšková 1402/5
Prague
18200
Czech Republic
E-mail: parma@it.cas.cz
Page: 93

Jiří Plešek

Institute of Thermomechanics, AS CR, v.v.i.
Dolejšková 1402/5
Prague
18200
Czech Republic
E-mail: plesek@it.cas.cz
Page: 49, 77, 85, 93

Alexey Porubov

Institute of Problems in Mechanical Engineering of the RAS
Saint Petersburg
199178 Bolshoy av., V.O. 61
Russia
E-mail: alexey.porubov@gmail.com
Page: 95

Zdeněk Převorovský

Institute of Thermomechanics, AS CR, v.v.i.
Dolejšková 1402/5
Prague
18200
Czech Republic
E-mail: zp@it.cas.cz
Page: 85, 97

Ivan Pšenčík

Institute of Geophysics
Boční 1401/22a
Prague
14131
Czech Republic
E-mail: ip@ig.cas.cz
Page: 103

Sofia Rejani

National School of Applied Sciences
M'haneche II, Avenue Palestine B.P. 2117
Tetouan
93000
Morocco
E-mail: Sofia.rejjani@gmail.com
Page: 99

Eduard Rohan

University of West Bohemia
Univerzitní 8
Pilsen
30614
Czech Republic
E-mail: rohan@kme.zcu.cz
Page: 101

Danijela Rostohar

HiLASE Centre, Institute of Physics, AS CR, v.v.i.
Na Slovance 1999/2
Prague
18221
Czech Republic
E-mail: rostohar@fzu.cz
Page:

Bohuslav Růžek

Institute of Geophysics
Boční 1401/22a
Prague
14131
Czech Republic
E-mail: b.ruzek@ig.cas.cz
Page: 103

Oren Sadot

Ben Gurion University of the Negev
P.O.Box 653
Beer Sheva
84105
Israel
E-mail: sorens@bgu.ac.il

Andrus Salupere

Tallinn University of Technology
Akadeemia tee 21
Tallinn
12618
Estonia
E-mail: salupere@ioc.ee
Page: 81, 105

Sergey Sorokin

Aalborg University
Fibigerstraede 16
Aalborg
9220
Denmark
E-mail: svb@m-tech.aau.dk
Page: 79

Yohanes Tjandrawidjaja

CEA-LIST
Bâtiment 565
Gif-sur-Yvette
91191
France
E-mail: yohanes.tjandrawidjaja@ensta-paristech.fr
Page: 29

Anton Tkachuk

Universität Stuttgart
Pfaffenwaldring 7
Stuttgart
70550
Germany
E-mail: tkachuk@ibb.uni-stuttgart.de
Page: 107

Vladimir Zakhmatov

St. Petersburg University of Fire Service of EMERCOM of Russia
149 Moskovsky Ave.
Saint Petersburg
196105
Russia
E-mail: zet.pulse@gmail.com
Page: 109

Eugene Zaretsky

Ben Gurion University of the Negev
P.O.Box 653
Beer Sheva
84105
Israel
E-mail: zheka@bgu.ac.il
Page: 111

© 2018, Institute of Thermomechanics
The Czech Academy of Sciences, v.v.i.
Dolejšková 1402/5
182 00 Prague 8
Czech Republic
<http://www.it.cas.cz>

ISBN: 978-80-87012-67-3